EVOLUTION OF NITROGEN IMPURITIES IN METAL-SILICON BINARY COUPLES AND THEIR EFFECT ON SILICIDE FORMATION

Thesis by

Kuo Ting Ho

In Partial Fulfillment of the Requirements

for the Degree of

Doctor of Philosophy

California Institute of Technology

Pasadena, Ca. 91125

1984

(submitted May 8, 1984)

ACKNOWLEDGEMENTS

The completion of this thesis has been a trying as well as rewarding experience. It is indeed a true pleasure to think back on the numerous people who have been my source of encouragements and inspirations. Foremost among these is my thesis advisor, Dr.Marc-Aurele Nicolet, whose extraordinary patience and liberal philosophy allowed me the freedom to pursue my own interests. His diligent scrutiny has always added extra refinements to all of my work. Gratitute goes to Dr. Leszek Wielunski who kindly guided me into the exciting field of nuclear reaction analysis, from which my thesis topic emerged. Ilkka Suni receives my high respect for his professional competence as well as his generous character in devoting a great deal of energy and time helping the students. Thanks go to Professor Silvanus Lau who is always a source of stimulating suggestions. My association with Dr. Marc van Rossum has been extremely interesting and valuable because of his conviction to apply sound scientific principles to all experimental works.

I want to express my appreciations to the fellow graduate students, Chuen Der Lien, Frank So, Tom Banwell, Dr. Meir Bartur and Dr. David Scott; all of whom have unselfishly offered their help in times of need, and have contributed to the dynamic research environment at Caltech, which nourished my scientific growth in the past few years. I only hope that whatever of their strong points I have absorbed will continue to benefit me in the future.

Special thanks go to Michell Parks who has been not only a great help due to her excellent typing skill but also a pleasant counselor in general. Thanks also go to Rob Gorris, Rouel Fernandez and Ali Ghaffari for their technical assistances.

I am indebted to the Jet Propulsion Laboratory, California Institute of

Technology (D. Burger), Sandia National Laboratory (M. B. Chamberlain) and Solid State Device Inc. (A. Applebaum) for their financial assistances.

Mrs. Laufer's hospitality made my six-year residence in Pasadena sweet and memorable. Her kind words provided me much comforting relief in stressful moments.

Last but not least, I want to pay a special respect to my parents, whose confidence and expectation in me have strengthened me at many difficult points, not only during graduate school, but throughout my life.

ABSTRACT

The possible ways in which nitrogen may be present in and interact with metal silicides are outlined. It is shown that, although contaminant nitrogen can be easily eliminated in deposition systems and processing ambients, understanding the role of nitrogen in metals and metal silicides may be important for various nitridation processes used for VLSI fabrication.

Nitrogen isotope ^{15}N is controllably introduced into either the metal or silicon in a metal-silicon binary couple. Silicide formation is induced by vacuum annealing. After various thermal treatments, ^{15}N is profiled by the $^{15}N(p,\alpha)^{12}C$ nuclear reaction. A detailed description of this technique is given.

The metals investigated are Pd, Ni, Co, Pt, Ta, Mo and Ti. Metal silicides are grouped into three categories according to the moving species during silicide formation: metal, silicon or both. The interpretation of nitrogen evolution during silicide formation is based on the identity of the moving species. A wide variety of nitrogen redistribution patterns (segregation, incorporation, accumulation, dilution and fast diffusion) are observed in different samples, depending on parameters such as nitrogen diffusivity and solubility in its host matrix, and nitrogen bond strength to the silicide forming species.

The presence of nitrogen sometimes will slow down the silicide growth rate. The degree of slowing down generally depends on the amount of nitrogen incorporated. In case of refractory metal, a large concentration up to 25 at% of oxygen is found to be incorporated during metal film deposition. The redistribution of oxygen during annealing is investigated using the $^{16}O(d,\alpha)^{14}N$ nuclear reaction.

Two additional studies on different subjects are reported. The first one investigates the dry and wet oxidation behavior of Ti and Hf nitrides. A parabolic

oxidation rate is found in all cases except the wet oxidation of HfN. The other study extends the work on dopant enhanced epitaxial regrowth of Si to three substrate orientations. It is found that the enhancement factor is the same, independent of the substrate orientation. An improved crystalline quality is observed for epitaxial Si regrown on an <111> substrate.

TABLE OF CONTENTS

CHAPTER 1 INTRODUCTION

The current trends in VLSI development is projecting a submicron feature size by 1985[1]. Continual scaling down of feature size raises many technological challenges such as propagation delay in interconnections[2], stability of contacts against thermal treatments and electromigration[3,4], planarization of dielectric insulations for multilevel interconnections[3], conformal coverage of anisotropically etched steps[4], interfacial cleanliness and low contact resistance in shallow contacts[5], etc. Of the many major research efforts undertaken on VLSI technology, the search for a new interconnection and gate material is a dominant sector[6].

Metal silicides have been proposed as the viable substitute for doped polysilicon as the interconnect and gate material as well as forming first level metallization to Si devices[2,3]. The various merits of metal silicides which warrant the intense attention that metal silicides have received are their low resistivity, good adherence to gate oxide, thermal stability against Si, wide selection of Schottky barrier heights, stability against chemical agents and oxidizability[2,7].

Many of these properties may come into interplay with impurity species that are present[8]. The interest in impurities generally comes in two ways. The first one has to do with redistribution of dopants during various processing steps. Dopant segregation at the silicide/Si interface during silicide growth was studied[9]. Some thoughts were also devoted to dopant diffusion in a polycide gate structure from poly Si into the adjacent silicide layer[10,11]. The other branch of impurity studies concentrates on the common contaminants in a vacuum system, such as N, O, and C, which may be incorporated into a metal or silicide layer during deposition[7]. Incorporated O has been reported to produce pest

silicide reactions, marked by nonuniform growth, and retard or suppress silicide growth rates[12,13,14]. The subject of this thesis is the effect of another type of impurity, the nitrogen.

During the sputter-deposition of metal films, nitrogen can be incorporated through one of three processes[15]:(i) Chemisorption of molecular N_2 with a sticking coefficient s. (ii) Adsorption of atomic nitrogen which is formed by bombardment of molecular ions against the substrate surface at energies $\geq$ 8 eV, by N_2 molecules first chemisorbed on the target surface and then sputtered off as atoms, and by dissociation due to electron collisional processes. The sticking coefficient for reactive atomic gases is usually taken to be unity. (iii) High energy ($\geq$ 100 eV) ions which become physically entrapped in the lattice. Such high energy ions can be produced with a substrate bias and are of negligible importance in a zero bias deposition system.

Winters and Kay[16] classified various sputtered materials into three classes. Class 1 consists of elements which both chemisorb molecular nitrogen and form nitrides, such as W, Ta, Hf, and Nb. Materials in class 1 can incorporate nitrogen through both processes (i) and (ii). However, process (i) is expected to dominate, since from cross-sectional data, it is estimated that the ratio of excited species (such as atoms and ions) to ground state molecules will be smaller than 10^{-3} in a typical discharge. The elements in class 2 do not chemisorb molecular nitrogen but form nitrides. These include Si, Al, Ni, and Fe. Nitrogen can be incorporated in these elements through process (ii). Noble metals such as Au and Ag fall in class 3, which do not chemisorb molecular nitrogen and do not form nitrides. This class of materials can only incorporate nitrogen through a large substrate bias, i.e. process (iii), and will not be considered further.

The sticking coefficients s of N_2 on a limited number of materials are available in the literature. For N_2 on W, s is a strong function of surface

coverage, and equal to 0.28 on a fresh W surface[17]. The sticking coefficient for N_2 on Ta has been suggested to be close to 0.5[18]. The incorporation of nitrogen by process (i) can be modeled based on elementary gas kinetic theories. The instantaneous rate of supply of gas to the surface flow is given by,

$$\text{flux} = \frac{P}{\sqrt{2\pi mkT}} \tag{1}$$

where P and m are the partial pressure and molecular mass of the gas. Using eqn.(1), the rate of N incorporation can be calculated by[15]

$$R^{(i)} = 7.7\times10^{20}\, sP_{N_2} \text{ atoms/cm}^2 \text{ sec} \tag{2}$$

where P_{N_2} is the partial pressure of nitrogen molecules in torr. The resultant N at% in a deposited film is given by

$$\text{N } at\% = 7.7\times10^{8}\frac{sP_{N_2}}{NR}\% \tag{3}$$

where N in the density of the material deposited in $10^{22}/\text{cm}^3$, and R is the deposition rate in Å/s. For a W film deposited at a rate of 20 Å/s, a nitrogen impurity level lower than 0.1% can be achieved with a N_2 partial pressure below 5.8×10^{-8}.

Predictions on the effects of process (ii) depend on a knowledge of the atomic nitrogen concentration in the discharge. Dissociation and ionization cross sections of N_2 have both been measured as a function of electron energy, and are found to be similar in magnitude and shape. The two cross sections reach values of 2.1 and 2.6 $\times$ 10^{-16} cm^2 at an electron energy of ~90 eV, respectively[19,20]. The atomic nitrogen concentration in a particular discharge configuration can be experimentally determined with an electron probe utilizing the similarty in the above two cross sections[21]. The nitrogen atom concentration can be assumed to be equal to the nitrogen ion concentration, which is equal to the electron concentration in the field-free negative glow

region. However, a generalized model for predicting such concentrations is still unavailable.

It is known from practical experiences that nitrogen in deposited materials exists in quantities much lower than oxygen. In sputtered and evaporated films, the nitrogen concentration is usually below the sensitivity of Auger electron spectroscopy[22]. Only trace amounts of N are reported to be detected by SIMS[23]. The difference can very likely be attributed to a larger partial pressure of H_2O, HO and O_2 compared to N_2 in common vacuum systems. Such a large offset in abundance of oxygen and nitrogen species has been observed using a monopole residual gas analyzer attached to the evaporation system used for this thesis work[24]. Another apparent difference between nitrogen and oxygen is the much larger dissociation energy of N_2 (9.83 eV) as compared to O_2 (5.15 eV)[25]. Thus, reactive atomic oxygen is expected to be much more abundant than atomic nitrogen given the same discharge configuration.

Another source of impurities is the annealing or storage ambient. Impurities may enter materials by diffusion at elevated temperatures. However, nitrogen indiffusion during annealing also is rarely seen, whereas, indiffusion of oxygen is frequently observed[26]. In fact, it is a common industrial practice to perform high temperature device processes in a N_2 ambient due to the inertness and immobility of nitrogen. Most of the published nitridation experiments have reported diffusion limited nitride growth[27,28]. The immobility of nitrogen is therefore very likely due to the lack of a fast diffusing nitridant. It is known for example, that ammonia is much more efficient than N_2 in nitriding Mo films[29]. This indicates that the nitridant involved must be in a form different from either ground state or ionized molecular nitrogen. The large dissociation energy of N_2 will then justify the scarcity of nitrogen incorporation by indiffusion from the ambient.

In a few cases, nitrogen in the form of unintended impurities has been reported. Cheung et al.[23] detected a thirtyfold increase of N content in Si that is sputtered in 5×10^{-7} torr residual gas pressure, as compared to Czochralski grown Si. Nowicki et al.[30] found up to 24 at% of N in sputtered Mo, when the residual pressure was at a high value of 3×10^{-5} torr. However, N content was reduced to below 0.1 at%, when a better vacuum system capable of 2×10^{-6} torr base pressure was used. Nagata and Shoji[31] also made a study on sputtered Mo. They observed a change in the phase of the sputtered film from bcc Mo to fcc γ-Mo_2N, when a low sputtering rate was used at a residual gas pressure of 2-3 $\times$ 10^{-6} torr. In actual industrial practice, deposition systems are generally pumped to a base pressure of $\sim 10^{-6}$ torr. At reasonably fast deposition rates, N contamination in these systems can be expected to be negligible.

However, there is abundant evidence in the literature which suggests that some N-intensive processing may rise to prominence in future VLSI fabrication. In such situations, N-impurities may become a major concern. Josquin and Jamminga[32] have demonstrated a new scheme for oxidation masking in self-aligned MOS fabrication. This scheme involves implanting 10^{16} N_2/cm^2 into the source and drain areas, and preannealing at 1000°C in dry N, prior to a 3hr. wet oxidation of the poly-silicon gate at 850°C. During the 1000°C preannealing, a large fraction of the N diffuses to the Si surface and becomes trapped under the thin gate oxide already formed. The trapped N forms a nitride-like layer and inhibits oxidation in the source and drain areas. They have also shown by resonant nuclear reaction analysis that a large amount of N remains inside the near surface region of Si. Formation of silicide contacts at these implanted areas will certainly be affected by the residual N.

Another application of N reported by Kim and Brown[33] is a partial nitridation of Mo gates to form a protective Mo_2N layer which provides

resistance against oxidation and processing reagents, as well as improves implantation masking. A few refractory metal and metal alloys other than Mo , namely W, TiW and Ta, are also being considered as potential interconnection and gate materials due to their high conductivity and fine-line patternability[34]. The nitride passivation method may be a major step in the improvement of processing tolerance of refractory metal gates, since lack of self-passivation capability is their major setback compared to polysilicon and silicide gates. An understanding of metal/nitrogen binary systems will therefore be valuable for such process innovations.

Novel and creative applications of Si_3N_4 also frequently appear in research journals. Silicon nitride formed by thermal nitridation of Si or SiO_2 is being tested for substituting SiO_2 as the thin gate dielectric, which is expected to scale down to 200 Å in VLSI circuits[35]. Thin SiO_2 films have various disadvantages such as high defect density, causing a high probability of low field breakdowns, tendency to react with electrodes, poor masking against dopant and impurity diffusion, a dielectric constant which changes with annealing and high field. Most of these disadvantages can be eliminated by using a nitride layer instead. Silicon nitride is also more suitable for use as the floating gate dielectric of avalanche-injection MIS devices such as electrically alterable ROM's[36]. The low energy barrier height of silicon nitride greatly enhances carrier injection. Still other new Si_3N_4 applications include oxidation masking[37], and encapsulation of Si film in zone-melting recrystallization processes[38]. The chemical stability of these Si nitrides or subnitrides against abutting metal contacts is clearly an important prerequisite. It is hoped that the materials reported in this thesis represent a first step in understanding metal reactions with nitrided Si.

In one type of diffusion barrier, N impurities have been proven to be desirable inclusions. Incorporation of N drastically improves the effectiveness of

Mo[39], W[40] and TiW[41] as diffusion barriers between two reactive elements. The role of N in these cases is explained as stuffing of grain boundaries thus eliminating short circuit diffusion paths in these polycrystalline barrier layers. Futhermore, N is found to inhibit reactions between these diffusion barriers and the Si substrate. This inhibition carries practical significance since contacts which can be annealed to minimize contact resistance without inducing reaction within the contact structure is highly desirable[42]. Recent experiments[43] demonstrated that even in the case of an amorphous NiW diffusion barrier, which does not have grain boundaries, N incorporation still serves a useful purpose. Nitrogen introduced through the sputtering gas decisively upgrades the stability and performance of the overall contact structure by suppressing reaction between Al and NiW, and between Si and NiW at annealing temperatures up to 500° for 150 min. These promising results demonstrate the concept that N impurities do not necessarily play the part of undesirable contaminants, but can actually have virtues which warrant practical applications.

As a final remark, application of N in material processing extends even into the realm of superconductors. Augmented-plane-wave band calculation has predicted a B1-structured MoN phase which should have a very high transition temperature (~29 K)[44]. Attempts at producing this metastable MoN phase are already under way[45,46]. Since the studies undertaken in this thesis provide some qualitative information about the behaviors of N in various metals (including Mo), it is hoped that the results reported may serve as a general reference for future material researches involving nitrogen processing.

CHAPTER 2 EXPERIMENTAL TECHNIQUE

2.1 Introduction

In thin film work, Rutherford backscattering spectrometry(RBS) is one of the primary techniques used for monitoring intermetallic reactions, determining alloy compositions, identifying surface elements, measuring layer thicknesses and profiling heavy impurities. However, RBS is insensitive to trace amounts of light impurities, such as carbon, oxygen and nitrogen, that are embedded in a high Z host material. Furthermore, if the host material is supported on a substrate composed of elements heavier than the impurity (eg. Si), the relatively large scattering section and high kinematic factor of the substrate element gives rise to an extended continuum of substrate signal which overlaps with the impurity signal and interferes with an accurate analysis.

Secondary Ion Mass Spectrometry (SIMS) and Auger Electron Spectrometry (AES) are common methods for profiling light elements employing ion milling. These methods have sensitivities of .001 and .1 at% respectively[47]. Their setbacks are that a suitable calibration sample is not always available to allow quantitative measurements, and that ion milling may alter the composition of the material being studied. A third technique, Nuclear Reaction Analysis (NRA), is an isotope-specific profiling technique, which is suitable for light elements, but is insensitive to sample matrix. It has a sensitivity close to that of AES. Its main advantages over the above two methods are its nondestructive nature and quantitative character. The common NRA techniques use an energetic beam of either deuterons or protons, at incident energies of order 1 MeV/ion, and can be performed with conventional RBS facilities. Thus, NRA and RBS are two compatible and complementary techniques.

Since RBS is a well established experimental technique, only NRA will

receive a detailed description in this thesis. There are two possible nuclear reactions for detecting nitrogen. A comparison is made in section 2.2. In subsequent sections, the discussion will focus on the $^{15}N(p,\alpha)^{12}C$ reaction only, which is the one chosen for this study.

2.2 $^{15}N(p,\alpha)^{12}C$ vs. $^{14}N(d,\alpha)^{12}C$

Nitrogen can be detected by two nuclear reactions[48]: the $^{15}N(p,\alpha)^{12}C$, hereafter referred to as (p,α), which detects the rare isotope ^{15}N (0.37% relative abundance), and the $^{14}N(d,\alpha)^{12}C$, hereafter referred to as (d,α), which detects the abundant isotope ^{14}N. A comparison of various characteristics will demonstrate the advantages of the former.

2.2.1 Reaction Cross Section

A compilation of nuclear reaction parameters has been published by Everling et al.[49]. Table I shows that for the experimental parameters specified, the (p,α) reaction has ~10 times the cross section σ of (d,α). The added charge collection efficiency and sensitivity due to a larger σ makes the former far superior from a practical point of view. It will be shown in the next section, that by using an incident proton energy of 1 MeV, the reaction cross section is enhanced to a value of 34.4 mb/sr. A typical NRA spectrum in this study is obtained in 20 min. of charge collection time with a beam current of 100 nA at this energy, which is only 3-4 times longer than that required for a typical 2 MeV $^4He^+$ RBS spectrum.

2.2.2 Energy Stopping Power

Before reaching the detector, the α particle emitted by the nuclear reaction must travel from the activation site, through the sample, to the surface. The energy loss of the α particle during this exit is the predominant factor which

TABLE I

Compilation of nuclear reaction parameters by Everling et al.

Reaction	Q value	Incident energy	Emitted energy	Approximate[a] $\sigma(E_0)$	Yield[b]
	(MeV)	(MeV)	(MeV)	(mb/sr)	(counts/μC)
$^{15}N(p,\alpha)^{12}C$	4.964	0.8	3.9	~15	90
$^{14}N(d,\alpha)^{12}C$	9.146	1.2	6.7	1.3	7

a) for laboratory emission angle of 150°.
b) yield from a $1 \times 10^{16}/cm^2$ surface layer for a solid angle of 0.1 sr.

gives NRA its depth scaling capability (see section 2.5.2). The depth resovling power of a particular NRA technique depends on a sufficiently high rate of energy loss. The emitted energy of the α particle usually lies in the 2-10 MeV range [48]. The energy stopping power at such high energy is given by the Bethe-Bloch formula[50],

$$S_\alpha \equiv \left[\frac{dE}{dX}\right]_\alpha = NZ_2\left[\frac{2\pi(Z_1 e)^2}{m_e(E/m)}\right]\ln\left[\frac{4m_e(E/m)}{kZ_2}\right] \qquad (1)$$

Where N and Z_2 are the atomic density and atomic number of the target material, respectively. m and E are the atomic mass and atomic number of the energetic α particle.

By referring to this formula or to the values tabulated by Chu et al.[50], it is clear that S_α(E) decreases with higher E. According to Table I, the emitted energy from the (d,α) reaction is 6.7 MeV, which is a factor of 1.7 larger than the emitted energy of 3.9 MeV for (p,α). For a Si target, $S_\alpha(E)$ for (p,α) is enhanced approximately 1.4 times over that for (d,α).

2.2.3 Radiation Safety

The (d,α) reaction requires extra safety considerations. A hazardous effect inherent to deuterium beam application is the neutron radiation produced by

the $^{12}C(d,n)^{13}N$ reaction. This reaction occurs as a result of divergent D^+ beam impinging on the carbon films that are deposited over time on the inside walls and slits of the beam line. Compliance with radiation safety standards inevitably sets limits in the maximum beam current and ion energy, as well as restricts the number of working hours allowed to an operator. These stringencies require constant cautions and reduce the flexibilities in experimental parameters which may be important for optimal results. These hazards and restrictions are eliminated by choosing the (p,α) reaction.

2.3 Geometry

An illustration of the sample mounting geometry is given in figure 1. The detector is placed in the plane of the sample normal and the incident proton beam, making an angle Θ w.r.t. the incident beam. During the setting up of the (p,α) experiments, a detector was already installed at $\Theta = 164°$, for previous $^{16}O(d,\alpha)^{14}N$ experiments. This detector angle was retained for this study to avoid modifications to the existing set up. The NRA spectra were taken with the sample tilted away from the detector around an axis normal to the beam-detector plane, at an angle $\Theta_1 = 60°$ from normal incidence. This configuration enhances the depth resolution by a factor $\left(\frac{1}{\cos\Theta_2}\right) = 2$ and minimizes the energy loss of the incident proton during its travel to an activation site at a sample depth x. Ideally, the proton energy loss should be reduced to zero, so that the reaction cross section σ remains constant throughout the thickness of the sample. Practically, a constant σ is approximated by selecting the incident energy E_0 from a range where the excitation curve of the nuclear reaction is nearly flat (see section 2.4).

In figure 1, E_1 is the proton energy immediately prior to activating an ^{15}N atom at a sample depth x in the target. It's value is given by

$$E_1 = E_0 - \int_0^x S_p \frac{dx}{\cos\Theta_1}, \tag{2}$$

where $S_p \equiv \left(\frac{dE}{dx}\right)_p$ stands for the rate of proton energy loss in the sample. The energy E_2 of the α particle emitted after the nuclear reaction takes place is calculated using the conservation of energy and momentum.

$$E_2(E_1) = \frac{m_1 m_2 E_1}{(M+m_2)^2}\left[2\cos^2\Theta + \frac{M(m_2+M)}{m_1 m_2}\left(\frac{Q}{E_1} - \frac{m_1}{M} + 1\right)\right.$$

$$\left. + 2\cos\Theta \sqrt{\cos^2\Theta + \frac{M(m_2+M)}{m_1 m_2}\left(\frac{Q}{E_1} - \frac{m_1}{M} + 1\right)}\right] \tag{3}$$

where m_1, m_2 and M are the masses of the proton, the α particle and the recoiling atom (^{12}C), respectively. Q is the energy liberated by the nuclear reaction and equal to 4.964 MeV for the (p,α) reaction. Finally, the α particle exits the sample with an energy E_3, given by

$$E_3 = E_2 - \int_0^x S_\alpha \frac{dx}{\cos\Theta_2}. \tag{4}$$

2.4 Excitation Curve

The excitation curve of a nuclear reaction is the figure of merit for its usefulness as a profiling tool. A high cross section (~10 mb/sr) and a constant yield over a sufficiently large energy range (~50 KeV) are the essential characteristics of a useful reaction. The excitation curve for the (p,α) reaction is determined from both experimental measurements and calculations based on information available in the literature. The errors involved by assuming that $\sigma(E)$ is a constant and equal to σ(1MeV) can be estimated using the obtained excitation curve. Some aspects of sample preparation for the experimental measurements of the excitation curve are discussed at the end of this section.

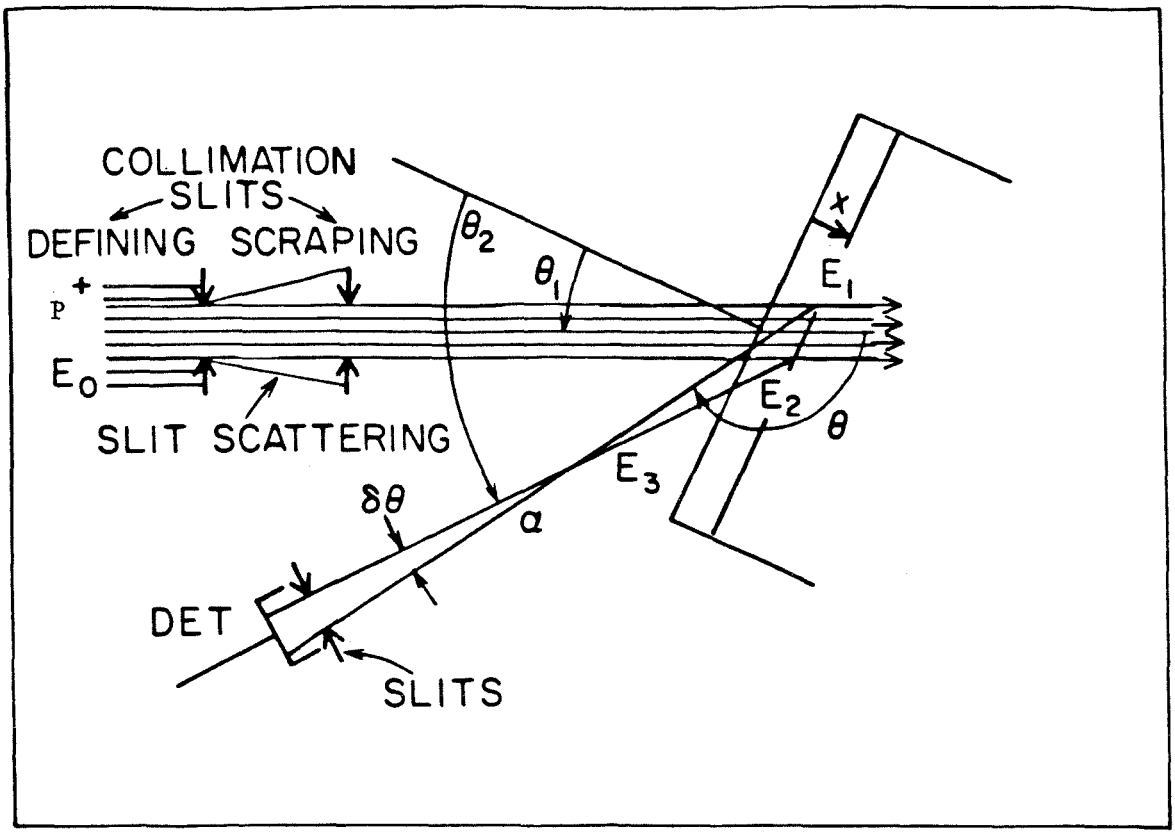

figure 1. The sample geometry used for NRA experiment. The proton beam size is set by the defining slits while the scraping slits remove the particles that scatter from the defining slits. Protons impinge on the sample which is tilted at Θ_1 against normal incidence. The emitted α particle enters the detector mounted at an angle Θ against the incident beam. A small angular divergence $\delta\Theta$ results from the finite width of the proton beam and detector opening. E_1, E_2 are the energy of the proton at incidence and immediately before the reaction. E_3 and E_4 are the energy of the α particle as emitted by the reaction and after exiting the sample.

2.4.1 Calculated and Experimentally Determined Excitation Curve

The cross section $\sigma(E)$ of the (p,α) reaction has been reported by various groups. Hagedorn and Marion[51] measured the angular dependence of $\alpha(E)$ at nine detector angles between 15° and 140°, covering the energy range from 0.9 to 1.3 MeV. Their σ values are normalized to the absolute measurements made by Schardt et al.[52] at E_0 = 1.03 MeV. Since the detector angle used in this study was fixed at Θ = 164°, due to required compatibility with other ongoing

experiments, the excitation curves published by Hagedorn et al. cannot be directly applied here. Hebbard[53] calculated the coefficients for a cosine expansion of $\sigma_\theta(E)$ for the energy range from 0.3 to 1.5 MeV. However, a discrepancy exists in the normalization adopted by Hebbard and Schardt et al.. Hebbard argued that the absolute yield reported by Schardt et al. should be scaled up by a factor of 1.33. The absolute measurement made in this study agrees extremely well with that of Schardt et al. In the following derivation of $\sigma_\theta(E)$ at $\Theta_1 = 164°$, the angular distribution coefficients of Hebbard will be applied but they are renormalized according to the yield given by Schardt et al..

The calculated excitation curve for energies from 0.8 to 1.2 MeV is shown in figure 2. The laboratory angle of 164° has been converted to the center-of-mass angle of 165.8° before entering into the cosine expansion. Experimental verification of this excitation curve is done using a ^{15}N enriched WN^2 calibration sample. The preparation method for the sample is described in section 3.4.3. The WN_2 sample has a thickness of 410Å, which at a 60° tilt, produces a proton energy loss of 5 KeV. The error in measured cross section due to this energy loss is estimated to be at worst 2%. No correction was made to compensate for this small error. Relative yields were obtained by bombarding the calibration sample at energy interval of 0.05 MeV from 0.8 to 1.0 MeV, keeping the charge collection constant in each run. The absolute cross section was measured for $E_0 = 1$ MeV, using the formula

$$\Sigma = \frac{Q\Omega\,\sigma(N^N T)^{cal}}{\cos\Theta_1} \tag{5}$$

where,

Σ = integrated yield,

Q = charge collection in number of particles

Ω = solid angle spanned by the detector

N^N = atomic density of nitrogen in the calibration sample

T = thickness of the calibration sample.

The italic form of N will be used to designate density to distinguish it from the roman N which stands for nitrogen. For the WN_2 sample used, $(N^N T)^{cal}$ has been determined to be 2.04×10^{16} $^{15}N/cm^2$ by RBS, using the Si substrate as the calibration reference. Ω can be measured using the signal of the protons elastically backscattered from W, since the cross section for proton backscattering is well known. An independent measurement of Ω was also performed using the 2 Mev $^4He^+$ yield from a Co film of a known thickness. From these measurements, the solid angle was determined to be $\Omega = (9.02 \pm 0.18) \times 10^{-4}$ sr. The absolute cross section at E_0 =1 MeV was then calculated to be (34.4 ± 0.2) mb/sr which agrees extremely well with the value 34.7 mb/sr obtained from the cosine expansion. By normalizing the other data points according to the experimentally determined yield at 1 MeV, a very good fit to the calculated excitation curve is obtained, as shown in figure 2.

It must be mentioned that the excellent agreement in the cross sections measured in this work and that by Schardt et al. may be fortuitous, since an elaborate effort was not made to determine charge integration errors due to neutralized beam, faulty electron suppression, imperfect detector efficiency, etc.. However, the data analysis performed for the NRA experiments does not depend on the absolute value of the reaction cross section, as will be clear from section 2.5.

2.4.2 Error in Dose Measurement Due to a Nonconstant Cross Section

As shown in figure 2, in the small region near E_0= 1 MeV, the excitation curve is fairly flat, and the yield is more than sufficiently high. In the analytical method to be described in the next section, σ is assumed to be constant and

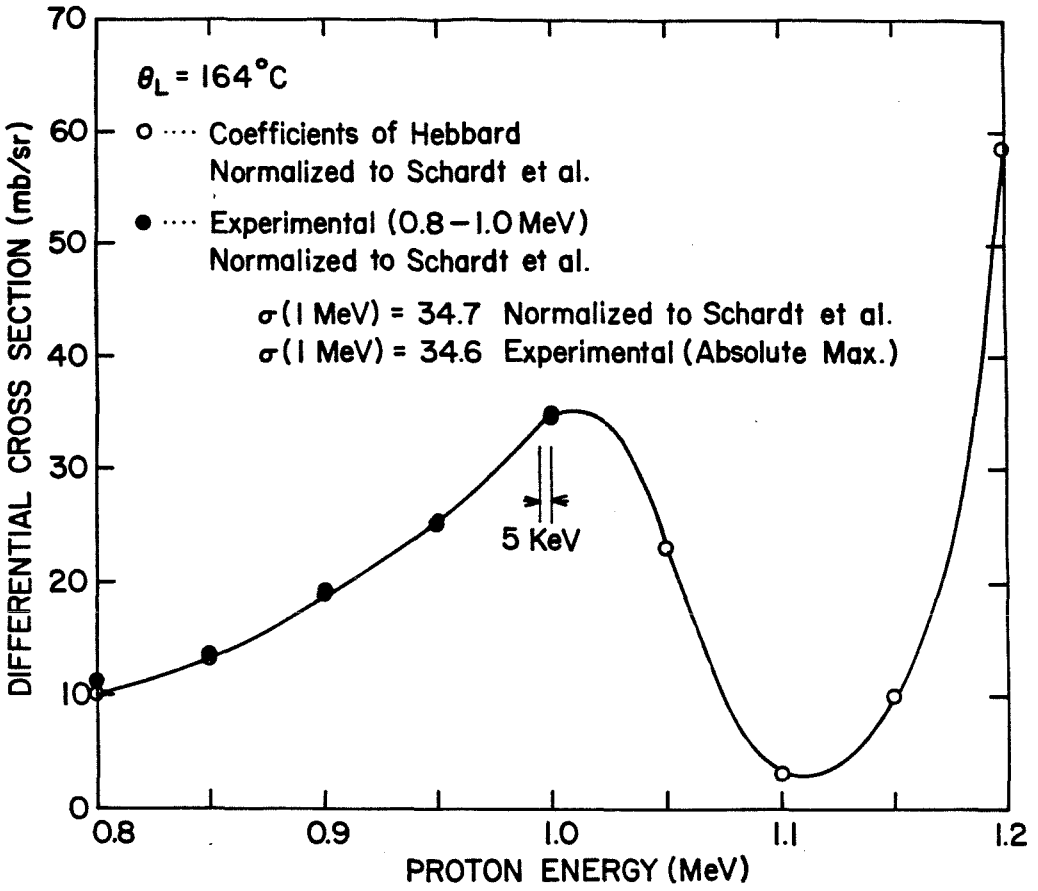

figure 2. The calculated excitation curve is shown as solid line. The coefficients of the cosine expansion are provided by Hebbard, while the normalization is that of Schardt et al. The yields experimentally determined in this study are shown as full circles. An absolute measurement is made for the experimental data point at E_2= 1 MeV.

equal to $\sigma_0 \equiv \sigma(1\ \text{Mev})$, which is the cross section at the sample surface. For samples with a heavy element or large thickness, the proton energy loss during its inward travel will be correspondingly large, producing a significant drop in σ. If the sample contains an uniform level of ^{15}N and has a thickness equivalent to

50 KeV of proton energy loss (eg. 3400 Å Pt), which represents the upper limit in sample thickness used in this study, the error in dose (areal density) measurement is given by the shaded area in figure 3(a) to be ~14%. For implanted samples with a gaussian shaped N profile, the error calculation initially seems more complicated than the case with an uniform N concentration. By taking a linear fit between σ(1 MeV) and σ(0.95 MeV), the drop in σ can be expressed as $\Delta\sigma$ = C ΔE, where

$$C=\frac{\sigma(1\,MeV)-\sigma(0.95\,MeV)}{(1-0.95)\,MeV}=0.17\,mb/sr-KeV.$$

Then, an approximate error can be obtained analytically, as illustrated by figure 3(b).

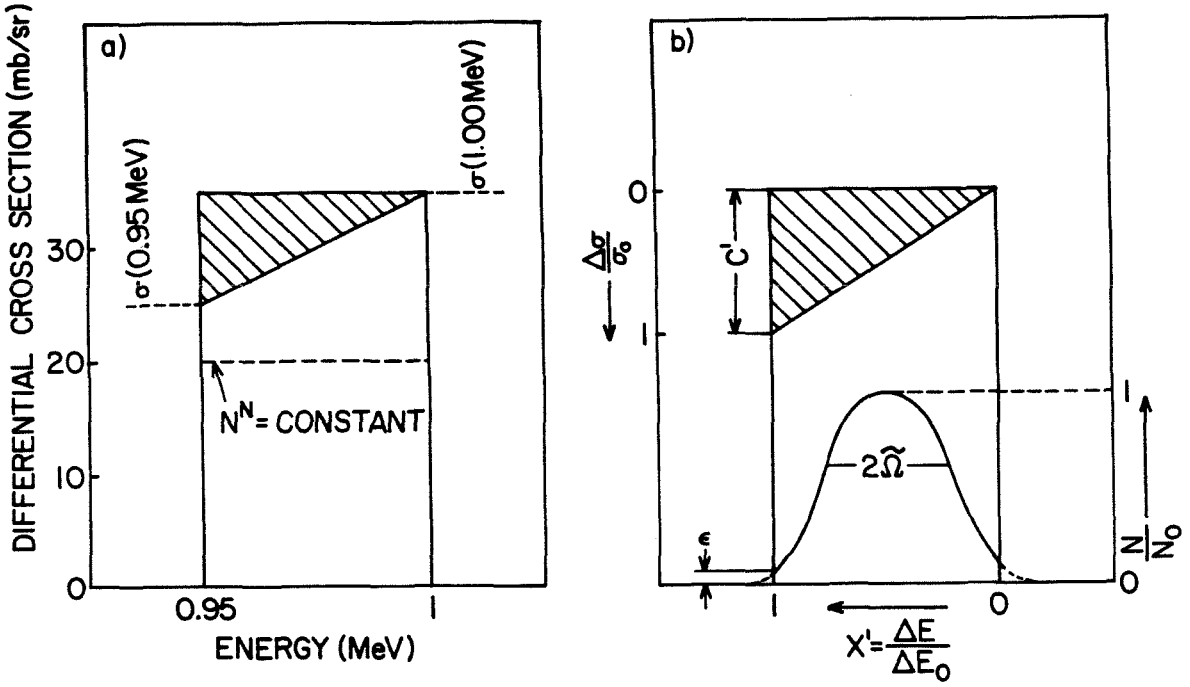

figure 3.(a) Shaded area represents the percentage error in measured N dose due to a nonconstant σ. (b) the tails in the gaussian shaped profile are truncated beyond a small fraction of the peak concentration. Sample depth is normalized to the total film thickness ΔE_0, while the change in cross section, $\Delta\sigma(\Delta E)$ is normalized to the cross section at 1 MeV, σ_0. C' is a function of total film thickness E_0, but is not a function of normalized thickness x.

For most of the implantation performed in this study, it is reasonable to describe the N profile as a modified gaussian with a normalized standard deviation $\tilde{\Omega}$, such that the N content drops to a small fraction of its peak concentration at the two boundaries of the implanted layer. By setting the N concentration outside the layer to be zero, the N profile is given by

$$\frac{N(x)}{N_0} = e^{\frac{-(x'-1/2)^2}{2\tilde{\Omega}^2}} \qquad ,0<x'$$

$$= 0 \qquad ,1<x' \text{ or } x'<0,$$

where $x' = \frac{\Delta E}{\Delta E_0}$ is the sample depth expressed as a fraction of total layer thickness ΔE_0. In normalized notations, the decrease in σ is $\frac{\Delta\sigma}{\sigma_0}=C'x'$. C' is a new constant, but is a function of the layer thickness,

$$C' = C\frac{\Delta E_0}{\sigma_0} = \left[\frac{0.005}{KeV}\right]\Delta E_0$$

the percentage of the rectangle occupied by the "weighted" area of the shaded area is given by

$$Error\,(\%) = \frac{100}{K}\int_0^1 C'x'e^{\frac{-(x'-1/2)^2}{2\tilde{\Omega}^2}}\,dx' \qquad (6)$$

where K is the appropriate normalization constant to set the modified gaussian equal to 1. After solving the integral, the error is expressed as a function of layer thickness,

$$Error\,(\%) = 100\ C' \frac{1}{2} \left[\frac{1}{K} \int_0^1 e^{\frac{-(x'-1/2)^2}{2\tilde{\sigma}^2}} \right] \tag{7}$$

The term in the parentheses is, by the definition of K, equal to 1. Finally,

$$Error\,(\%) = 100\ C \frac{\Delta E_0}{\sigma_0} \tag{7b}$$

Equation (7b) is the same result as for the case of an uniform N concentration. The error correction has been reduced to no more than a calculation of the area of a triangle. The error as a function of layer thickness in KeV is plotted in figure 4. The horizontal axis is also labeled in terms of equivalent sample thickness of various metal films studied in this thesis. A sample tilting angle of $\Theta_1 = 60°$ has been taken into account. Some of the discrepancies between measured and implanted doses oberved during this study are plotted here for comparison.

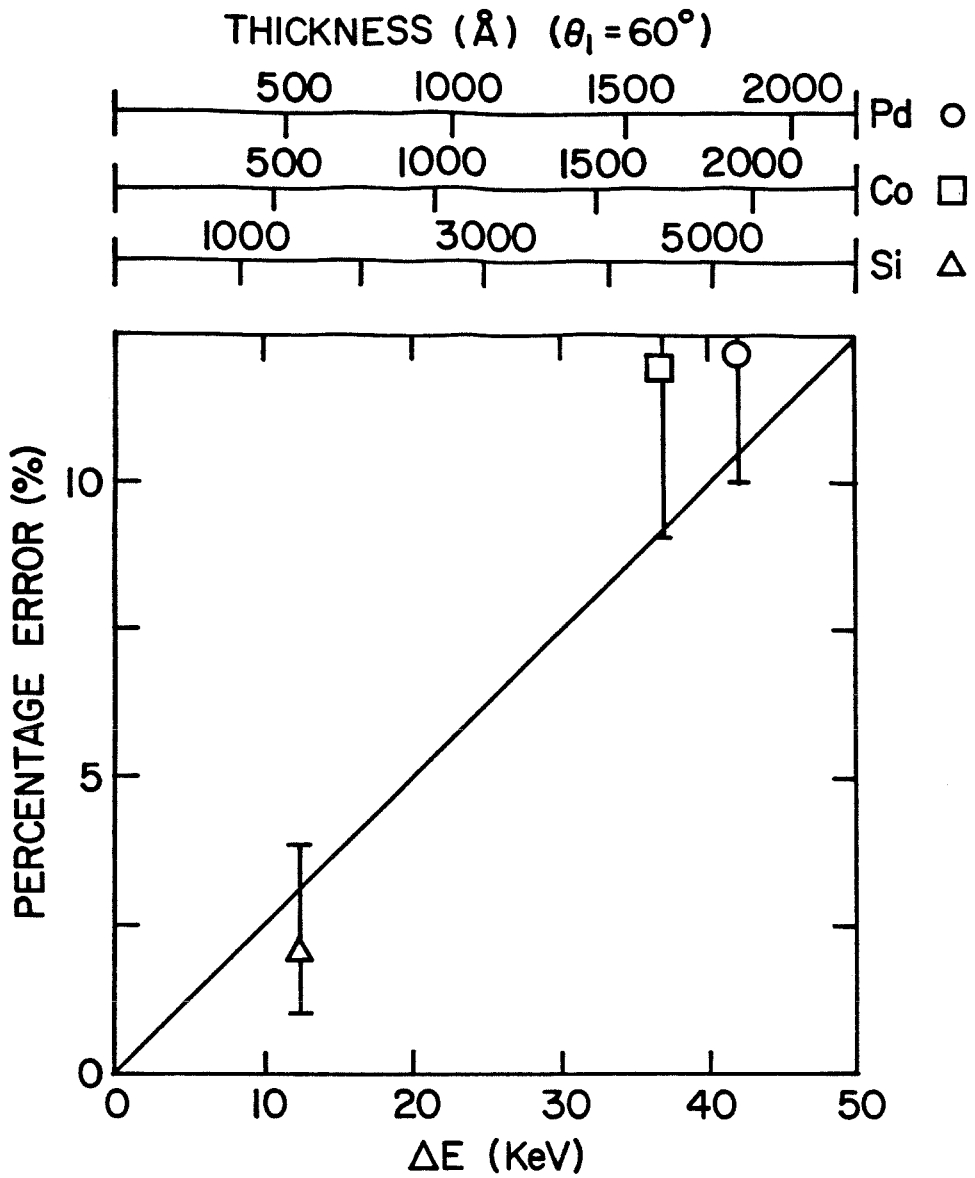

figure 4 The percentage error in total dose measured by NRA due to a nonconstant cross section.

2.4.3 *Preparation of the WN_2 Calibration Sample*

The WN_2 calibration sample was reactively sputter-deposited from a 99.9% W target. The plasma gas was 98.0% ^{15}N enriched nitrogen, throttled to a pressure of 40 μm. Deposition was performed at 800 mW power in 3 min. time on a Si substrate. Integration of the RBS yields for W and ^{15}N signals indicate a

stoichiometric ratio of exactly 1 : 2. The presence of ^{14}N is beyond the detection limit of RBS. For calibration purposes, this sample is assumed to be stoichiometric WN_2 with 100% ^{15}N enrichment. A N areal density of 2.04 × $10^{17}/cm^2$ is determined by using the signal height of the Si substrate as the calibration. The density of WN_2 is tabulated by Goldschmidt[54] as 2.55 × $10^{22}/cm^3$. Thus, the thickness of the WN_2 film is determined to be 410 Å, which is equivalent to 5 KeV of proton energy loss when the sample is tilted at 60° w.r.t. the beam.

2.5 Data Analysis

The data analysis generally involves extracting three types of information from the N profile in a nuclear reaction spectrum. They are the total dose, the depth scale of the profile and the concentration in a local region. The analytical methods are based on tabulated stopping cross section $\varepsilon(E)$ for both a proton and an α particle, and sometimes depend on reliable calibration samples of various types, as described in the following subsections.

2.5.1 Measuring the Total Dose

The total N dose in a sample is derived by comparing its integrated yield to that of a calibration sample. The integrated yield for the calibration sample is given by eqn.(5), written here with extra superscripts,

$$\Sigma^{cal} = \frac{Q^{cal}\,\Omega\,\sigma_0\,(N^N T)^{cal}}{\cos\Theta_1} \qquad (5a)$$

For the WN_2 calibration sample described in section 2.4, the proton energy loss in the sample is small enough so that the approximation $\sigma(E) = \sigma_0$ holds throughout the sample. The superscript on Q is necessary since the dose used in a different run may vary according to the amount of N present. The yield for the experimental sample under study is given by

$$\Sigma^{sample} = Q\Omega \int_{E_0}^{E_1(x_0)} \frac{\sigma(E)N^N dE}{\cos\Theta_1 S_p(E)} \tag{8}$$

or alternatively,

$$\Sigma^{sample} = Q\Omega \int_0^{x_0} \frac{\sigma(E(x))N^N(x)dx}{\cos\Theta_1 S_p(x)} \tag{8a}$$

where the nitrogen concentration is generally a nonconstant function of the sample depth (eg. a gaussian). x_0 denotes the sample thickness. It was shown in 2.4.2 that, for the samples studied in this thesis, the error introduced by setting $\sigma(E) = \sigma_0$ is always smaller than 14%. After making this simplification,

$$\Sigma^{sample} = \frac{Q^{sample}\Omega\,\sigma_0 \int_0^x N^N(x)dx}{\cos\Theta_1} = \frac{Q^{sample}\Omega\,\sigma_0}{\cos\Theta_1} D \tag{5b}$$

where D is the measured total dose.

The ratio of eqns. (5a) and (5b) gives

$$\frac{\Sigma^{cal}}{\Sigma^{sample}} = \frac{Q^{cal}(N^N T)^{cal}}{Q^{sample} D}$$

or,

$$D = \left[\frac{(N^N T)^{cal} Q^{cal}}{\Sigma^{cal}}\right]\left[\frac{\Sigma^{sample}}{Q^{sample}}\right] \tag{9}$$

The term in the first bracket is intrinsic to the calibration sample.

2.5.2 Depth Scaling

The sample depth x can be directly converted to an energy scale with a linear multiplication constant. For sample depth small enough, eqns.(2) and (4) can be linearized using a surface energy approximation,

$$E_1 = E_0 - \frac{S_p}{\cos\Theta_1} x \tag{2a}$$

$$E_3 = E_2 - \frac{S_a}{\cos\Theta_2} x \tag{4a}$$

If the variation of E_2 with E_1 is not large, eqn.(3) can also be simplified to

$$E_2(E_1) = E_2(x=0) - \frac{dE_2}{dE_1}\Big|_{E_0}(E_0 - E_1)$$

eqns. (2a), (4a) and (3a) can be combined to give

$$\Delta E(x) = E_3(x=0) - E_3(x)$$

$$= \left[\frac{dE_2}{dE_1}\Big|_{E_0}\frac{S_p}{\cos\Theta_1} + \frac{S_a}{\cos\Theta_2}\right] x$$

$$= [S]_n\, x \quad . \tag{10}$$

Thus a linear dependence of ΔE on x is obtained by defining an energy loss factor $[S]_n$. By inspection, the S_p term generally contributes ~5% to $[S]_n$. The estimated error in the linearized energy loss calculation for a 5000 Å Pd film is 7.4%.

A frequently used method for presenting NRA data in this thesis is superimposing the nuclear reaction signals of N with the RBS signals of its host matrix. A great advantage of this method is that the conversion factor for the energy losses varies very little with different matrix material. Thus the method can be applied even when the matrix is an alloy with an unidentified composition or when a large composition gradient exists. Another advantage is that, the uncertainty in the sample tilting angle becomes unimportant, as will be explained in the following text.

This method relies on a calibration sample (different from the WN_2 sample previously described), which has very thin layer of ^{15}N enriched WN_2 buried

under a thick Pd layer. A conversion ratio for NRA and RBS energy losses pertaining to the Pd film is first obtained from spectra taken for this calibration sample.

The energy losses for any given sample in RBS and NRA are given by

$$\Delta E_r^i = (NT)^i \, [\varepsilon]_r^i \qquad (11)$$

$$\Delta E_n^i = (NT)^i \, [\varepsilon]_n^i$$

respectively. Where $[\varepsilon]$ is called the stopping cross section and is defined as $[\varepsilon] = \frac{[S]}{N}$. The superscript i identifies the sample as either the calibration sample or the experimental sample under study. The ratio of the two eqns. (11) is

$$\frac{\Delta E_r^i}{\Delta E_n^i} = \frac{[\varepsilon]_r^i}{[\varepsilon]_n^i} \qquad (12)$$

Eqn (12) can be written for both the calibration sample and the experimental sample. By dividing the two, we get

$$\frac{\Delta E_r^{sample}}{\Delta E_n^{sample}} = \left[\frac{\Delta E_r^{cal} [\varepsilon]_n^{cal}}{\Delta E_n^{cal} [\varepsilon]_r^{cal}} \right] \frac{[\varepsilon]_r^{sample}}{[\varepsilon]_n^{sample}}, \qquad (13)$$

which provides the conversion factor needed to plot NRA and RBS spectra together.

Some values of $\frac{[\varepsilon]_r^{sample}}{[\varepsilon]_n^{sample}}$ are tabulated in Table II. It is evident that the energy conversion ratio is very nearly constant for a large variety of materials.

The sample tilting angle enters into the calculation of $[\varepsilon]$. An erroneous reading of tilting angle σ_1 will not lead to a large change in the conversion factor, since the angle enters into both $[\varepsilon]_r$ and $[\varepsilon]_n$, and the error is largely compensated by taking the ratio of these two factors.

TABLE II

ratio of RBS and NRA stopping cross section for various sample matrices.

sample matrix	$\frac{[\varepsilon]_r}{[\varepsilon]_n}$
Si	.62
Pd	.58
Pd_2Si	.59
Co	.56
Co_2Si	.58
CoSi	.59
Mo	.62
$MoSi_2$	.64

2.5.3 Nitrogen Concentration

Nitrogen concentration can be determined from the height of the nuclear reaction spectrum, by the equation,

$$H = \frac{Q\Omega\,\sigma N^N \Delta E}{N[\varepsilon]_n} \tag{14}$$

Where N and $[\varepsilon]_n$ are the atomic density and stopping cross section, respectively, of the sample matrix, which contains nitrogen concentration N^N. ΔE is the energy per channel in the NRA spectrum. Its value can be determined by three data points: (1) surface energy of nitrogen, (2) energy of the WN_2 burried layer under a Pd film, (3) the energy of proton backscattered from a known sample.

In practice, errors may be contained in the values of Q, Θ_1 and ΔE, unless they are remeasured for each experimental run. therefore, concentration can be more accurately measured with the help of a calibration sample, which has a constant nitrogen concentration and whose thickness is above the depth resolution of the NRA set up. In this method, N^N is found by the equation

$$\left[\frac{N^N}{N}\right]^{sample} = \left[\frac{N^N}{N}\right]^{cal}\left[\frac{Q}{H[\varepsilon]_n}\right]^{cal}\left[\frac{H[\varepsilon]_n}{Q}\right]^{sample} \tag{15}$$

When the sample matrix is elemental, the nitrogen concentration expressed in atomic per cent is given by

$$N\ at\% = 100 \times \frac{N^N}{N}$$

In case of a compound matrix, it becomes

$$N\ at\% = 100 \times \frac{N^N}{mN}$$

where m is the number of atoms in the compound formula (eg. m=3 in $MoSi_2$)

2.6 Resolution and Sensitivity

The basic quality of a profiling technique can be evaluated by its depth resolution and detection sensitivity. Therefore this last section is devoted to a discussion of these two parameters.

2.6.1 Resolution

The resolution of the nuclear reaction technique is limited by a few broadening effects which degrade the energy definition of the signal. Assuming a gaussian distribution for those effects, their standard deviation becomes additive. The standard deviation of the system energy resolution is given by[55],

$$\delta E^2 = \delta E_b^2 + \delta E_d^2 + \delta E_s^2 + \delta E_g^2 \qquad (16)$$

where the terms on the right are

δE_b = energy spread of the beam, only a few Kev and can be neglected,

δE_d = detector resolution, ~30 KeV,

δE_s = straggling,

δE_g = geometrical effect.

The straggling effect has been discussed by several authors based on Bohr's

theory[57,5],

$$\delta E_s^2 = 4\pi (Z_1 e^2)^2 N Z_2 x \tag{17}$$

where Z_1 is the atomic number of the energetic ion (i.e. proton and α particle), N and Z_2 are the atomic density and atomic number of the sample matrix, and x is the distance in the sample traversed by the ion.

The geometrical effect is the result of the angular spread due to a finite beam width. δE_g can be derived by differentiation of eqn.(3), and neglecting the second order term[55],

$$\delta E_g = \left[-A \sin\Theta + x S_\alpha \frac{\sin\Theta_2}{\cos^2\Theta_2} \right] \delta\Theta,$$

where,

$$A \approx 2E_0 \sqrt{\frac{M m_1 m_2}{(M+m_2)^3} \left[\frac{Q}{E_0} - \frac{m_1}{M} + 1 \right]} \tag{18}$$

$\delta\Theta$ is taken to be 2° in this experimental set up.

The calculated depth resolution for a Pt film as a function of film thickness, is shown in figure 5. For a Pt film thickness under 3000 Å, the system depth resolution is better than 430 Å.

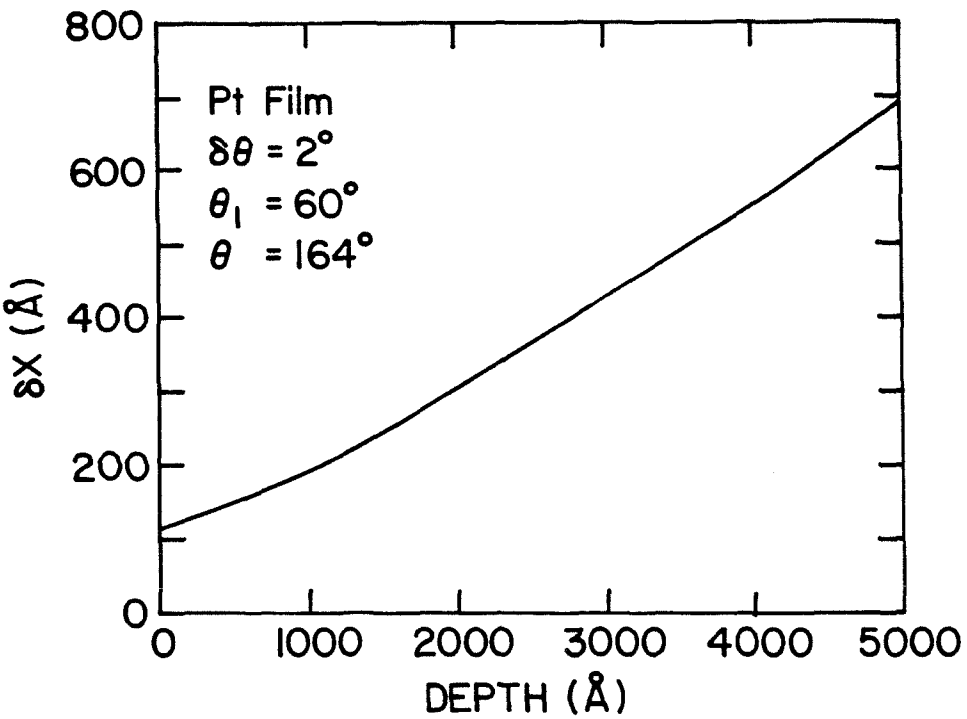

figure 5. Resolution vs. sample thickness for a Pt films.

2.6.2 Sensitivity

The energy of the emitted α particle (3.963 MeV) is approximately 4 times the incident proton energy (1 MeV), so that it is the third pileup from backscattered signals that can interfere with nuclear reaction signals. The magnitude of pileup signals drops by a factor of ~60 for each higher order[58], at a current of 100 nA. Therefore, pileup interference is generally negligible for the (p,α) reaction. The sensitivity of this technique is then only set by the practical limits of charge collection time. Good statistics (~10%) requires about running time of 5 hr per sample; a realistic sensitivity limit can be set at 0.05 at%, which is

comparable to the AES.

CHAPTER 3 THE EVOLUTION OF NITROGEN IMPURITIES IN METAL-SILICON BINARY COUPLES AND THEIR EFFECTS ON SILICIDE FORMATION.

3.1 Introduction

The sample configurations used generally fall into the two forms shown in figure 1. Nitrogen is implanted into the top layer, whether it is the metal or the silicon.

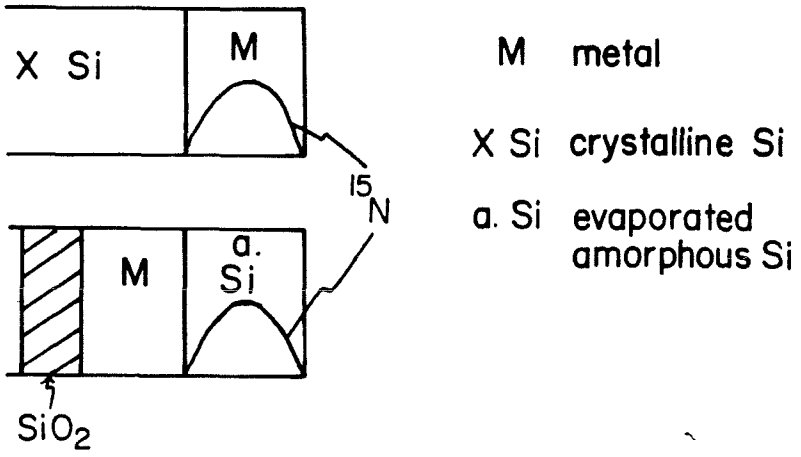

figure 1. The two sample configurations generally used in this study.

When a refractory metal film is on top, a Si cap ~200 Å is deposited to prevent indiffusion of oxygen contaminants after removing from the vacuum deposition system. The Ni and Pt experiments had a slight variation in sample configuration and will be explained in the corresponding subsections.

The various nitrogen and silicide properties elucidated by the experimental capabilities of this study are :(1) N mobility in its initial host lattice, at the silicide forming temperature appropriate for each metal. A high mobility can be correlated to a host material which either does not form nitrides or forms nitrides but has a large solubility for N. The range of N mobilities varies in different host lattices, from extremely mobile (Ni, Co), mobile but slow (Mo), to

immobile (Si). (2) N segregation effects. After silicide reaction, N is either completely incorporated into the silicide (Ni/Si+N), partially rejected from the silicide (Ta+N/Si), or completely left out of the silicide (Pt+N/Si). Each outcome is explainable in terms of the moving species responsible for the formation of that silicide phase. (3) Piling up of N in its initial host lattice, which occurs whenever it is not completely incorporated into the growing silicide layer. This pile up inevitably retards the silicide growth rate (Ta+N/Si, Pt+N/Si) and in certain cases will completely suppress further silicide growth (Co/Si+N). When N is completely incorporated into the silicide, the silicide growth rate is either unaltered (Ni/Si+N, Pt/Si+N) or slowed down (Mo+N/Si). (4) Any change in the first phase silicide formed. It will be shown later that no such change was ever observed in this study.

Since much of the data interpretation is linked to identification of the moving species during silicide growth, the presentation of experimental results will be categorized accordingly. For the near noble metals such as Ni, Co and Pt, it is known that metal is the moving species for the first phase silicide, which is generally metal rich. Another common feature of these metals is that their second phase silicide, which is generally a monosilicide, forms at about the same temperature as the first phase, with Si as the moving species in CoSi and metal in NiSi and PtSi[59]. The N redistribution which results from the second phase formation is discussed in detail for the case of Co. The near noble metal silicides are presented in section 3.2.

The refractory metals (Ta, Mo) form a disilicide phase at relatively high temperature (500-700°C), and the moving species is always Si. Those silicides fall in the second group which is discussed in section 3.3.

The moving species in Pd_2Si formation is a subject of prolonged debate. Therefore, a part of this thesis is devoted towards clarification of this issue,

before N impurity effects in Pd_2Si formation is studied. It was determined that Si is the only moving species under "normal" conditions. A "normal" condition is considered to be in effect when the silicide growth rate is equal to that for impurity-free Pd and Si. However, Pd motion is activated whenever Si diffusion becomes obstructed as was found when a Ti or W marker was inserted between Pd and Si, or N was implanted into Si. Palladium silicide, thus exists in a category by itself and is discussed in section 3.4.

3.2 Silicides in Which Metal Is The Moving Species

The moving species studies are summarized by Nicolet and Lau[59]. Most of the near noble metals form their first phase silicide with metal as the moving species. Another feature common to these metal silicides is a low formation temperature (200-400°C) compared to that for the refractory metal silicides (500-700°C)[59]. This implies that N impurity effects in these silicides are likely to be more pronounced. The reasoning can be generalized by modelling impurities as a kinetic barrier to chemical reactions or mass transport processes, and realizing that such barriers can often be compensated by thermal agitations. The same concept is put to practice when diffusion barriers are tested at high temperatures[60], and when an Al-Si structure is sintered to overcome the interfacial oxide and form an intimate contact[3].

3.2.1 Platinum (see reference I)

Pt_2Si formed from a nitrogen implanted Pt film was investigated at an annealing temperature of 282°C. Nitrogen in the dose range from 0.5 to 2 × $10^{16}/cm^2$ has an visible retardation effect on Pt_2Si growth rate. Nitrogen accumulates at the Pt side of the Pt/Pt_2Si interface, which is consistent with the Pt_2Si growth mechanism as depicted in figure 2. In order for the growth of the Pt_2Si layer to continue, Pt must diffuse past the already grown layer. The

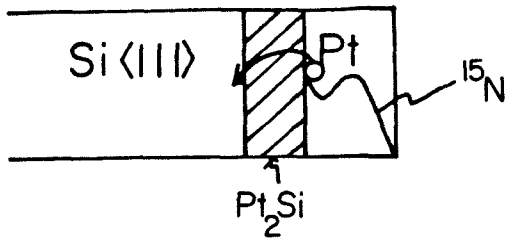

figure 2. Platinum silicide growth by Pt diffusion, leaving nitrogen behind to accumulate at the Pt/Pt_2Si interface.

implanted N apparently does not diffuse through Pt_2Si alongside the Pt traffic. The accumulation near the Pt/Pt_2Si interface is due to the N left behind by Pt. The nitrogen profile does not vary in shape in parts of the Pt film that are far from the silicide region, indicating that the diffusivity of N in Pt is neglible. The total amount of N is conserved after long annealing.

The interfacial N accumulation severely suppresses Pt_2Si growth rate. To check its effectiveness as a Pt diffusion barrier, a sample was implanted with 3.5 $\times 10^{16}/cm^2$ of N, and an annealing sequence of 286°C for 50 min., plus 290°C for 150 min., plus 300°C for 180 min. was applied. We found that the silicide reaction does not come to a stop completely even after this prolonged annealing, although the growth rate becomes extremely slow as compared to the published growth rates at this temperature range.

In the second part of this study, N was implanted into an <111> Si substrate. The substrate was then annealed at 550°C for 2800 min. to remove the implantation damage. The Si surface was plasma oxidized and etched in HF, followed by a standard cleaning procedure described in reference I. Finally, a Pt film was evaporated on the N-implanted Si. The sample configuration is shown in figure 3a. After annealing, it is found that N is incorporated into the silicide

layer at the same rate as the Si atoms of its host lattice. This result can be explained by the diffusion of Pt and by the strong bonds ($\Delta H_f^{Si_3N_4}$=−179.3KCal/g mole)[25] between N and Si. The strong bonds will restrain N to remain fixed with respect to the Si lattice surrounding it. When Pt infiltrates the Si lattice and transforms it into the Pt_2Si lattice, N which keeps a constant concentration ratio with respect to the Si sublattice, will become diluted in atomic concentration (number of N per 3×100 Pt_2Si molecules) by a factor of 3 (see figure 3b). This dilution is quantitively verified by the N concentration profile obtained with NRA.

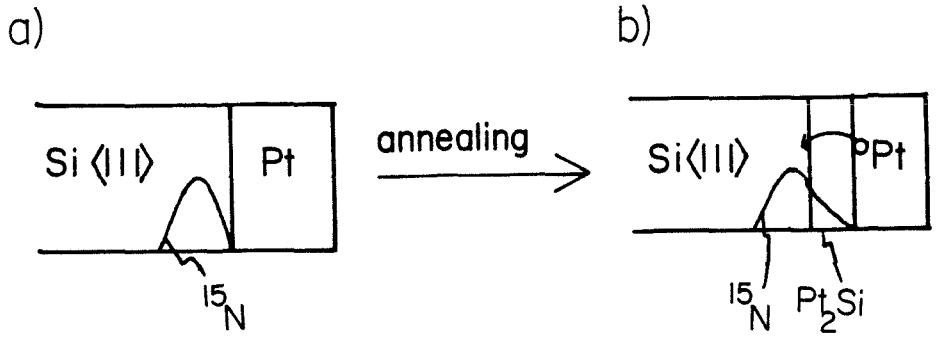

figure 3a) Sample configuration with N implanted into a Si substrate prior to deposition of a Pt film. b) Pt penetrates the Si lattice to form Pt_2Si. Nitrogen is incorporated into the silicide but remains fixed to the Si sublattice during the process.

3.2.2 Nickel (see reference I)

When N is implanted into Ni, a fast N diffusion is observed at 350°C. RBS shows that the diffusion process occurs in a time too short for a significant amount of silicide reaction to occur. Nitrogen forms a thin layer (≤ 300 Å) at the Ni side of the Ni/Si interface, with a partial loss in quantity due to outdiffusion. At a low implantation dose ($0.5 \times 10^{16}/cm^2$), Ni_2Si grows uninhibitedly in spite of the N accumulation. Since Ni is the moving species, it apparently diffuses past the N layer, through the Ni_2Si layer and continues silicide growth at

the Si/Ni_2Si interface, so that the N layer finally emerges at the top surface of the sample, when Ni becomes exhausted.

When a high implantation dose ($\geq 10^{16}/cm^2$) is used, the interfacial N layer has a higher areal density, and becomes strong enough to block Ni diffusion, so that Ni_2Si growth is suppressed.

The fast diffusion of N in Ni is consistent with the fact that N and Ni have very weak bonds. The interfacial layer of N most likely gets its strength from Si-N bonds. The molecular form N takes is probably close to Si_3N_4. This requires the capability of XPS or AES to clarify.

For studying implanted N in Si, the same sample preparation as the Pt case was used. The subsequent Ni_2Si formation also produced the same results as Pt; namely, Ni penetrates into Si during Ni_2Si formation and dilutes N concentration in the same proportion as the Si lattice atoms. The close analogy is expected, considering the parallel nature of the moving species involved and the same bonding between N and the Si host lattice.

3.2.3 Cobalt (see reference II)

Nitrogen implanted into Co shows the same fast diffusion previously observed in Ni. A thin nitride layer forms at the Co/Co_2Si interface. For low implantation dose ($0.5 \times 10^{16}/cm^2$), the full implanted amount is retained in this interfacial layer and no change in Co_2Si or CoSi growth rate can be seen as compared to an unimplanted reference sample. Simultaneous formation of Co_2Si and CoSi prior to the complete consumption of Co is consistent with previously reported results. After a finite width of both silicide phases are reached, a second N peak can be resolved, but is much smaller in size than the one at the Co/Co_2Si interface. This smaller peak is located at the CoSi side of the Si/CoSi interface, and remains at the same position relative to this interface

when the CoSi layer thickens. By using the smaller peak as an inert marker, it can be concluded that Si is the dominant moving species in CoSi, in agreement with previous studies.

For higher implantation doses (1 and $2\times10^{19}/cm^2$), the interfacial N layer always amounts to an areal density of $0.86 \times 10^{16}/cm^2$, losing the rest of N by outdiffusion. This areal density value is reproducible to within 10%, and apparently represents a saturation value of areal coverage N can have on a smooth <111> Si surface. At this areal density, the interfacial layer acts as a barrier, which suppresses Co silicide reaction at temperatures lower that 550°C. After annealing at 550°C for 30 min., a nonuniform reaction through local breakdowns of the barrier occurs. A detailed NRA study shows that at the onset of barrier failure, the interfacial N layer is reduced in areal density to a value of $0.57 \times 10^{16}/cm^2$. Evidently, at high annealing temperatures (~550°C), Si-N bonds are not strong enough against the thermal agitation. Nitrogen can break away and outdiffuse from the sample.

When N is implanted into Si, a retardation of Co_2Si and CoSi growth rates is observed for all three implanted doses (0.5, 1 and $2 \times 10^{16}/cm^2$). For the highest dose, the thickness of the CoSi layer is restricted below the resolution limit of RBS (~250 Å), even after 270 min. annealing at 415°C. However, the evolution of the N profile in this case reassures that a thin layer of CoSi does exist. The N profile peaks up slightly at the Si/silicide interface, and its position shows a small shift toward the unreacted Si. Since Co is the moving species in Co_2Si, Co will penetrate into Si and dilutes the N peak if only the metal rich phase is growing next to Si. The only possible explanation for the piling up of N is for Si to be moving through the Si/Silicide interface and leaving N behind. Knowing that Si is the moving species through CoSi, the existence of this silicide phase next to Si is thus substantiated.

Electrical measurements were made on the contact structure. A contact resistivity of ~1.42 $\mu\Omega\,cm^2$ was measured by applying the transmission line model to a test pattern with phosphorous diffused n^+ channels. The measured value is in good agreement with that predicted by tunneling theory[61] for the Schottky barrier height of Co silicide on n-type Si (~0.67 eV) and the n^+ channel sheet resistance of 35 Ω / ■ . This low contact resistivity qualifies for the requirement of VLSI applications. Since only a negligible amount of substrate Si has reacted with Co before N forms a barrier, the Co/nitrogen structure may be an alternative scheme for making shallow contacts.

3.3 Silicides in Which Si Is The Moving Species

Silicon has been identified as the moving species for all of the refractory metal silicides[59]. Those silicides generally form at a high temperature (500-700°C) and are often plagued by oxygen contamination[7]. It is found that by encapsulating the evaporated metal film with a thin layer of Si, O contamination is limited to only the amount incorporated during deposition. The incorporated O is profiled by $^{16}O(d,\alpha)^{14}N$ nuclear reaction. In the Ta and Mo samples studied, oxygen concentration rises monotonically with film thickness, starting at ~0.5 at% near the metal/silicide interface, and increasing to over 25 at% at the top surface of the metal film. The large O concentration gradient does not have an apparent effect on the growth rate or pattern ($x \propto t$ for $TaSi_2$, $x \propto \sqrt{t}$ for $MoSi_2$). The effect of implanted N is therefore easily discernable by comparing the kinetics of implanted samples with an unimplanted reference.

3.3.2 Tantalum (see reference III)

Implanted nitrogen in Ta is primarily segregated by the growing $TaSi_2$ layer. Only a small portion is incorporated into the silicide. Due to the segregation effect, N concentration accumulates in the remaining Ta. The silicide growth rate is gradually slowed down with increasing silicide thickness, coincident with the build up of N concentration in Ta. After 6 hrs. annealing at 675°C, a narrow (~800 Å) Ta rich region remains near the surface corresponding to the position of a large surface N peak. Presumably the excess Ta is stabilized by the N peak from completely reacting into $TaSi_2$. The total quantity of N remains conserved; N is very likely refrained from diffusion out by the Si cap. The Si cap itself reacts with Ta at a much slower rate than the Si substrate. It can be conjectured that if the Si cap can be eliminated without introducing more O contamination, $TaSi_2$ formation becomes a self-cleaning process in which N is mostly pushed out of the sample during the growth of the $TaSi_2$ layer.

The N segregation effect can be understood in terms of the large solubility of N in Ta (1.8 at% at 500°C)[63]. The solubility of N in $TaSi_2$ is most likely small but finite, as evidenced by the small amount (~2at%) incorporated into the silicide. When N accumulates to a high enough concentration at the top region of the Ta film, Ta nitride is expected to form. This may explain the stability of the Ta rich region against a complete transformation into stoichiometric $TaSi_2$. Incorporated oxygen is also seen to primarily segregate out of the silicide, and accumulate in this Ta rich region[III]. The presence of O may enhance effects of N in strengthening the chemical inertness of this region.

When N is implanted into Si at doses of 0.5, 1 or $2 \times 10^{16}/cm^2$, $TaSi_2$ formation virtually comes to a halt at the rising edge of the N profile, without visibly altering the N signal in the NRA spectrum. The barrier effect of the implanted N can be understood in view of the strong bonding between Si and N, and the fact

that Si is the moving species in $TaSi_2$. A surprising aspect of the results is that the interface between Si and $TaSi_2$ is much sharper than the rising edge of the N profile. Apparently there is a strong tendency for Si and $TaSi_2$ to adjoin with a abrupt boundary, even though the barrier which inhibits the reacting species increases in strength gradually.

3.3.2 Molybdenum (see reference IV)

The effect of N implanted into Mo on $MoSi_2$ growth rate is pronouncedly dependent on the implanted dose. The unimplanted Mo sample showed a growth with a parabolic time dependence and an incubation time of 15 min. at an annealing temperature of 510°C. At an implanted dose of $0.5 \times 10^{16}/cm^2$, no change in silicide growth rate or incubation time can be seen. When the implanted dose is increased to $1 \times 10^{16}/cm^2$, the parabolic growth constant ($K=\frac{x^2}{t}$) is decreased by a factor of 4, and the incubation time is increased to 50 min. At an even higher dose of $2 \times 10^{16}/cm^2$, no signs of $MoSi_2$ can be seen until after 120 min. annealing. However, when the annealing temperature is raised to 550°C, silicide reaction is completed in less than 30min., leaving only a Mo rich region near the surface.

The N profile after 120 min. annealing at 510°C shows the existence of a sharp N peak near the Mo/Si cap interface. Nitrogen is otherwise uniformly distributed in the Mo film with a concentration of ~1.5 at%. By forcing the silicide formation to proceed at 550°C, the uniformly distributed N is completely incorporated by the growing silicide with no segregation. The N to Mo ratio is preserved before and after Mo is transformed into $MoSi_2$. Finally a N peak remains in the near surface Mo rich region. The excess Mo is presumably stabilized by this N peak, analogous to the Ta case.

Oxygen profiling by $^{16}O(d,\alpha)^{14}N$ shows that the incorporated O has an initial profile very much like the one in deposited Ta film. Oxygen is apparently able to redistribute in the Mo film during 510°C annealing. In the high dose implanted sample ($2\times10^{16}/cm^2$) which reacted only insignificantly after 120 min. annealing, there is a net O transport towards the sample surface, resulting in a broad O peak next to the Mo/Si cap interface. In the low dose ($0.5\times10^{16}/cm^2$) implanted sample, which almost reacted to completion after 180 min., O is fairly uniformly incorporated into the silicide, except for a large near surface peak in the Mo rich region, coincident in position with the N peak.

3.4 Silicide in Which The Moving Species Is Undetermined: Pd_2Si

The first silicide phase of Pd, Pd_2Si, has continued to be an intriguing subject to study, not only because of its practical usefulness as a contact material, but also because of the many inconsistent results reported in the past decade, which have obscured the identity of its moving species. The perplexities involved can be sampled from the listing in table I.

Since a meaningful interpretation of results from the impurity experiments rests upon the knowledge of the moving species, a carefully designed inert marker experiment was first conducted.

3.4.3 *Marker Study of Pd_2Si Formation* (see reference V)

Silicon of three types of crystallinity : amorphous, <100> and <111> single crystalline, are used to form Pd_2Si with an evaporated Pd films at various temperatures from 250 to 350°C. A thin (~6 Å) W marker is used to study amorphous Si samples, while thin (~10 Å) Ti markers are used for crystalline Si samples of the two different orientations. The markers are initially located between Pd and Si. Care is taken to avoid possible interfacial drag problems by depositing a very thin (~20Å) layer of Si between the marker and Pd, and a thin layer of Pd

TABLE I

Results of previous studies.

AUTHORS	REF.	MARKER	INITIAL LOCATION OF MARKER	YEAR	Si TYPE	IDENTI-FICATION
W.K.Chu et al.	64	Argon	in Si	1975		Both
R.Pretorius et al.	13	^{31}Si	Top layer of Si	1978	<100>	Both
N.Cheung et al.	66	Kirkendall voids	at Pd/Pd_2Si & Pd_2Si/Si interfaces	1979	<111> <100> a. Si	Both Pd Pd
H.Föll et al.	67	Interfacial oxide	at Pd/Si interface	1981	<111>	Both
D.M.Scott et al.	68	oxygen	in Pd	1983	<100>	Si
C.D.Lien et al.	69	Epitaxial structure	Pd_2Si	1984	<111>	Pd
C.D.Lien et al.	16	Interfacial oxide	at Pd_2Si interface	1984	<111>	no i.i.[a]: Both w. i.i.[b]: Si
K.T.Ho et al.	This work	W,Ti	in Pd_2Si	1984	<111> <100> a.Si	Si(Pd)

between the marker and Si, such that the marker will be incorporated in a silicide layer as soon as annealing begins. From the slopes of marker shift vs. thickness plot, it is determined that Si is the only moving species. However, there is always an initial growth stage (~500-1000 Å)in which no marker shift is observed within the resolution of RBS. A corresponding phenomenon oberved in the growth rate plot indicates that there is an incubation time in all marked samples, whereas a reference sample without a marker starts its silicide growth as soon as annealing starts. The growth rates of marked samples are otherwise identical to the unmarked sample annealed at the same temperature.

It is postulated that in the initial stage of silicide formation, Pd must move to penetrate and break up the marker layer (W or Ti) which apparently acts as a diffusion barrier for Si. During this time an inhibition or retardation in growth rate will take place, as compared to the reference sample. To test this postulate, the same experiment is repeated with a thicker (~20 Å) Ti layer as a marker. It is found that the marker shift initially shows a predominant Pd motion,

simultaneous with an initial Pd_2Si growth pattern which is erratic and slow. When the silicide layer becomes thick (~1500 Å), the growth constant ($K=\frac{x^2}{t}$) approaches that of the reference sample, while the slope in the marker shift vs. silicide thickness plot changes sign and indicates a predominant Si motion.

From these unusual inert marker results, we construct a dual-moving-species model, in which Si is the dominant moving species under a "normal" condition. A "normal" condition is experimentally demonstrated to be in effect, when the Pd_2Si growth rate matches that of an impurity-free reference sample. However, if the Si flux is obstructed by certain impurities present in the system (e.g., Ti, W, SiO_2), Pd motion is activated to penetrate the impurity concentrated region. The regime in which Pd diffusion dominates is experimentally monitorable by a slowdown in Pd_2Si growth rate. A predominant Si diffusion resumes when the impurity concentration is sufficiently diluted in Pd_2Si to allow an unrestrained Si flow.

This dual-moving-species model is fruitfully applied in the following impurity study.

3.4.2 Palladium (see reference VI)

When N is implanted into Pd, it slows down the Pd_2Si growth rate by only a small amount. Furthermore, the amount of slowing down is independent of the implantation dose used (0.5, 1 and $2\times10^{16}/cm^2$). During Pd_2Si growth, a strong segregation effect of N is apparent. Nitrogen is primarily pushed forward by the advancing Pd/Pd_2Si interface. Only a small amount is incorporated into the silicide, equivalent to 0.7 at%, uniformly across the silicide layer. At the completion of Pd consumption, the segregated portion of N is pushed out of the sample through the top surface, resulting in 36% loss in total quantity. Since the

growth rate of N implanted sample does not deviate from the reference sample by any significant amount, the model described in the previous section indicates that Si is the dominant moving species in spite of the nitrogen's presence. The movement of N is then a "snow-plowing" effect which may be due to different N solubilities in Pd and Pd_2Si.

When N is implanted into Si, the retardation in silicide growth rate at 230°C is very severe and varies pronouncedly with implanted dose. In the high dose ($2\times10^{16}/cm^2$) sample, the reaction rate is virtually reduced to zero when the Si/Silicide interface reaches the N concentrated region of Si. The reaction can be, however, forced to completion by raising the annealing temperature to 350°C and extending the annealing time for ~10 hrs. longer. After this annealing stage, RBS shows that both Pd and Si are completely consumed, except for a small bump in the Si signal at a position corresponding to where N is finally situated. In the Pd signal, a small dip is found at an equivalent position. Calculations support the assumption that this perturbation in Pd_2Si stoichiometry is due to competition for Si atoms by nitride formation in a ratio close to Si_3N_4. The N signal, unexpectedly, remains in approximately the same position in NRA energy space, before and after annealing, even though its host lattice has had a complete transformation in composition. The stationary behavior of the N peak can only be explained by having an equivalent amount of Pd and Si traffic across it. By an equivalent amount it is meant that the quantity of each produces the same energy loss. This result may be a direct observation of a realization of the dual-moving-species model. It can be conjectured that, the implanted N forms a barrier to Si diffusion. During the high temperature (350°C) annealing stage, Pd diffusion becomes activated, and both elements contribute to the mass flow during the subsequent silicide growth.

CHAPTER 4 SUMMARY OF ADDITIONAL WORK

Three additional projects were completed within the time frame in which this thesis work was carried out. The first one investigates the influence of N impurities on $TiSi_2$ formation, and falls within the integral part of the thesis. However, since the manuscript for this project is not currently in its final publication form, it is briefly mentioned here instead of discussed in chapter 3. Two other studies are already published but do not correlate with the main topic covered by chapter 3. These two are described here briefly with references to the corresponding publications.

4.1 Nitrogen Impurity Effects on Titanium Silicide Formation

Thermally grown $TiSi_2$ layers do not form sharp boundaries with adjoining Ti and Si. It is therefore not possible to make a simple growth rate comparison between N implanted and as deposited samples. Therefore, only a visual inspection of silicide growth and N motion can be made. This is carried out by superimposing RBS and NRA spectra. Here also, a Si encapsulation (~300 Å) is evaporated on top of the Ti film to protect it against post deposition oxygen contamination.

When N is implanted into Ti, a predominant "snow-plow" effect of N by the growing $TiSi_2$ is observed, very similiar to the Ta case. Only a small fraction is incorporated by the silicide but this amount increases in concentration with silicide thickness. Segregated N accumulates in the remaining Ti, gaining in peak concentration as Ti becomes continuously consumed. One interesting feature is that, although the $Ti/TiSi_2$ interface is very unsharp and ill-defined, the segregated N peak still drops off very abruptly at the vicinity of that interface. Finally, after a total of 890 min. annealing at 575°C, $TiSi_2$ formation terminates leaving a surface region that is slightly Ti rich. The excess Ti is most likely stabilized by

the segregated N which finally resides in this surface region after being pushed by the growing silicide.

When N is implanted into Si, $TiSi_2$ formation is inhibited when the $Si/TiSi_2$ interface reaches near the peak of the N profile. The edge of the N profile on the side of the silicide reaction is sharpened noticeably exhibiting a "pushing" action by the $Si/TiSi_2$ interface. Apparently, Si diffusion is not completely choked off until after a slight N redistribution, leading to a more compacted N barrier at the $Si/TiSi_2$ interface.

4.2 Thermal Oxidation of Reactively Sputtered Titanium and Hafnium Nitride (see reference VII)

Titanium nitride and hafnium nitride have been extensively studied for their applicability as diffusion barriers for solar cell and IC contacts. One of the relevant properties for evaluating potential applications is their behavior in oxidation ambients.

The thermal oxidation characteristics of TiN is studied in both dry and wet oxidation ambients at 425°C-600°C. The oxide thickness follows a parabolic time dependence in both cases. The activation energies associated with the parabolic rate constants are 2.1 eV for the dry oxidation and 1.5 eV for the wet oxidation. The oxide phase which formed is shown by x-ray diffraction to be rutile TiO_2.

Dry oxidation of HfN also yields an oxide growth with a parabolic time dependence. The activation energy is found to be 2.5 eV and the oxide phase obtained is monoclinic HfO_2. The wet oxidation behavior is more complex, with an initial slow oxidation followed by a rapid increase after a certain delay time. The oxide film has a rough surface morphology with severe pitting. The change in surface morphology may be attributed to an impeded outdiffusion of nitrogen which breaks up the rather brittle HfO_2. The broad grain boundary and pores

which are created due to the breaking up gives ways to fast diffusion of the oxidant and therefore the fast oxidation rate observed.

4.3 *Substrate Orientation Dependence of Enhanced Epitaxial Regrowth of Silicon* (see reference VIII)

Past studies have shown that the solid phase epitaxial regrowth of Si can be accelerated by introducing electrically active dopants, ie. boron, phosphorous and arsenic, into the amorphous Si. However, this enhanced regrowth effect has not been systematically demonstrated for substrates of different orientations. Since various models have pointed out the definite relevance of the seed atomic arrangements at the epitaxial regrowth plane, a natural extension of this branch of research is therefore an investigation of orientation dependence of enhanced regrowth. Three Si substrates of different orientations, <100>, <110> and <111>, were amorphized by Si irradiation at liquid nitrogen temperature, to a depth of ~6000 Å. The amorphous region was then uniformly doped with B or P to a concentration of $2 \times 10^{16}/cm^2$, by means of well calibrated triple implantations. Thermally induced regrowth takes place in a vacuum furnace at a temperature of 500°C or 550°C. Thickness of the amorphous region after each annealing stage is measured by channeling RBS.

Enhanced regrowth is verified for all three orientations. A constant enhancement factor of 8.1 ± 0.9 is determined for P doped samples, and 12.2 ± 1.2 for B doped samples.

Epitaxially regrown Si on an <111> substrate is known to contain high density of crystalline defects, particularly twins[71]. The defective crystalline quality gives rise to a high channeling yield. It is found that doped amorphous Si is regrown epitaxially with a much improved crystalline quality as indicated by an overall reduction in channeling yield. This improved crystallinity can be

explained by assuming that twins nucleate at a constant rate at the amorphous-crystalline interface, in competition with epitaxial regrowth. A fast regrowth rate due to doping therefore reduces the total nucleation sites per regrown layer thickness.

REFERENCES

I - General

II - Papers written by Kuo Ting Ho, including both published and unpublished work.

I- General

1 K.C.Sarawat and F.Mohammadi, *IEEE Trans.on Electron.Dev.*, ED-29(1982)645.

2 A.K.Sinha, *J.Vac.Sci.Technol.*, 19,(1982)778.

3 P.B.Ghate, *Thin Solid Films*, 93(1982)359.

4 J.L.Vossen, *J.Vac.Sci.Technol.*, 19,(1982)761.

5 K.N.Tu, *J.Vac.Sci.Technol.*, 19,(1982)766.

6 E.A.Torrero, ed., *Tomorrow's Computer- The Quest*, *IEEE Trans.on Electron.Dev.*, Nov.1983,p.59.

7 T.P.Chow, *IEEE Trans.on Electron.Dev.*, ED-30(1983)1480.

8 C.D.Lien, *Proceedings of the Refractory Metal Silicide for VLSI*, University of California Extension, Berkeley, 1983.

9 A.Kikuchi and S.Sugaki, *J.Appl.Phys.*, 53(1982)3690.

10 F.Pelleg and S.D.Muraka, *J.Appl.Phys.*, 54(1983)1337.

11 H.Norstrom,F.Runovc,R.Buchta,P.Wiklund,M.Östling and C.S.Petersson, *J.Vac.Sci.Technol.*, A1(1983)463.

12 R.J.Blattner,C.A.Evans,Jr.,S.S.Lau,J.W.Mayer and B.M.Ullrich, *J.Electrochem.Soc.* 122(1975)1732.

13 P.J.Grunthaner,F.J.Grunthaner,D.M.Scott,M-A.Nicolet and J.W.Mayer, *J.Vac.Sci.Technol.* 19(1981)641.

14 C.D.Lien,M-A.Nicolet and K.Stika, *Thin Solid Films*, 104(1983)235.

15 H.F.Winters,D.L.Raimondi and D.E.Horne, *J.Appl.Phys.*, 40(1969)2996.

16 H.G.Winters and E.Kay, *J.Appl.Phys.*, 42(1972)794.

17 G.Ehrlich, *J.Chem.Phys.*, 34(1961)29.

18 L.T.Lamont,Jr., *J.Vac.Sci.Technol.*, 10(1973)251.

19 H.F.Winters, *J.Chem.Phys.*, 44(1966)1472.

20 J.T.Tate and P.T.Smith, *Phys.Rev.*, 39(1932)270.

21 H.F.Winters and E.Kay, *J.Appl.Phys.*, 38(1967)3928.

22 J.Angilello,J.E.E.Baglin,F.Cardone,J.J.Dempsey,F.M.d'Heurle,E.A.Irene, R.MacInnes,C.S.Petersson,R.Savoy,A.P.Segmuller and E.Tierney, *J.Electron.Mat.*, 10(1981)59.

23 N.W.Cheung,M-A.Nicolet,M.Wittmer,C.A.Evans,Jr.,T.T.Sheng, *Thin Solid Films*, 79(1981)51.

24 M.Bartur, private communications.

25 R.C.Weast (ed.), *Handbood of Chemistry and Physics*, CRC Press,Cleveland,1975.

26 D.M.Scott and M-A.Nicolet, *Nucl.Instr.Meth.*, 209/210(1983)297.

27 J.T.Clenny and C.J.Rosa, *Met.Trans.A*, 11A(1980)1575.

28 K.N.Strafford, *Corrosion Science*, 19(1979)49.

29 M.J.Brown,D.M.Brown and W.Katz, *J.Electrochem.Soc.*, 130(1983)1196.

30 R.S.Nowicki,W.D.Buckley,W.D.Mackintosh and I.V.Mitchell, *J.Vac.Sci.Technol.*, 11(1974)675.

31 S.Nagata and F.Shoji, *Jap.J.Appl.Phys.*, 10(1971)11.

32 W.J.M.J.Josquin and Y.Jamminga, *J.Electrochem.Soc.*, 129(1982)1804.

33 M.J.Kim and D.M.Brown, *IEEE Trans.on Electron.Dev.*, ED-30(1983)598.

34 P.L.Shah, *IEEE Trans.on Electron.Dev.*, ED-26(1979)631.

35 J.A.Nemetz,T.E.Tressler, *Solid St.Technol.*, Feb.1983,p.79.

36 T.Ito,S.Hijiya,T.Nozaki,H.Arakawa,H.Ishikawa and M.Shinoda, *IEEE Trans.on Electron.Dev.*,

37 T.Enomoto,R.Ando,H.Morita and H.Nakayama, *Jap.J.Appl.Phys.*, 17(1978)1049.

38 M.W.Geis,H.I.Smith,B.Y.Traur,J.C.C.Fan,F.W.Maby and D.A.Antoniadis, *Appl.Phys.Lett.*, 40(1982)158.

39 R.S.Nowicki and I.Wang, *J.Vac.Sci.Technol.*, 15(1978)232.

40 R.S.Nowicki and M-A.Nicolet, *Thin Solid Films*, 96(1982)317.

41 R.S.Nowicki,J.M.Harris,M-A.Nicolet and I.V.Mitchell, *Thin Solid Films*, 53(1978)195.

42 J.Y-T.Chen,D.B.Rensch, *IEEE Trans.on Electron.Dev.*, ED-30(1983)1542.

43 M.F.Zhu,F.C.T.So and M-A.Nicolet, *Thin Solid Films*, to be published.

44 W.E.Pickett,B.M.Klein and D.A.Papaconstantopoulos, *Physica* 107B(1981)667.

45 W.W.Fuller,S.A.Wolf,D.U.Gubser,E.F.Skelton and T.L.Francavilla, *J.Vac.Sci.Technol.*, A1(1983)517.

46 M.van Rossum,private communications.

47 G.Mezy, E.Kotoi,T.Nagy, L.Lohner, A.Manuaba, J.Gyulai, V.R.Deline, R.J.Blattner and C.A.Evans, Jr., *Nucl.Instr.Meth.*, 167(1979)279.

48 J.W.Mayer and E.Rimini, *Ion Beam Handbook for Material Analysis*, Academic Press, New York, 1977, p.118.

49 E.Everling, L.A.Koenig, J.H.E.Mattauch and H.H.Wapstra, *1960 Nuclear Data Tables, Part I*, National Academy of Science, Washington, (1961).

50 W.K.Chu, J.W.Mayer and M-A.Nicolet, *Backscattering Spectrometry*, Academic Press, New York (1978).

51 F.B.Hagedorn and J.B.Marion, *Phys.Rev*, 108(1957) 1015.

52 A.Schardt, W.A.Fowler and C.C.Lauritsen, *Phys.Rev*, 86(1952)527.

53 D.F.Hebbard, *Nucl.Phys.*, 15(1960)289.

54 H.J.Goldschmidt, *Interstitial Alloys*, Plenum Press, New York, 1967,p.227.

55 D.M.Scott, Ph.D.thesis., California Institue of Technology, (1980).

56 N.Bohr, *Mat.Fys.Medd.Dan.Vid.Selsk.* 18, No8(1948).

57 W.K.Chu, *Phys.Rev.A*, 13(1976)2057.

58 C.D.Lien,L.Wielunski,M-A.Nicolet *Nucl.Instr.Meth.*, 213(1983)463.

59 M-A Nicolet and S.S.Lau, in *VLSI Electronics* vol.6,edited by N.G.Einspruch and G.B.Larrabee, (Academic Press,New York,1983),chap.6.

60 M-A.Nicolet and M.Bartur, *J.Vac.Sci.Technol.*, 19(1981)786.

61 A.Y.C.Yu, *Solid St.Electr.* ,13(1970)239.

62 H.N.Yu,A.Reisman,C.M.Osburn and D.L.Critchlow, *IEEE Trans.on Electron Dev.*, ED-26(1979)318.

63 R.P.Elliott, *Constitution of Binary Alloys, First Supplement*, McGraw-Hill,New York,1965.

64 W.K.Chu, S.S.Lau, J.W.Mayer, H.Müller and K.N.Tu, *Thin Solid Films*, 25,(1975)393.

65 R.Pretorius, C.L.Ramiller, M-A.Nicolet, *Nucl.Instr.Meth.*, 149(1978)629.

66 N.Cheung, S.S.Lau, M-A.Nicolet and J.W.Mayer, in J.E.E.Baglin and J.M.Poate(eds.), *Proc. Symp. on Thin Film Interfaces and Interactions* Electrochem.Soc., Princeton, New Jersey, 1980,V80-2, p494.

67 H.Föll and P.S.Ho, *J.Appl.Lett.*, 52(1981)5510.

68 D.M.Scott and M-A.Nicolet, *Nucl.Instr.Meth.* 209/210(1983)297.

69 C.D.Lien and M-A.Nicolet, to be published.

70 C.D.Lien and M-A.Nicolet, to be published.

71 L.Csepregi,J.W.Mayer and T.W.Sigmon, *Appl.Phys.Lett. 29* ,92(1976).

II - papers written by Kuo Ting Ho

I K.T.Ho, M-A.Nicolet and L.Wielun'ski, "Influence of Nitrogen Impurities on Nickel and Platinum Silicide Formation", *Thin Solid Films* ,104(1983)243 : paper presented at Materials Research Society Conference,Boston,(November, 1982).

II K.T.Ho and M-A.Nicolet, "Application of Nitrogen in a Cobalt Silicide Forming System", see Appendix A.

III K.T.Ho, C.D.Lien, M-A.Nicolet and D.M.Scott, "Effect of Nitrogen and Oxygen Impurities on Tantalum Silicide Formation", MRS Proceedings Volume *Thin Films and Interfaces*, edited by J.E.E.Baglin,D.R.Campbell and W.K.Chu, (North-Holland,New York,in press) :paper presented at Materials Research Society Conference,Boston (November,1983). see Appendix B.

IV K.T.Ho and M-A.Nicolet, *Effect of Nitrogen Impurities on Molybdenum Silicide Formation*, see Appendix C.

V K.T.Ho,C.D.Lien,U.Shreter and M-A.Nicolet, *An Inert Marker Study for Palladium Silicide Formation:Si moves in* Polycrystalline "Pd_2Si, see Appendix D.

VI K.T.Ho and M-A.Nicolet, *Palladium Silicide Formation under the Influence of Nitrogen and Oxygen* Impurities", see Appendix E.

VII I.Suni,D.Sigurd,K.T.Ho and M-A.Nicolet, Nitride Films", *J.Electrochem.Soc.*, 130(1983)1210.

VIII K.T.Ho,I.Suni and M-A.Nicolet, *J.Appl.Phys.*, (in press) see Appendix F.

FINAL REMARKS

It was very astonishing for me to find out that the cross section of the $^{15}N(p,\alpha)^{12}C$ nuclear reaction was measured by Caltech nuclear physicists 30 years ago, using the same Van de Graaff accelerator at Kellogg laboratory, which I now use for material analysis. It must be rather rare to find such a interesting coincidence which links a basic research to a later day application.

APPENDICES

A) Application of Nitrogen in a Cobalt Silicide Forming System

B) Effect of Nitrogen and Oxygen Impurities on Tantalum Silicide Formation

C) Effect of Nitrogen on Molybdenum Silicide Formation

D) An Inert Marker Study for Palladium Silicide Formation:
Si Moves in Polycrystalline Pd_2Si

E) Palladium Silicide Formation under the Influence of Nitrogen and Oxygen Impurities

F) Substrate Orientation Effect of Enhanced Epitaxial Regrowth of Silicon

APPENDIX A

APPLICATION OF NITROGEN IN A COBALT SILICIDE FORMING SYSTEM

K.T.Ho and M-A.Nicolet

California Institute of Technology,

Pasadena, California, 91125

ABSTRACT

Implanted nitrogen exhibited an interesting fast diffusion in Co films evaporated on crystalline Si substrate. A nitride barrier layer forms at the Co/Si interface with a saturation areal density of $0.85 \times 10^{16} N/cm^2$, and prevents reaction between Co and Si for annealing temperatures up to 550°C. A Co/nitrogen shallow contact structure was tested using this nitride barrier. A contact resistivity of $1.42 \pm 0.25 \mu\Omega\, cm^2$ was obtained. Nitrogen implanted into Si inhibits the Si flux which is responsible for CoSi growth. Nitrogen redistribution and preferential growth of Co_2Si over CoSi was observed. These results are explained based on the dominant moving species involved during the growth of each silicide phase.

I INTRODUCTION

In recent studies of the behavior of nitrogen in a Ni/Si binary couple, it was found that N, when implanted into the Ni film on a Si substrate, diffused rapidly to the Ni/Si interface and formed a thin layer of nitride barrier[1,2]. For doses equal to or greater than $1 \times 10^{16}/cm^2$, the nitride barrier inhibited Ni_2Si formation at annealing temperatures up to 450°C. In view of the similiarity in metallic valence and radii of Ni and Co[3], we have pursued an analogous investigation with the Co/Si system. High nitrogen mobility and nitride barrier formation were also observed. Local breakdown of the nitride barrier at the Co/Si interface is observed at 550°C.

The subject of cobalt silicide formation presents itself as an challenging transport problem due to simultaneous appearance of two silicide phases prior to the consumption of pure Co[4]. By altering the Si supply rate with implanted N, various characteristics of the silicide growth such as the moving species and kinetics can be explored. Our results agree with the implanted oxygen results reported by Lien et al[5].

One of the new processing requirements in the fabrication of VLSI devices is making reliable shallow contacts which minimize the consumption of substrate Si during thermal annealing to form intimate contacts[6]. The thermal stability of the N barrier which forms at the interface of Co/Si or Ni/Si[7] suggests a new concept for making shallow contacts. In this study, we examined the electrical properties of the more stable Co/nitrogen contact.

II EXPERIMENTAL PROCEDURES

To study the effect of N implanted into Co, a Co film of 1814 Å thickness was evaporated on < 111> oriented Si wafers. The sample for studying N implanted Si had a reversed configuration with 2750 Å of Si evaporated on 1570 Å of Co, which was evaporated first on an oxidized wafer. The evaporation was carried out in an oil-free e-gun system, the background pressure in the chamber during evaporation was $\sim 3\times10^{-7}$ torr. The evaporation rate for both Co and Si was ~20 Å/s. Immediately before loading into the evaporation system, both bare and oxidized Si wafers were ultrasonically cleaned in trichloroethylene, acetone, and methanol sequentially for 5 min. each. The bare wafer was, in addition, etched in 20% HF, then slightly oxidized in an RCA solution (1 H_2O_2:1 NH_4OH:5 H_2O), and finally in 6% HF.

Nitrogen isotope ^{15}N was implanted into Co, at an energy of 200 Kev/N_2^+, with an expected projected range of 960 Å [8]. For N implantation into Si, the

energy used was 120 Kev/N_2^+, with an expected projected range of 1620 Å. Implantation doses used were 0.5, 1 and 2 $\times 10^{16} N/cm^2$ for both types of samples.

The samples were annealed in a vacuum furnace at an ambient pressure of 4×10^{-7} torr. Silicide growth was monitored by MeV $^4He^+$ backscattering spectrometry(RBS), and ^{15}N was profiled by the isotope specific $^{15}N(p,\alpha)^{12}C$ nuclear reaction analysis (NRA). An incident proton energy of 1 Mev was selected to utilize the optimally flat region in the excitation curve[9]. The detector was mounted in the plane of the sample normal and the proton beam, making an angle of 164° with the incident beam. Samples were tilted at 60° against normal incidence to obtain a depth resolution of ~300 Å.

To test the shallow contact feasibility of the Co/nitrogen scheme, contact resistivity measurements were made on an <100> P type Si wafer with phosphorous diffused n^+ channels ($N_D \sim 2\times10^{20}/cm^3$, $X_j \sim 0.3$ μm), with a sheet resistance of ~35 Ω /■ . Channel regions were defined photolithographically by opening windows on a thermally grown silicon oxide layer of ~4000 Å prior to dopant diffusion. Subtrates were etched in 10% HF solution before loading into the evaporation system. Contact pads were defined by standard photoresist lift-off. Geometry of the test pattern is shown in figure 1. More details concerning the test pattern have been published elsewhere[10]. A Co layer of 1415 Å thickness was evaporated for the electrical measurement sample; it was then implanted with 2×10^{16} $^{15}N/cm^2$ at an energy of 60 KeV/N_2^+, with a calculated projected range R_p of 257 Å and and ΔR_p of 194 Å. The implantation energy was purposely made low to minimize the irradiation damage to the substrate. A large area reference sample was prepared simultaneously to be used for RBS and NRA studies. Samples were annealed at 450 °C for 165 min. An unimplanted Co of the same thickness reacts completely into CoSi after the same thermal treatment.

II RESULTS AND DISCUSSION

A. Nitrogen in Cobalt

Figure 2 gives the RBS and NRA spectra for the samples implanted with three different doses after annealing for 3 hr. at 475 °C. The energy axis of the NRA spectra was adjusted to align the N signals with respect to the RBS peaks of its host material. Samples implanted with 1 and 2 $\times 10^{16}/cm^2$ do not show any signs of reaction. Apparently, when annealing begins, N diffuses rapidly to the Co/Si interface and forms a barrier in a time too short for any significant reaction or interdiffusion between Co and Si to occur. For both implanted doses, the interfacial N amounts to an areal density of 0.86 $\times$ $10^{16}/cm^2$, determined to within 10% reproducibility of the NRA technique. This amount, in the form of N atoms, can cover the lattice sites of a smooth <111> Si surface 11 times. Alternatively, this amount of N is equivalent to 3.5 monolayers of Si_3N_4, which is the chemical form favored by thermodynamical considerations[11]. It appears that this amount represents a saturation value of N that can bond to a <111> Si surface. For implanted doses exceeding this value, all excess N outdiffuses from the sample. When the nitride barrier is tested with high temperature(550°C) annealing, failure occurs by a process in which the total amount of N is slowly lost, presumably through bond breaking and outdiffusion. Figure 3 shows that the N barrier has a markedly reduced areal density ($.57\times10^{16}/cm^2$) at the onset of its breakdown. The rough back edge of the RBS peak of Co may indicate that breakdown occurs in localized weak spots of the barrier where we suspect attrition of N is most severe.

Also shown in figure 2 are the result for an implanted dose of 0.5 $\times$ $10^{16}/cm^2$. The fully implanted amount is retained in the interfacial barrier after 180 min. annealing at 475°C. Nitrogen accumulation below the saturation value does not suppress the formation of Co silicide phase nor does it affect the

silicide growth rates, as compared to an unimplanted sample. After the above thermal treatment, Co and the first phase silicide Co_2Si have both transformed into CoSi, as shown in figure 2. Nitrogen is predominantly located in a relatively broad peak near the sample surface, while a small amount resides near the CoSi/Si interface.

The evolution of N in the low dose sample ($0.5 \times 10^{16}/cm^2$) has been monitored throughout the annealing sequence at 475°C, and is illustrated in figures 4a) to 4d). In figure 4a), the as-implanted sample showns a gaussian profile in the Co film. In figure 4b), after 30 min. annealing, both Co_2Si and CoSi coexist with still unreacted Co film. A dominant N peak is situated at the Co/Co_2Si interface. This redistribution is consistent with marker experiments which identify Co as the dominant moving species in Co_2Si formation[12]. Since interfacial N accumulation at this low dose does not produce a barrier effect to silicide reaction, Co will diffuse across the N layer to support the Co_2Si formation. The advancing Co/Co_2Si interface will then drive N further into the unreacted Co. However, an inclination for this N peak to be incorporated into Co_2Si can be observed. A minor N peak is observed in the relatively thin CoSi layer. This small amount is presumably incorporated when CoSi nucleates at the Co/Si or the Co_2Si/Si interface. In figure 4c), By annealing for 60 min., the Co film becomes completely consumed. The dominant N peak emerges near but not at the sample surface, and the peak width has broadened during annealing relative to the 30 min. profile. The fact that N is not pushed all the way to the surface and its broadening can be explained by a partial contribution of Si diffusion to the mass transport. It is not clear why implanted N should produce the above results, whereas, in the case of implanted O, the O emerges all the way at the top sample surface after Co is consumed[5]. The minor peak trails right behind the CoSi/Si interface. Since this N peak is inside the CoSi layer from the

start, it can justifiably serve as a diffusion marker for that phase. Its motion then indicates that Si is the moving species in CoSi growth. In figure 4d), the Co_2Si phase has been depleted due to further growth of CoSi, after a total of 3 hr. annealing. The N redistribution shown here corresponds to that previously illustrated in figure 2.

B. Nitrogen in Silicon

The growth kinetics of the two silicide phases and the consumption rates of Co and Si for the samples with three doses of N implanted into Si are plotted in figure 5, along with an unimplanted reference sample. the annealing temperature used was 415°C. There are a few important feature to be extracted from the kinetic behaviors of these samples. (1) Growth rate of Co_2Si follows a parabolic ($\sqrt{t}$) time dependence in all implanted and reference samples. The same applies to CoSi growth for the reference sample. (2) From 5b), N apparently inhibits the release of Si. According to the simplified model presented in the appendix, a reduction of the Si supply results in the preferential growth of Co_2Si at the expense of CoSi growth. In figure 5a) and 5c), this preferential growth is indeed evident and becomes more pronounced with higher N dose. (3) When release of Si becomes the rate limiting factor in CoSi growth, its growth should approach linear ($\propto$ t)behavior, especially after the complete consumption of Co. However, limited data points and statistical fluctuations do not allow an exact determination of growth pattern in figure 5c). Deviation from a parabolic time dependence can not be excluded, although for simplicity, such a dependence is assumed here to fit a straight line through the data points. (4) While implanted samples demonstrate a suppression of the Si supply, and altered growth rates of the two silicide phases, the consumption rate of Co does not differ from that of the unimplanted sample.

One result which clearly sets apart the effects of N and O implantation into Si is that, at a dose of $2 \times 10^{16}/cm^2$, O completely suppresses the formation of CoSi, even after Co is completedly consumed by the Co_2Si [5]; the Co_2Si phase is growing immediately adjacent to pure Si even after prolonged annealing. Since Co is the moving species in Co_2Si formation, O initially situated in Si becomes diluted by the infiltration of Co along with the Si lattice atoms which bond to it. Contrarily, when 2×10^{16} N/cm^2 is implanted into Si, a thin layer of CoSi always exists between Co_2Si and Si. This thin layer is barely visible in the RBS spectrum but its thickness remains resolution(~250 Å) limited, even when annealing extends beyond the complete consumption of Co. However, the presence of this thin layer is reassured by the piling up of N during the growth of the much more visible Co_2Si. Figure 6b) shows that N is pushed further into Si, after 120 min. annealing, as a large portion of the Si layer becomes consumed by the growing Co_2Si layer. This can only be explained by the presence of a CoSi layer, which is estimated to be about 100 Å from RBS at this annealing stage between Co_2Si and Si. Since Si is the moving species that diffuses through CoSi, N is left behind and accumulates in the remaining Si. As the Si transport continues, it must move past this accumulated layer of N. After further annealing to a total of 270 min, this CoSi growth is still suppressed, whereas, in the samples with lower doses (0.5 and $1\times10^{16}/cm^2$), CoSi contiues to grow at rates not very different from the reference sample. A prolong thermal treatment for 710 min. completely transforms Si and Co_2Si into CoSi in the low dose ($0.5\times10^{16}/cm^2$) sample, N is finally situated at the top sample surface. The movement of the N profile sharply contrasts the case of $TaSi_2$ formation[13], where the dominant moving species is also Si. It was found that Si does not diffuse through the N implanted region to continue Ta silicide growth even at a high annealing temperature of 675°C. The explanation for the large difference in the strength of the N barriers may be related to the diffusion mechanism(interstitial or lattice diffusion etc.) of each

case.

C. Electrical Measurements

After 165 min. annealing at 450°C, an unimplanted sample had completely transformed Co into CoSi, while the implanted sample showed no signs of reaction in the RBS spectrum(see figure 7). The measured contact resistance for the Co/nitrogen contact structure was 1.2 ± 0.2 Ω . From the transmission line model[14] interpretation, the contact resistivity is given by $\rho_c = \frac{R_c^2 W^2}{R_s}$, where W is the width of the contact region, R_c is the contact resistance, and R_s is the sheet resistance of the n^+ channel. The value of ρ_c calculated using this model is 1.42 ± .25 $\mu\Omega\,cm^2$. The low ρ_c obtained for this type of contact is sufficient for VLSI applications[20]. This value also closely agrees with the theoretical prediction of Yu[15] based on an electron tunneling mechanism, which takes in consideration of the dopant concentration N_D and the Schottky barrier height φ_B. The Schottky barrier height of Co silicide (φ_B = 0.65 eV for Co_2Si and 0.67 eV for CoSi)[16] is used in analogy to the case of Ni, for which Cheung and Mayer[17] and Banwell[18] have shown that a finite layer of Ni silicide is present at the Ni-Si[7] interface even for as deposited Ni.

IV. CONCLUSIONS

Nitrogen implanted into a Co film on a Si substrate will diffuse rapidly to the Co/Si interface at the Co silicide forming temperature of ~450°C. A diffusion barrier of a maximum areal density ~0.85 × 10^{16}N/cm^2 forms at this interface for implanted doses equal or greater than this value, inhibiting Co silicide reaction up to 550°C. Nitrogen content in excess of this amount presumably outdiffuses from the Co film. At 550°C, the interfacial nitride barrier fails by slowly losing the total quantity of N. Finally, when the nitride layer becomes thin enough local breakdown occurs, and silicide forms in a laterally nonuniform

manner. When a low dose ($0.5\times10^{16}/cm^2$) implantation is used, Co silicide formation proceeds as if no N is present, and N subsequently emerges at the sample top as soon as Co becomes completely consumed.

When N is implanted into Si in a Si/Co bilayer, N reduces the Si flux which is responsible for CoSi growth. This alteration results in preferential growth of Co_2Si over that of CoSi. For low dose ($0.5\times10^{16}/cm^2$) implanted samples, Si reacts completely after prolonged annealing, and N emerges at the sample surface, confirming a dominant Si diffusion. For high dose ($2\times10_{16}/cm^2$) implanted sample, the Si flux becomes totally suppressed before CoSi formation is completed, due to the built up of a N barrier in Si.

A contact resistivity of $1.42 \pm 0.25\ \mu\Omega\ cm^2$ was measured for a new contact structure made by annealing a N-implanted Co film on n^+ Si, which is acceptable for VLSI applications.

ACKNOWLEDGEMENT

The authors would like to acknowledge Ali Ghaffari for technical assistance and M. Finnetti for invaluable instructions on sample preparations for electrical measurements. Discussions with C. D. Lien and T. Banwell disclosed many new insights and enlivened the subject matter investigated.

APPENDIX

This simplified model takes the results of van Gurp et al.[12] which state that Co is the dominant moving species in Co_2Si formation, while Si plays the corresponding role in CoSi formation. The situation is depicted in figure 7.

The reaction at the $Co^2Si/CoSi$ interface can be described by the formula

$$n\ Co + m\ Si = (\ n - m\ )\ Co_2Si + (\ 2\,m - n\ )\ CoSi$$

The ratio of the integral coefficients m and n is given by the fluxes of the two moving species.

$$\frac{J_{Si}}{J_{Co}} = \frac{m}{n} = R$$

The ratio of the growth rates for these two phases then can be calculated to be:

$$\frac{\Delta X_1}{\Delta X_2} = \frac{(2m - n)/N_1}{(n - m)/N_2} = \frac{(2R - 1)/N_1}{(1 - R)/N_2}$$

where ΔX_i and N_i stand for the differential thickness and density of the Co_iSi phase.

When J_{Si} becomes impeded by a N barrier, R decreases, and the ratio of ΔX_1 diminishes with respect to ΔX_2, corresponding to preferential growth of Co_2Si.

REFERENCES

1 D.M.Scott, L.Wielun'ski, H.von Seefeld and M-A.Nicolet, *Nucl.Instr.Meth* ,182/183(1981)661.

2 K.T.Ho, M-A.Nicolet and L.Wielun'ski, *Thin Solid Films* ,104(1983)243.

3 L.Pauling, *The Nature of The Chemical Bonds*. (Cornell University Press Inc.,Ithaca,1967), p.396 and 417.

4 S.S.Lau, J.W.Mayer and K.N.Tu, *J.Appl.Phys.* ,49,(1978)4005.

5 C.D.Lien and M-A.Nicolet, MRS Proceedings Volume *Thin Films and Interfaces*, edited by J.E.E.Baglin,D.R.Campbell and W.K.Chu, (North-Holland,New York,in press).

6 K.N.Tu, *J.Vac.Sci.Technol.*, 19(1981)766.

7 T.Banwell, M-A.Nicolet and D.M.Scott, *Thin Solid Films.* ,107(1983)67.

8 J.P.Biersack, *Nucl.Instr.Meth.* ,182/183(1981)199.

9 F.B.Hagedorn and J.B.Marion, *Phys.Rev.* ,108(1957)1015.

10 M.Finnetti, I.Suni and M-A.Nicolet, *Solar Cells* ,9(1983)179.

11 R.C.Weast (ed.), *Handbook of Chemistry and Physics*, (CRC Press,Cleveland,1975).

12 G.J.van Gurp, W.F.van der Weg and D.Sigurd, *J.Appl.Phys.* ,49(1978)4011.

13 K.T.Ho, C.D.Lien, M-A.Nicolet and D.M.Scott, MRS Proceedings Volume *Thin Films and Interfaces*, edited by J.E.E.Baglin,D.R.Campbell and W.K.Chu, (North-Holland,New York,in press).

14 H.H.Berger, *J.Electrochem.Soc.* ,119(1972)507.

15 A.Y.C.Yu, *Solid St.Electr.* ,13(1970)239.

16 C.D.Lien and M-A.Nicolet, to be published.

17 N.W.Cheung and J.W.Mayer, *Phys.Rev.Lett.* ,46(1981)671.

18 T.Banwell, private communication.

19 H.N.Yu,A.Reisman,C.M.Osburn and D.L.Critchlow, *IEEE Trans.on Electron Dev.*, ED-26(1979)318.

FIGURE CAPTIONS

figure 1 Test pattern for contact resistivity measurement. Highly doped region is opened in the oxide.

figure 2 After 3 hr. annealing at 475°C, the sample implanted with 0.5 × $10^{16}N/cm^2$ has transformed completely CoSi, while silicide reactions in the higher dose samples are inhibited.

figure 3 Local failure of the nitride barrier occurs after 550°C annealing for 30 min. A reduction in the areal density of N is observed at the onset of the breakdown.

figure 4 The evolution of N profiles at various annealing stages. Regions I and II correspond to the Co_2Si and CoSi phases. The N redistribution observed is consistent withN the reported moving species: Co for Co_2Si and Si for CoSi.

figure 5 Growth rates of Co_2Si and CoSi and consumption rates of Co and Si. Nitrogen suppresses the release of Si, leading to the preferential growth of Co_2Si over CoSo. The high dose (2×10^{16}) implant suppresses CoSi growth.

figure 6 After 120 min. annealing at 475°C, N pile up occurs in Si. From moving species considerations, this accumulation indicates that a thin layer of CoSi exists between Co_2Si and CoSi, even though its thickness is below the depth resolution of RBS.

figure 7 Simplified model of diffusion processes during Co_2Si and CoSi formation. Co moves in Co_2Si while Si moves in CoSi.

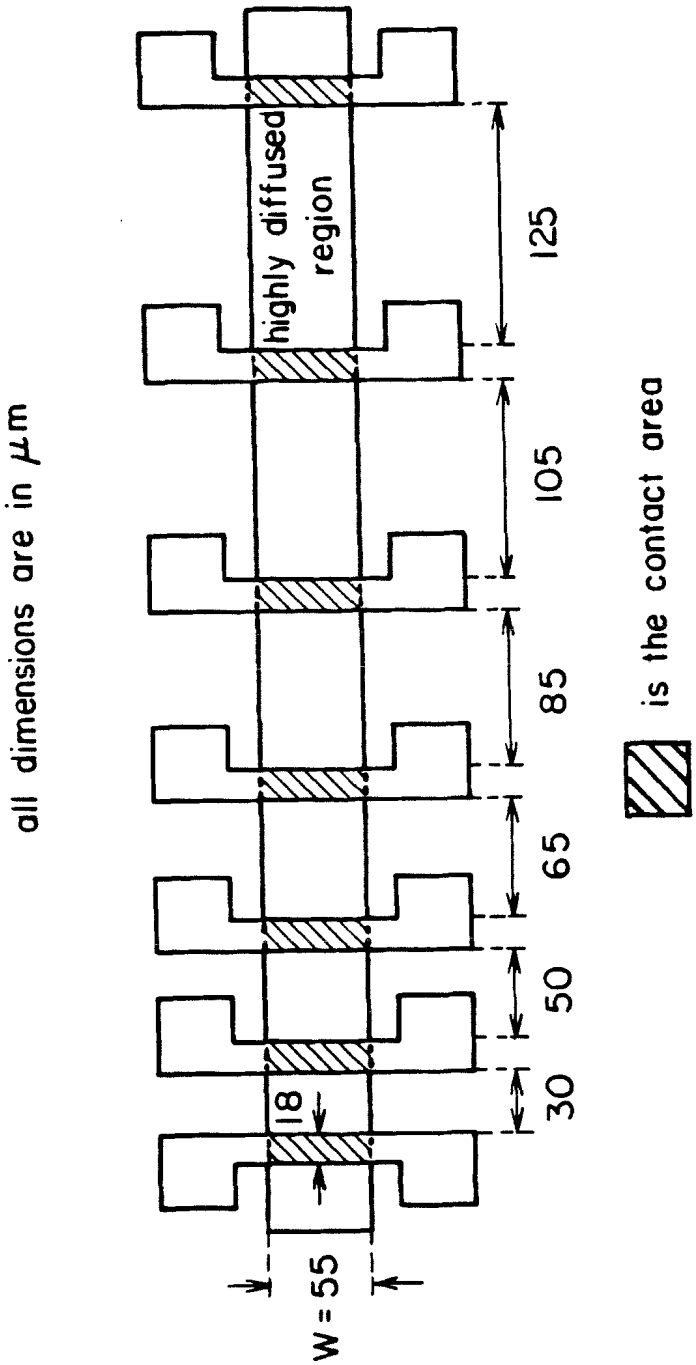
all dimensions are in μm
highly diffused region
125
105
85
65
50
30
18
W = 55
is the contact area

fig.1

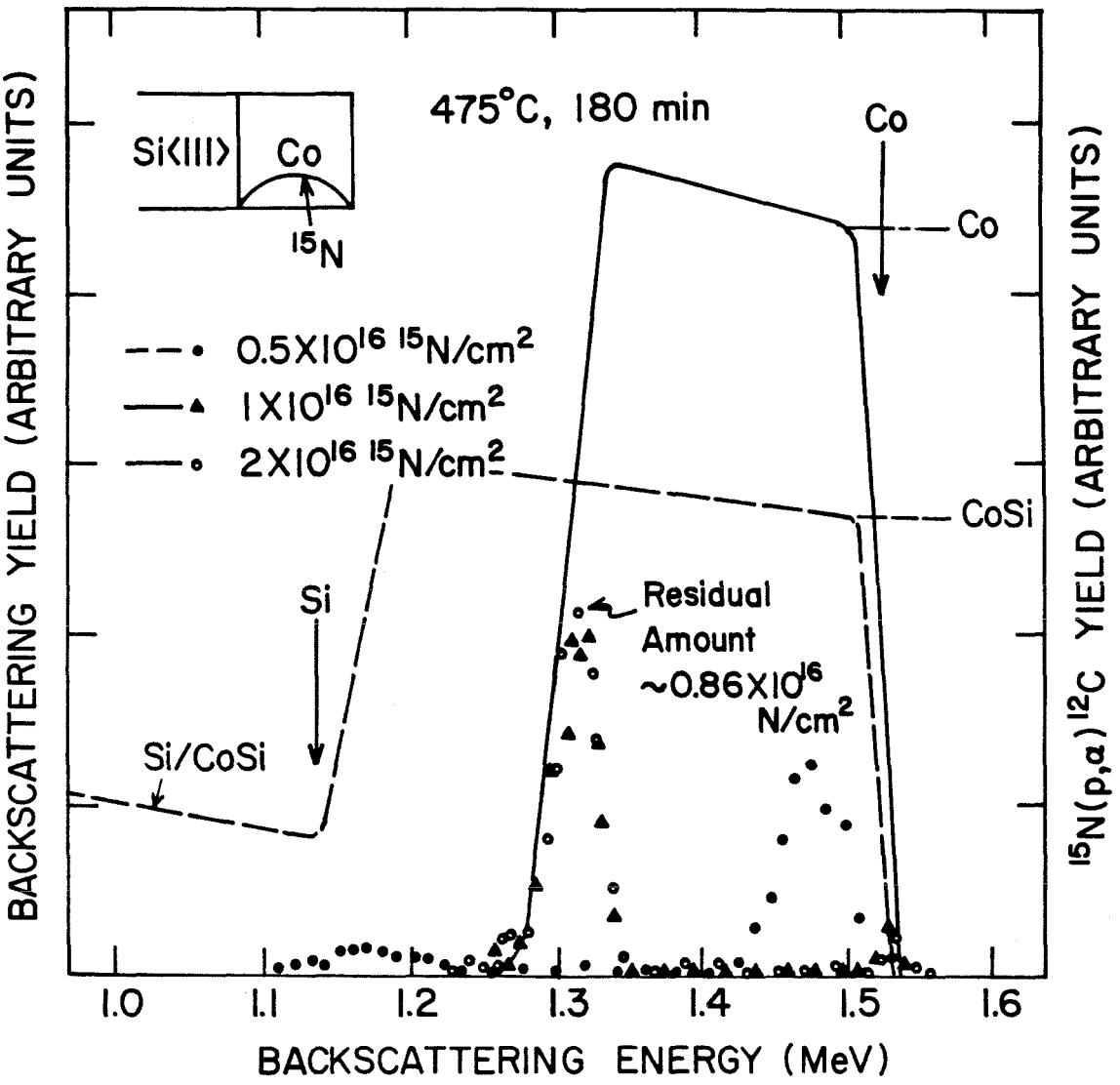
475°C, 180 min
Si⟨111⟩
Co
15N
Co
Co
0.5X10^16 15N/cm^2
1X10^16 15N/cm^2
2X10^16 15N/cm^2
CoSi
Si
Residual
Amount
~0.86X10^16
N/cm^2
Si/CoSi
BACKSCATTERING YIELD (ARBITRARY UNITS)
15N(p,α)12C YIELD (ARBITRARY UNITS)
1.0
1.1
1.2
1.3
1.4
1.5
1.6
BACKSCATTERING ENERGY (MeV)

fig.2

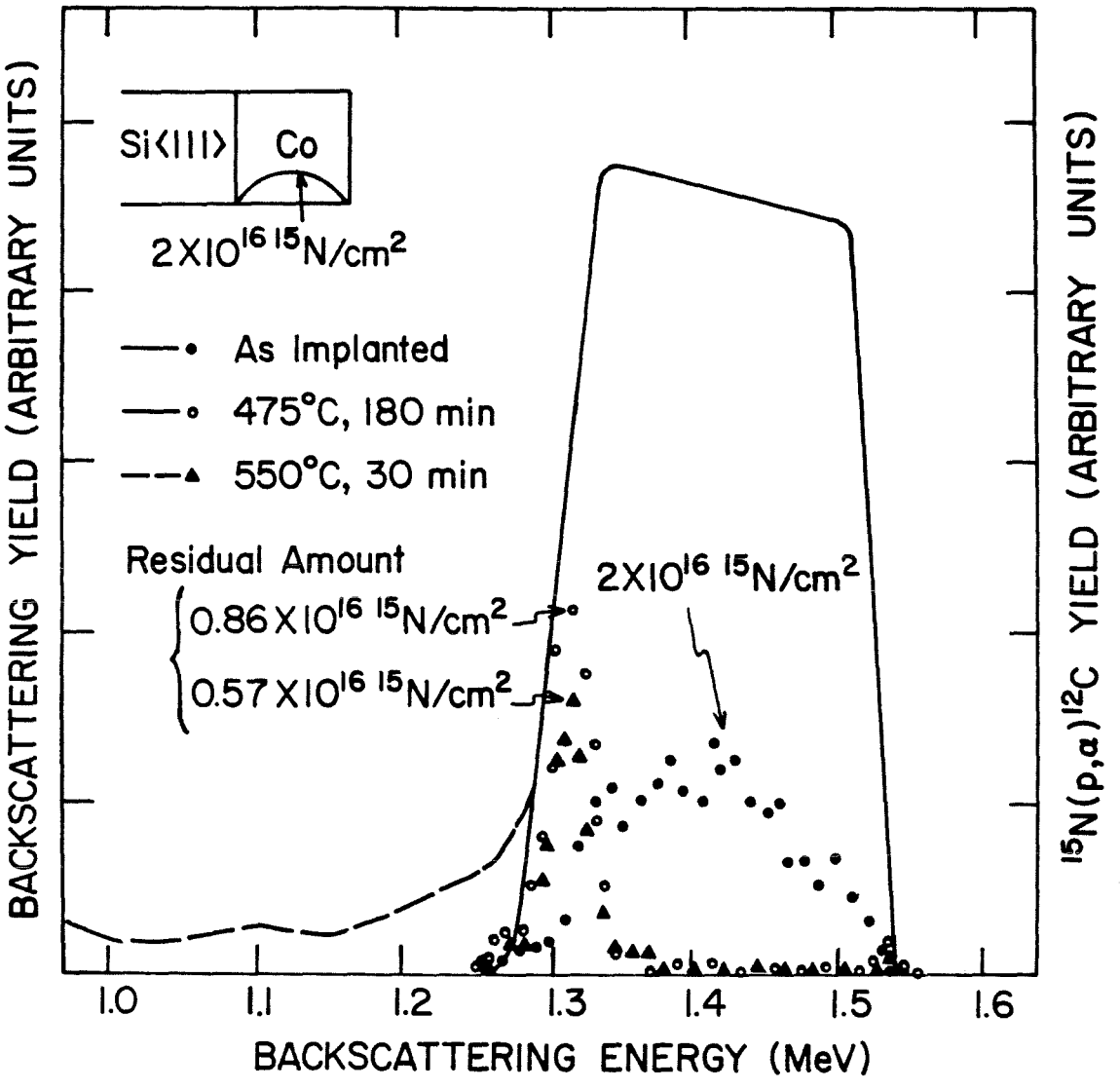
Si⟨111⟩
Co
2X10^16 15N/cm2
As Implanted
475°C, 180 min
550°C, 30 min
Residual Amount
0.86X10^16 15N/cm2
0.57X10^16 15N/cm2
2X10^16 15N/cm2
BACKSCATTERING YIELD (ARBITRARY UNITS)
15N(p,α)12C YIELD (ARBITRARY UNITS)
1.0
1.1
1.2
1.3
1.4
1.5
1.6
BACKSCATTERING ENERGY (MeV)

fig.3

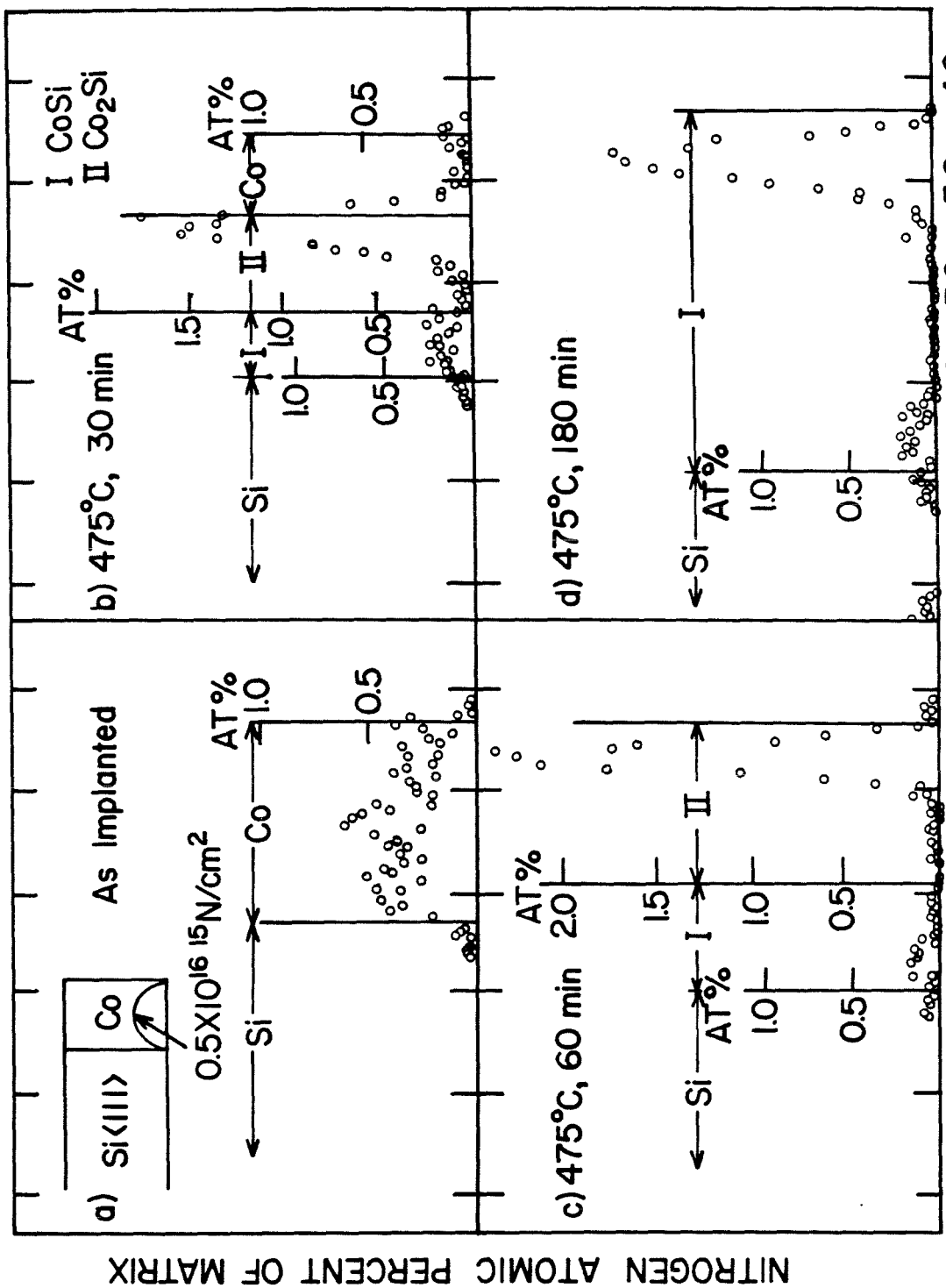
a) Si⟨111⟩
Co
0.5X10^16 15N/cm2
As Implanted
b) 475°C, 30 min
I CoSi
II Co2Si
c) 475°C, 60 min
d) 475°C, 180 min
AT%
Si
Co
I
II
15N(p,α)12C ENERGY (MeV)
NITROGEN ATOMIC PERCENT OF MATRIX

fig.4

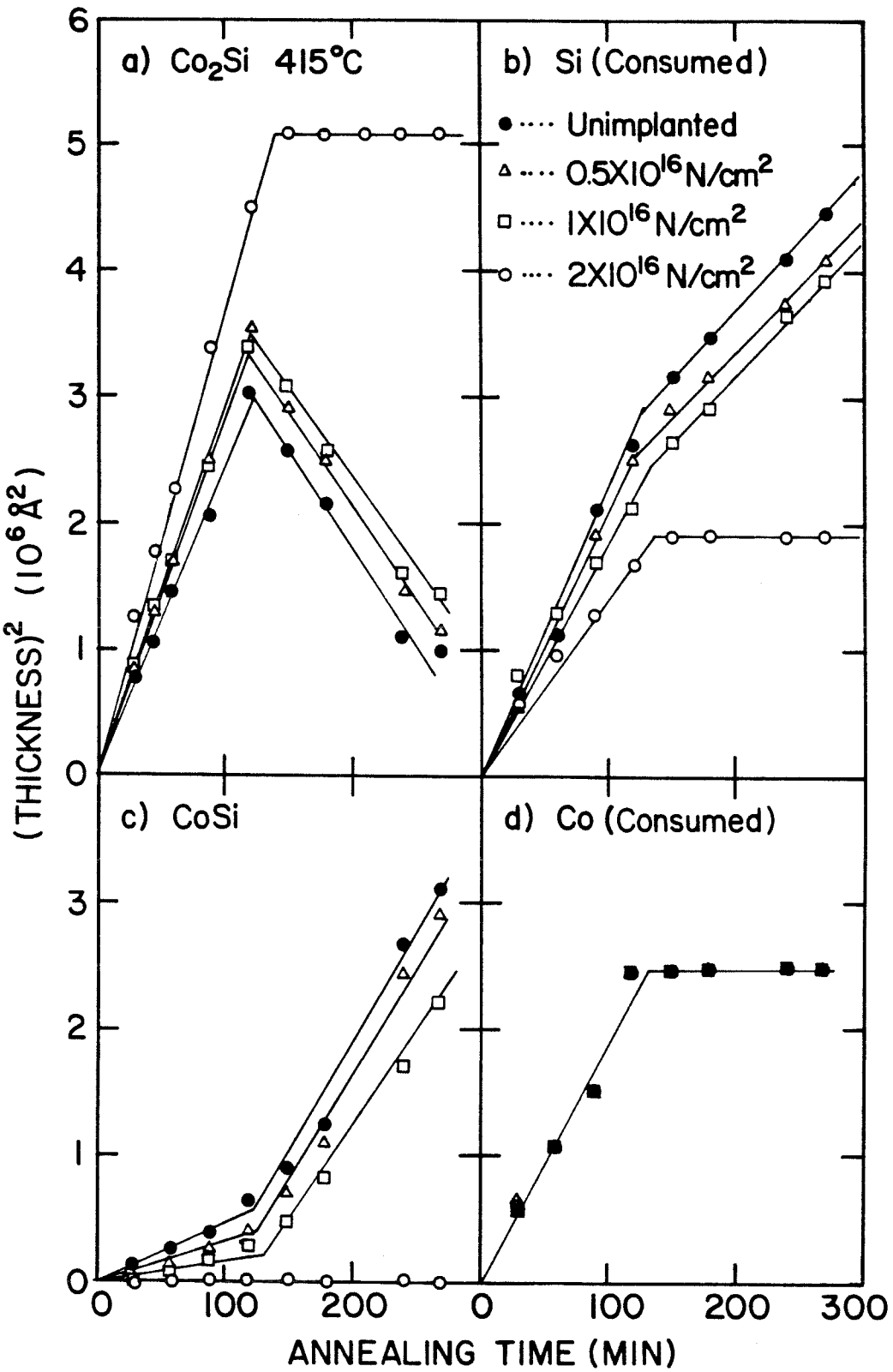
a) Co_2Si 415°C
b) Si (Consumed)
Unimplanted
$0.5X10^{16}$ N/cm^2
$1X10^{16}$ N/cm^2
$2X10^{16}$ N/cm^2
c) CoSi
d) Co (Consumed)
(THICKNESS)^2 (10^6 Å^2)
ANNEALING TIME (MIN)
0
1
2
3
4
5
6
100
200
300

fig.5

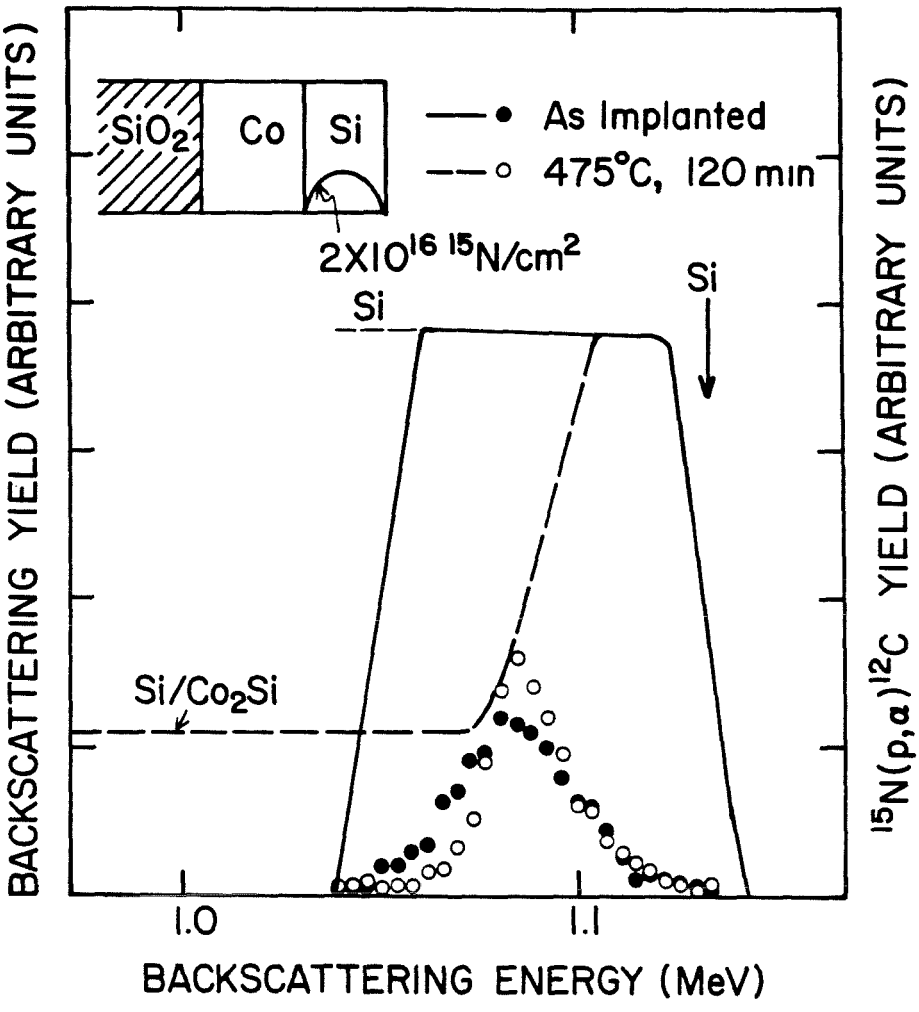
BACKSCATTERING YIELD (ARBITRARY UNITS)
$^{15}N(p,\alpha)^{12}C$ YIELD (ARBITRARY UNITS)
SiO_2
Co
Si
As Implanted
475°C, 120 min
$2X10^{16}$ $^{15}N/cm^2$
Si
Si
Si/Co_2Si
1.0
1.1
BACKSCATTERING ENERGY (MeV)

fig.6

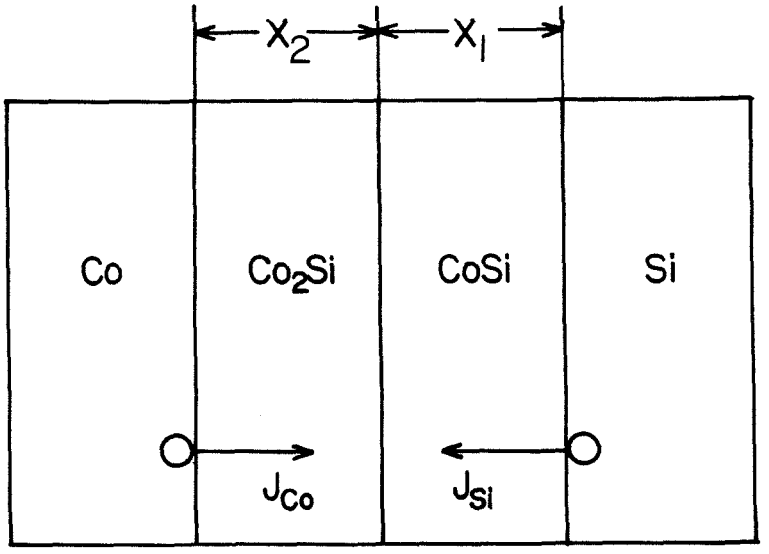

fig.7

APPENDIX B

EFFECT OF NITROGEN AND OXYGEN IMPURITIES ON TANTALUM SILICIDE FORMATION

K.T.Ho, C.D.Lien, and M-A. Nicolet

California Institute of Technology,

Pasadena, California, 91125

D.M.Scott

University of California at San Diego,

La Jolla, California, 92093

ABSTRACT

Tantalum, being a refractory metal, is sensitive to ambient impurities when forming a silicide. By introducing nitrogen and oxygen impurities into a tantalum-silicon system, interesting chemical and physical effects are observed in their subsequent reactions. Nitrogen and oxygen behave similarly in such a system. If initially present in Ta, they segregate into still unreacted Ta, as the silicide layer grows at a somewhat retarded rate. The same impurities initially present in Si are immobile in the form of stable compounds, and suppress $TaSi_2$ growth. The rare isotopes ^{15}N and ^{18}O are introduced by implantation and profiled by $^{15}N(p,\alpha)^{12}C$ and $^{18}O(p,\alpha)^{15}N$ nuclear reaction analysis, respectively. In addition, unintentionally incorporated ^{16}O is checked by $^{16}O(d,\alpha)^{14}N$ nuclear reaction. Results are explained in terms of the moving species Si and chemical affinity, solubility and diffusivity of the impurities in their host lattice.

I INTRODUCTION

Thermally induced silicide formation from evaporated metal films on Si often inadvertently incorporate impurities which have deleterious effects on the growth of the silicide[1-3]. Past investigators of transition metal silicides have

generally shunned or minimized complications due to these impurities by chemically etching or plasma cleaning the Si surfaces, utilizing oil-free high vacuum evaporation systems, annealing in vacuum or reducing ambients, and capping sample tops with thin Si or Pt/W layers[4,5]. Some authors also suggested implantation through the interfacial oxides[6]. Recently, more concentrated work addressing impurity effects is being pursued[7-9].

The refractory metal (Ti,Ta,Mo,W,V etc.) silicides have so far eluded a comprehensive understanding due to irreproducible growth behaviors (e.g., linear or square-root of time growth rate)[10,11]. It has been proposed that some of the complexities are to be attributed to impurity influences, since refractory metals are strong getters of oxygen impurities[12]. Impurities in refractory metals are especially interesting because of their usually high solubility and diffusivity in, as well as large heat of compound formation with these metals. Previous work on vanadium and titanium silicide has reported an interesting interfacial "plowing" behavior of oxygen[3,13].

In this work we intentionally introduce the most common impurities, nitrogen and oxygen, in tantalum-silicon reactions, and study their effects by both monitoring the silicide growth rates and observing the impurity motion by nuclear reaction profiling. The understanding of their effects can be approached based on thermodynamical arguments and other physical properties such as the moving species and diffusivity. Since we expect a priori that the deposiited film will contain unintended oxygen impurity, a comparison of this background level with those purposely introduced was performed and considered in interpreting the experimental results.

II EXPERIMENTAL PROCEDURES

For impurity implantation into Ta, Ta films were evaporated onto < 100> Si for nitrogen studies, and onto amorphous Si on an oxidized Si wafer for oxygen studies. For impurity implantation into Si, amorphous Si was evaporated on top of Ta, which was first evaporated on oxidized Si wafers. The < 100> Si wafer was commercially polished, p-type, with a resistivity of 1.5-2.5 Ω cm. Both bare and oxidized Si wafers were ultrasonically cleaned with trichloroethylene, acetone, and methanol. The bare wafer was then etched in 20% HF, followed by an RCA solution etch (H_2O_2 :NH_4OH:H_2O in the ratio 1:1:5), and finally another etch in 6% HF. Samples were loaded into an oil-free high vacuum system immediately after cleaning.

The base pressure of the system was 6×10^{-8} torr and was maintained at 2×10^{-7} torr during evaporation. The Ta films were evaporated at a rate of 20Å/s to approximately 1600Å thick, and the Si films at a rate of 20Å/s to thicknesses of approximately 3200Å. The samples which had the Ta films on top were always covered with ~200Å Si cap to protect the metal films from oxygen contamination from the annealing ambient.

Nitrogen isotope ^{15}N was implanted into Ta with an energy of 200 kev/N_2^+, with an expected range of 770Å and a ΔR of 634Å[14]. Nitrogen implantation into Si was done at 130 kev/N_2^+, with an expected range of 1764Å and a ΔR of 705Å. The corresponding values of oxygen isotope ^{18}O implantations into Ta were performed at the energy of 210 kev/O_2^+, range of 697Å, and ΔR of 586Å, and oxygen into Si, at the energy of 130 kev/O_2^+, range of 1520Å, and ΔR of 631Å. Implantation doses of both nitrogen and oxygen for all sample configurations were 0.5, 1.0, and 2.0×10^{16} atoms/cm^2.

Silicide formation took place by thermal annealing in a vacuum furnace

with 5×10^{-7} torr pressure. The annealing temperature used was always 675 °C. Silicide growth was tracked over a 3-hr period at half-hr intervals. Silicide thicknesses were monitored by 2 Mev $^4He^+$ Rutherford backscattering spectrometry (RBS), with a detector angle of 170 °, and a sample tilting angle of 50 °. Nitrogen and oxygen were profiled by the $^{15}N(p,\alpha)^{12}C$ and $^{18}O(p,\alpha)^{15}N$ nuclear reaction analysis(NRA), at incident energies of 1 and .75 Mev, respectively. Samples were tilted at 60° with respect to the beam to obtain a depth resolution of ~300Å for both techniques. The detector was mounted in the plane of the sample normal and the proton beam at an angle of 164°. Unintentional ^{16}O contamination was checked using the $^{16}O(d,\alpha)^{14}N$ nuclear reaction. Description of this technique was given elsewhere[15].

III RESULTS

A. Nitrogen in Tantalum

Figure 1a gives the RBS and NRA spectra for both as-implanted and annealed samples with 2×10^{16} N/cm^2 implanted into Ta. The NRA energy axis is adjusted to show the position of N relative to the edges of the Ta film. Nitrogen in the as-implanted sample has a gaussian profile with a range of ~800 Å, in good agreement with the calculated range. The peak concentration amounts to 1.8 at%. After 1.5 hrs. annealing at 675°C, 1900 Å of $TaSi_2$ has formed. Nitrogen is pushed by the Ta/silicide interface into the untreated portion of Ta, leaving approximately 0.2 at% of residual N in the silicide layer. After 6 hrs. annealing, an amount equivalent to about 570 Å of Ta has not completely formed $TaSi_2$. Nitrogen accumulates at the top surface with no loss in total quantity. The kinetics of $TaSi_2$ formation is shown in figure 1b. The unimplanted sample has a linear silicide growth rate as reported previously. Retardation effect of implanted N becomes apparent only after a large Ta consumption.

B. Oxygen in Tantulum

The same segregation effect as for N is seen for O in Ta, as depicted in figure 2a. For the sample with one hr. annealing, the NRA spectrum shows that O has diffused rapidly towards sample surface, in addition to segregating out of the silicide. The sample with 3 hrs. annealing showed a much more complete reaction than that in the N case. Total quantity of O in this sample is reduced by approximately 15%. This outdiffusion correlates well with the lack of surface oxygen peak. The kinetics curves are shown in figure 2b. Unimplanted films become nonuniform after annealing, therefore only one data point can be obtained for that curve. Growth rates of implanted samples deviate from linearity, with the higher dose samples giving more pronounced retardation effects.

C. Nitrogen in Silicon

Figure 3a shows that the silicide formation proceeds until the Si/silicide interface reaches the region of Si with high N content. From NRA spectra we could not observe any N movement after up to 6 hrs. annealing (indicating a strong bonding between N and the host Si). The kinetics curve in figure 3b points out that silicide growth starts out linearly and indeed comes to a halt when the interface of the growing layer sees high N concentration. The sample with 0.5×10^{16} N/cm^2 dose has a larger final silicide thickness than the higher dose samples (apparently because there is more N-free Si between the N maximum and Ta).

D. Oxygen in Silicon

Figures 4a shows that the $TaSi_2$ growth also stops at the region of Si where O content builds up. No O movement is observed after 3 hrs. annealing. The kinetics curve in figure 4b shows suppression of silicide growth after 1350 Å of Si

has been consumed.

IV DISCUSSION

Studies of impurities in near noble metal and Cr have reported incorporation of impurity into the silicide when the impurity is initially in the stationary species[7-9]. In contrast, even with Si as the moving species in $TaSi_2$ formation, our results for N and O implanted into Ta showed impurity segregation rather than incorporation, in agreement with the results reported for V and Ti silicides[3,13]. This can be understood in terms of the solid solubility of N (1.8% at 500°C)[16] and O (9.3% at 1050°C)[17] in bulk Ta as well as each's high diffusivity in Ta[18].

A free Si atom which diffuses to the Ta/silicide interface can undergo two possible reactions in the presence of either impurity,

$$(1) Si + \frac{4}{3}(\,N\ s.\ s.\ in\ Ta\,) \rightarrow \frac{1}{3} Si_3N_4$$

or

$$Si + 2(\,O\ s.\ s.\ in\ Ta\,) \rightarrow SiO_2$$

$$(2) Si + \frac{1}{2} Ta \rightarrow \frac{1}{2} TaSi_2$$

The fact that N(O) impurity segregates means that neither Si nitride(oxide) nor Ta nitride(oxide) has formed, since nitrogen(oxygen) in the molecular form is expected to have very small diffusivity and become incorporated by the advancing silicide layer. There is the possibility that a submonolayer of nitride(oxide) is dragged by the Ta/silicide interface, since the signal from such a layer will not be detected on top of the residual N(O) in the silicide. As the

N(O) concentration in Ta gets high towards the end of the growth stage, it can eventually exceed its solid solubility limit and react into a nitride(oxide), which is then incorporated into the silicide in increasing proportions, as shown by the rising N(O) profile in the silicide layer of figure 1(3)a.

Interpretations of growth kinetics will depend on the background ^{16}O contamination, which we have checked by $^{16}O(d,\alpha)^{14}N$ nuclear reaction. We find, as shown in figure 5a, a continuous O concentration gradient starting from 3 at% to 26 at% near the top Ta interface with the cap. Increased O content towards the top of the Ta film is attributed to a higher rate of outgassing from the high vacuum system which heats up continuously during evaporation. This raises the question whether the high background O concentration is the cause of linear growth rate of $TaSi_2$ (see fig.1b) or the silicide simply has an intrinsic linear growth rate regardless of any interference from O. The unintended O significantly overlaps with and by far exceeds the peak of the implanted impurities. Therefore, the oxygen dose-dependent growth retardation shown in figure 2b is either due to implantation damages or due to different chemical forms of ^{16}O (e.g. CO) and ^{18}O; whereas, implanted N may still be chemically changing the reaction environment. The phenomenon of fast oxygen diffusion towards metal surfaces has also been observed in Mo films[19]. After annealing for 3 hrs., most of the ^{16}O segregates into the unreacted Ta. Oxygen concentration that remained in the silicide dropped to approximately 5 at%. There is no change in total ^{16}O quantity within our experimental accuracy. We can not exclude the possibility that ^{16}O has diffused into as well as out of the sample.

Nitrogen and oxygen initially in Si can be assumed to take the forms of Si_3N_4 and SiO_2, respectively[20,21]. The suppression of silicide reaction shows that the nitride and oxide regions do act as barriers to Si diffusion. The immobility

of impurities indicate that Ta does not compete favorably with Si in forming either nitrides or oxides. Thermodynamically, the reaction

$$SiO_2 + \frac{13}{10} Ta \rightarrow \frac{2}{5} Ta_2O_5 + \frac{1}{2} TaSi_2$$

yields a marginal positive heat of formation[22], whereas the reaction

$$Si_3N_4 + \frac{11}{2} Ta \rightarrow 4\ TaN + \frac{3}{2} TaSi_2$$

is strongly favorable, with -7.16 kcal/gatom as the heat of formation. The apparent stability of the nitride must then be attributed to kinetic barriers. These results are to be compared to the previous work on Cr, where Cr is reported to decompose SiO_2 and causes O accumulation at the Si/silicide interface[4].

V CONCLUSIONS

Nitrogen and oxygen have similar effects on the tantalum-silicon system. When these impurities are implanted into Ta, they have minor interferences with $TaSi_2$ formation. Both impurities are pushed by the advancing silicide layer into unreacted Ta. In addition, O exhibits a fast diffusion towards Ta surface. When N and O are implanted into Si, reaction with Ta is suppressed once the silicide/Si interface reaches the region of high impurity concentration; no impurity motion in Si is detected using nuclear reaction analysis. Evaporated Ta films contain unintentional oxygen inclusions which build up in concentration with film thickness, but do not interfere with silicide reaction.

ACKNOWLEDGEMENTS

The authors would like to acknowledge Ali Ghaffari for technical assistances, and Frank So for helpful discussions. One of the authors

(D.M.Scott) wishes to acknowledge financial support from DARPA (S.Roosild). This work was partially supported by SSDI (A. Applebaum)

REFERENCES

1 C.D.Lien and M-A.Nicolet in: *Proceedings of the Workshop on Refractory Metal Silicide for VLSI*, San Juan Bautista, California - September 1983, (University of California Extension,Berkeley,1983).

2 C.Canali,C.Catellana,M.Prudenziati,W.H.Wadlin and C.A.Evans.Jr., *Appl.Phys.Lett.* ,31(1977)43.

3 R.J.Schultz and L.R.Testardi, *J.APPl.Phys.* ,50(1979)5773.

4 G.Bomchil,D.Bensahel,A.Golanski,F.Ferriell,G.Auvert,A.Perio and J.C.Pfister, *Appl.Phys.Lett.* ,41(1982)46.

5 K.N.Tu,R.D.Thompson and B.Y.Tsaur, *Appl.Phys.Lett.* ,38(1981)626.

6 L.S.Wielunski,C.D.Lien,B.X.Liu and M-A.Nicolet, in S.T.Picraux and W.J.Choyke(eds.), *Proc.Symp.on Metastable Materials Formation by Ion Implantation* ,(North Holland,New York,1982).

7 K.T.Ho,M-A.Nicolet and L.Wielunske, *Thin Solid Films* ,104(1983)243.

8 C.D.Lien,L.Wielunske and M-A.Nicolet, *Thin Solid Films* ,104(1983)235.

9 D.M.Scott and M-A.Nicolet, *Nucl.Instr.Meth.* ,182-183(1981)655.

10 K.N.Tu and J.W.Mayer in J.M.Poate, K.N.Tu and J.W.Mayer(eds.), *Thin Films-Interdiffusion and Reactions* ,(Wiley,New York,1978),p.359.

11 C.S.Petersson,J.E.E.Baglin,F.M.d'Heurle,J.J.Dempsey,J.M.E.Harper,C.M.Serrano and M.Y.Tsai in J.E.E.Baglin and J.M.Poate(eds.), *Thin Films and Interfaces*, (Electrochemical Society,Princeton,1980),Vol.80-2,p.290.

12 H.Kräutle,M-A.Nicolet and J.W.Mayer, *J.Appl.Phys.* ,45(1974)3304.

13 A.Guldan,V.Schiller,A.Steffen and P.Balk, *Thin Solid Films* ,100(1983)1.

14 J.P.Biersack, *Nucl.Instr.Meth.*, 182/183(1981)199.

15 S.T.Picraux, *Nucl.Instr.Meth.* ,149(1978)289.

16 R.P.Elliott, *Constitution of Binary Alloys, First Supplement*, McGraw-Hill,New York,1965.

17 M.Hansen and K.Anderko, *Constitution of Binary Alloys*, McGraw-Hill,New york,1958.

18 R.Kelly, *J.Vac.Sci.Technol.* ,21(1982)778.

19 F.Arnaud,D'Avitaya,G.Bomchil and C.Arena, *Extended abstract of the Electrochemical Society spring meeting(1983)*, #389;(to be published in Proceedings of the Electrochemical Society).

20 T.Tsujide,M.Nojiri and H.Kitagawa, *J.Appl.Phys.* ,51(1980)1605.

21 P.J.Grunthaner,F.J.Grunthaner,D.M.Scott,M-A.Nicolet,J.W.Mayer, *J.Vac.Sci.Technol.* ,19(1981)641.

22 R.Pretorius,J.M.Harris,M-A.Nicolet, *Solid-State Electron.* ,21(1978)667.

FIGURE CAPTIONS

figure 1 Nitrogen implanted into Ta. (a) NRA shows a pile-up of N in the unreacted Ta film. (b) Kinetics curves indicate that implanted N retards the silicide growth.

figure 2 Oxygen implanted into Ta. (a) O segregates out of the advancing silicide layer and at the same time outdiffuses through Ta surface. (b) O implantations produce a dose-dependent retardation effect on silicide growth.

figure 3 Nitrogen implanted into Si. (a) Silicide growth proceeds until silicide front reaches region of high N concentration. (b) N completely supresses further silicide growth.

figure 4 Oxygen implanted into Si. (a) silicide growth stops at region of high O concentration. (b) O also completely suppresses silicide growth.

figure 5 (a) Unannealed Ta film contains from 3 to 26 at% of ^{16}O which by far exceeds the implanted impurity concentrations(shown as dashed line). (b) After 3 hr. annealing, ^{16}O segregates into remaining Ta. Up to 5 at% oxygen is incorporated into the silicide.

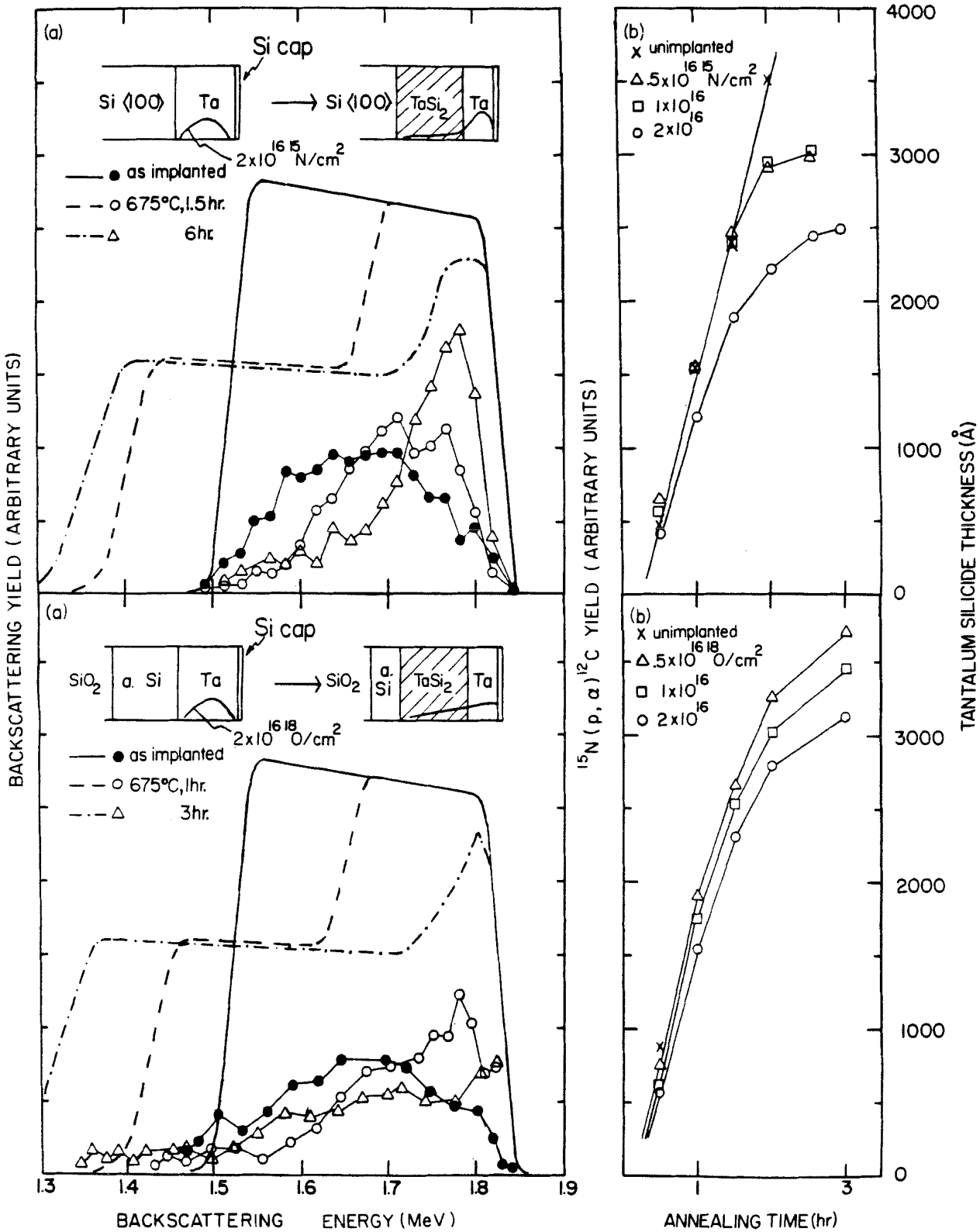
(a)
Si cap
Si ⟨100⟩ Ta
Si ⟨100⟩ TaSi2 Ta
2x10^16 15 N/cm^2
● as implanted
o 675°C, 1.5hr.
△ 6hr.
(a)
Si cap
SiO2 a. Si Ta
SiO2 a. Si TaSi2 Ta
2x10^16 18 O/cm^2
● as implanted
o 675°C, 1hr.
△ 3hr.
BACKSCATTERING YIELD (ARBITRARY UNITS)
1.3
1.4
1.5
1.6
1.7
1.8
1.9
BACKSCATTERING ENERGY (MeV)
(b)
x unimplanted
△ 5x10^16 15 N/cm^2
□ 1x10^16
o 2x10^16
(b)
x unimplanted
△ 5x10^16 18 O/cm^2
□ 1x10^16
o 2x10^16
15N(p,α)12C YIELD (ARBITRARY UNITS)
4000
3000
2000
1000
0
TANTALUM SILICIDE THICKNESS (Å)
1
3
ANNEALING TIME (hr)

fig.1,2

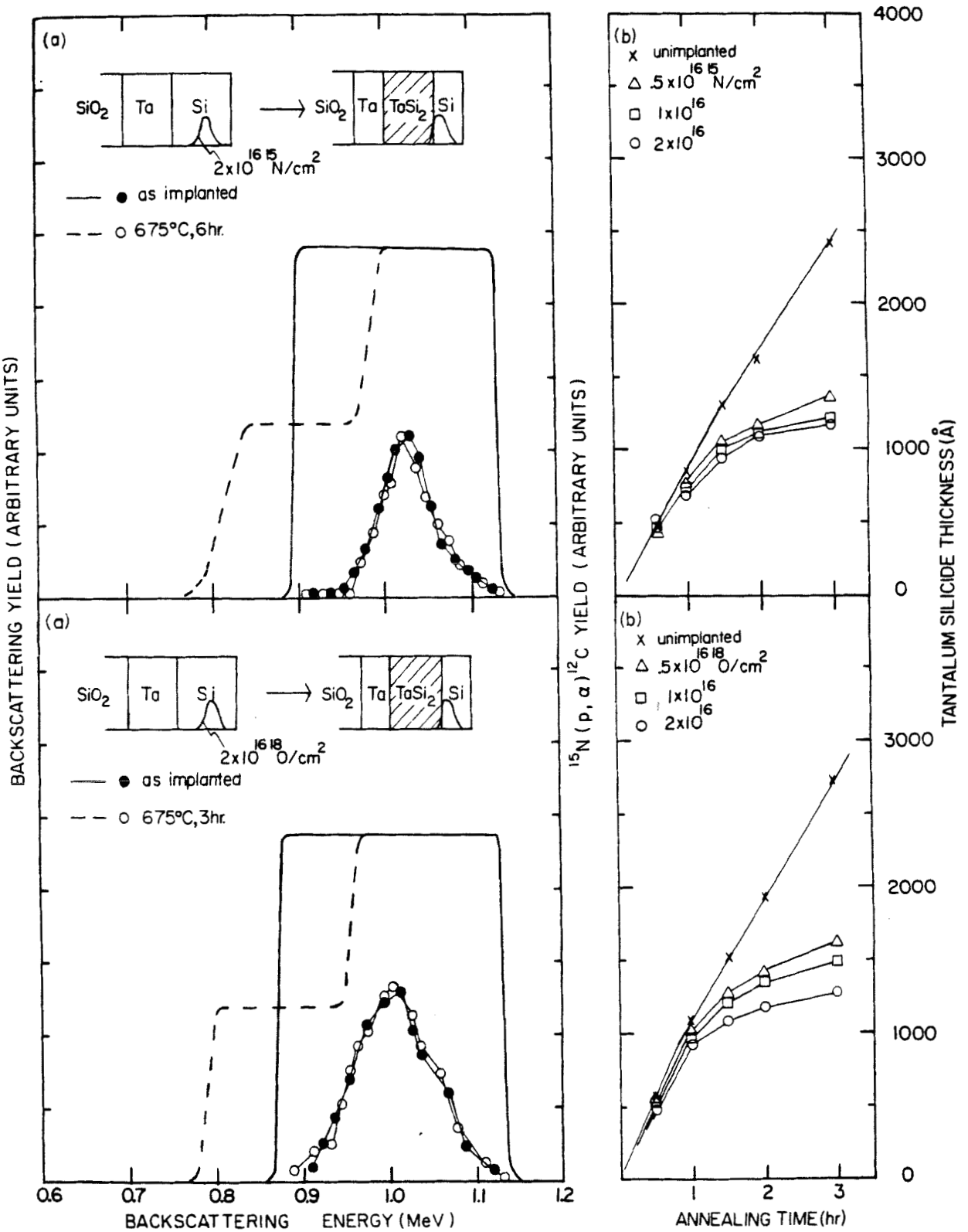
(a)
SiO2 Ta Si
SiO2 Ta TaSi2 Si
2x10^16 15 N/cm^2
as implanted
675°C,6hr.
(a)
SiO2 Ta Si
SiO2 Ta TaSi2 Si
2x10^16 18 O/cm^2
as implanted
675°C,3hr.
BACKSCATTERING YIELD (ARBITRARY UNITS)
0.6 0.7 0.8 0.9 1.0 1.1 1.2
BACKSCATTERING ENERGY (MeV)
(b)
unimplanted
.5x10^16 15 N/cm^2
1x10^16
2x10^16
(b)
unimplanted
.5x10^16 18 O/cm^2
1x10^16
2x10^16
15N(p,α)12C YIELD (ARBITRARY UNITS)
4000
3000
2000
1000
0
TANTALUM SILICIDE THICKNESS (Å)
1 2 3
ANNEALING TIME (hr)

fig.3,4

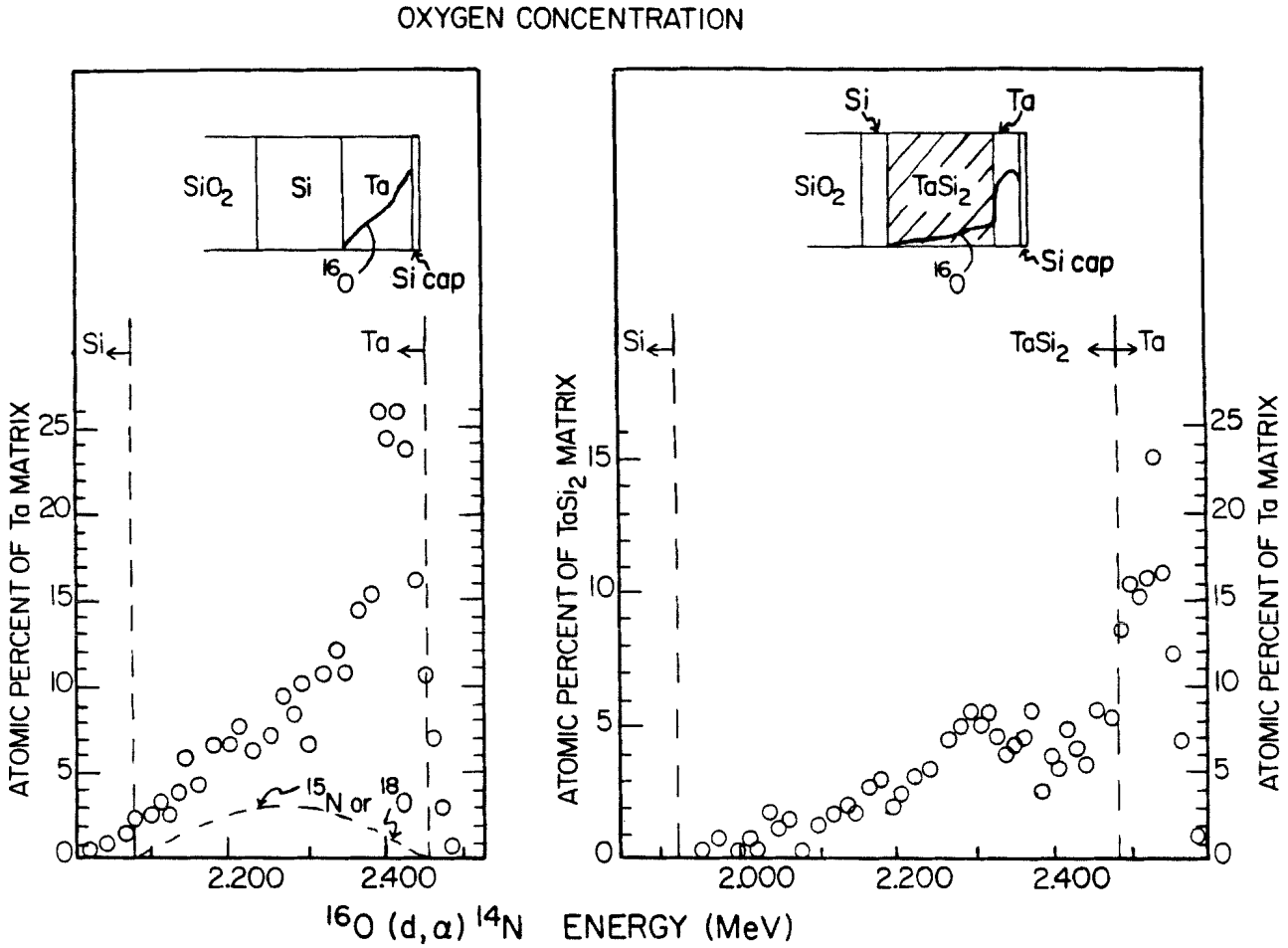
OXYGEN CONCENTRATION
SiO2
Si
Ta
16O
Si cap
Si
Ta
ATOMIC PERCENT OF Ta MATRIX
15N or 18O
2.200
2.400
16O (d,α) 14N
ENERGY (MeV)
SiO2
TaSi2
Si cap
TaSi2
ATOMIC PERCENT OF TaSi2 MATRIX
2.000

fig.5

APPENDIX C

EFFECT OF NITROGEN IMPURITIES ON MOLYBDENUM SILICIDE FORMATION

K.T.Ho and M-A. Nicolet

California Institute of Technology

Pasadena, California, 91125

D.M.Sott

University of California at San Diego,

La Jolla, California, 92093

ABSTRACT

In this study, N is introduced into a Mo film evaporated on a Si wafer. Nitrogen redistribution and alteration of silicide formation during subsequent annealing is investigated. It was found that N redistributes uniformly in the Mo film and becomes incorporated into the growing $MoSi_2$ layer without any segregation effect taking place. Nitrogen incorporation causes an incubation time in the growth of Mo_2Si, which lengthens with increasing nitrogen dose. Nitrogen also slows down the silicide growth while the parabolic growth pattern is retained.

I INTRODUCTION

Due to their low resistivity and high temperature stability, refractory metals and their silicides are vigorously investigated for their applicability as MOS gate, interconnect and contact materials in VLSI circuits[1,2]. Metal silicides have the additional desirable property of forming thermal silicon oxides for passivation[2,3]. In particular, both Mo and its disilicide have been demonstrated to be good gate materials from the point of view of their work function, resistance to chemical agents, ambient sensitivity and oxidizability[4].

In many of the reported works on Mo, nitrogen figures as a crucial partner in determineing the properties of Mo related materials. Kim and Brown[5] report a new process which nitridizes the top portion of a Mo layer to make Mo_2N/Mo gate MOSFET's. The nitride layer provides resistance against oxidation and processing agents, and improved ion-implantation masking. Nitridation of Mo also arouses interests in the field of superconductors[6], since theoretical calculations predict a very high transition temperature(~29°K) in the case of a metastable B1 structured MoN phase[7].

Another application of N in Mo comes n the form of a stuffed diffusion barrier between Au and Si[9]. This concept is further strengthened by a recent study of N incorporated in amorphous NiW diffusion barriers in which the highly sensitive technique of Schottky barrier height measurement is used to characterize the effectiveness of the barrier[10].

Nitrogen, oxygen and water vapor are the main constituents in the residual gas in a vacuum system[11]. Nitrogen and oxygen can be incorporated into materials deposited either by evaporation or sputtering[12]. In the future VLSI fabrication, plasma processing becomes attractive for anisotropic etching, in situ surface cleaning, chemical vapor deposition[13], or simply sputter deposition[4]. The concentraction of reactive atomic N species generated by the plasma rises rapidly with increasing residual gas pressure, and enhances the level of nitrogen contamination[14]. Impurity effects can affect metal and metal silicides in general. In the particular case of Mo, a few studies have already been reported. As an example, by increasing the residual gas pressure or substrate temperature, or decreasing the sputtering rate, Nagata and Shoji[14] has shown that the deposited Mo film starts out having the bcc structure of pure Mo, gradually incorporates increasing amounts of fcc γ-Mo_2N, and finally transforms completely into the nitride phase. In the same samples, deuterium activation

analysis shows that oxygen concentration is generally less than N, and no oxide phase is detectable. Nowicki et al.[15] pointed out that N and O incorporation can actually be beneficial by relieving the high compressive stress normally observed in Mo films, thereby allowing films as thick as 3 μm to be deposited without buckling. This stress free but impure Mo film still has a resistivity low enough(~130 $\mu\Omega$ cm) for many technical uses.

When N is incorporated into co-evaporated $MoSi_2$, it is found to have no effect on the resistivity of the silicide[16]. In this study, we investigate the metallurgical aspect of $MoSi_2$ which is formed from a Mo film evaporated on a Si substrate, when N is controllably incorporated in the Mo layer.

II EXPERIMENTAL PROCEDURES

An Mo film of 910 Å was evaporated on an <111> Si wafer. The deposition was carried out in an oil-free e-gun vacuum system with a base pressure of ~5 × 10^{-8} torr. Deposition rate was set at ~20 Å/s. A 310 Å thick Si cap was then deposited on top of the Mo film to prevent in-diffusion of ambient oxygen during annealing and sample storage. Nitrogen isotope ^{15}N was implanted into the Mo film at doses of 0.5, 1 and 2 × $10^{16}/cm^2$. The implantation energy was set at 90 KeV/N_2^+ for a calculated range of 415 Å and a ΔR of 340 Å. The thin Si cap has been neglected in the range calculation. Annealing was done in a quartz tube vacuum furnace pumped to a pressure of 5 × 10^7 torr.

Silicide thicknesses were monitored by 2 Mev $^4He^+$ Rutherford backscattering spectrometry (RBS). Nitrogen was profiled by $^{15}N(p,\alpha)^{12}C$ nuclear reaction analysis (NRA), using an incident proton energy of 1 Mev. Samples were tilted at 60° against normal incidence to obtain a depth resolution of ~250 Å. The detector was mounted in the plane of the sample normal and the proton beam, making an angle of 164° with the beam. Unintentional ^{16}O contamination

was checked using the $^{16}O(d,\alpha)^{14}N$ nuclear reaction. Description of this technique was given elsewhere[17].

III RESULTS AND DISCUSSION

Depending on the dose, implanted nitrogen can significantly alter the $MoSi_2$ growth kinetics. However, the silicide phase formed is unaltered. Thermal treatment at 510°C transforms the Mo and Si in the implanted samples into a single phase $MoSi_2$. Figure 1 shows that the $MoSi_2$ growth is diffusion controlled, with a $\sqrt{t}$ time dependence. The growth rate of the unimplanted reference sample and the low dose (0.5×10^{16}) implanted sample are the same within experimental accuracy. An extrapolation to zero silicide thickness seems to indicate an incubation time of ~15 min for these two samples. An implantation dose of $1 \times 10^{16}/cm^2$ reduce the growth rate substantially and lengthen the incubation time to ~50 min. At the even higher dose of 2×10^{16} N/cm^2, no silicide formation is observed up to 90 min. Some signs of silicide formation is finally visible after 120 min. annealing, and a measurable amount (~380 Å) is observed after 180 min. However this suppression of silicide growth is strongly temperature sensitive. By raising the annealing temperature to 550°C, $MoSi_2$ formation is completed in 30 min. even for the high dose ($2 \times 10^{16}/cm^2$) sample.

It is interesting that N reduces the $MoSi_2$ growth rate, but the diffusion limited growth pattern is still preserved. We can exclude any possibility that the slowing down of the growth is due to an interfacial mechanism since the kinetics demonstrates diffusion limited process. However, the incubation time observed is likely due to the existence of a interfacial barrier which is related to the implanted nitrogen. To investigate further the mechanism of N interference, nitrogen profiles at various annealing stages are obtained by NRA and plotted against the RBS peaks of the host Mo or $MoSi_2$ lattice.

Nitrogen profiles for the low dose ($0.5\times10^{16}/cm^2$) sample are shown in figure 2. The positions of the N and Mo signals are aligned by taking into consideration the different energy stopping powers of the two techniques used. After annealing for 180 min., The $MoSi_2$ reaction is almost completed. A thin Mo-rich layer still remains at the surface. A heavy N peak is located at the Mo/Si cap interface. The concentration is estimated to be $5 \times 10^{20}/cm^3$. NRA spectrum of a sample which was annealed only 90 min. (not shown here) shows that this sharp N peak exists even before the complete reaction of Mo into $MoSi_2$. The same spectrum also shows that N which is not a part of the peak begins to redistribute uniformily throughout the Mo layer. It can be seen in figure 2 that after 180 min. annealing, the N outside the surface peak is incorporated into the silicide layer, within which N concentration levels off at 0.2 at% (0.2 N per 100 lattice atom in $MoSi_2$), It can be seen that, other than the near surface peak, the incorporated N level is uniform throughout the silicide layer. This may imply that N is being incorporated at the same rate as Mo when the Mo/$MoSi_2$ advances toward the unreacted Mo layer. This scheme is consistent with the fact that Si is the moving species in $MoSi_2$ growth[18], provided that no segregation effect of N occurs. Further clarification is provided by the data from high dose samples, described in the following text.

The reaction of the Si cap with Mo is very slow compared to the Si substrate. This slow reaction is similiar to that reported by Bomchil et al.[19] in their study of laser induced $MoSi_2$ formation. The inertness of the Si cap is very likely due to the near surface oxygen peak which will be described later.

The large and uniform concentration of N throughout the silicide layer can interfere with the Si flux diffusing through it. For the sample implanted with a dose of $1 \times 10^{16}/cm^2$, the N content in the $MoSi_2$ layer rises and causes an enhanced interference in Si diffusion. Therefore, a slower and still diffusion

limited growth rate like the one shown in figure 1 results.

Nitrogen profiles for the high dose ($2\times10^{16}/cm^2$) sample are shown in figure 3b),c) and d). After annealing at 510°C for 120 min., the RBS spectra in figure 3a) shows a slight sign of reaction at the boundary of Mo and Si. Here also, a high N peak accumulates at the Mo/Si cap interface with a concentration of $\sim 18.5 \times 10^{20}/cm^3$, which is about 4 times larger than the corresponding peak in the low dose sample described before. A smaller peak appears at the Mo/Si interface. The rest of the N content spreads uniformly throughout the Mo layer at a concentration of $\sim 9.8 \times 10^{20}/cm^3$ or 1.5 at%. When the sample is further annealed at a higher temperature of 550°C for 30 min., a complete transformation of Mo into $MoSi_2$ occurs, except for a bump in the RBS peak of Mo, indicating an excess Mo over the stoichiometric composition of $MoSi_2$ at the near surface region. The sharp N peak appears unchanged by the silicide reaction. All the N outside this sharp peak now resides in the silicide layer at a level of $5.2 \times 10^{20}/cm^3$ or .53 at% (.53 N per 100 lattice atom of $MoSi_2$). Alternatively, this can be expressed as 1.6 N per 100 $MoSi_2$ formula. Within experimental error, the concentration ratio of N to Mo is the same before and after the conversion of pure Mo into the silicide.

Based on these results, the following model can be constructed, as illustrated in figure 4. During the initial period of thermal annealing, N in Mo has enough mobility to redistribute quickly, and either becomes trapped at the Mo/Si cap interface, the Mo/Si interface, or spread uniformily in the Mo film. Both the trapped interfacial N and the uniformily distributed portion have quantities proportional to the implanted dose. The effect of implanted N on the growth rate should be caused by the uniform portion and is, therefore, dependent on the implantation dose. When silicide formation proceeds, Si diffuses into the Mo lattice, incorporating N into the growing silicide at the same

rate as Mo, thus keeping the concentration ratio of N to Mo the same. The large N concentration incorporated by $MoSi_2$ contrasts with the results for $TaSi_2$[20] and $TiSi_2$[21], where N in the metal is predominantly rejected from the silicide layer, even though Si the dominant moving species in all three cases.

The N accumulation at interfaces may be due to the danggling bonds, vacancies and atomic steps and ledges which are associated with abruptly terminated lattices. From the high ^{15}N dose ($2\times10^{16}/cm^2$) sample, it is seen that a N peak also exists at the Mo/Si interface. This interface peak connot be observed in the two samples with lower implanted doses, due to faster reactions in them. However, it can be conjectured that the same N peak also exists in the two low dose samples with densities proportional to the implanted doses, since such a proportional relationship is observed for the Mo/Si cap interface peak. The incubation time for silicide formation can then be explained by suppression of interfacial reaction by the bulid-up of the N peak.

From bulk diffusivity data[22], the diffusion length of N in Mo exceeds the Mo film thickness in less than 1 second. The experimentally observed fast N diffusion in Mo is therefore consistent with such data. Although caution is required in extrapolating bulk data for thin film applications. In addition, implanted N may take a different chemical form compared to the nitrogen species involved in diffusion studies. From the same collection of diffusion data[22], a fast diffusion should also be expected for N in Ta. However, it was reported in a previous study that N seems to be immobile in Ta, except when subjected to a "snow ploughing" action of $TaSi_2$ growth[23]. This differing result may be due to either inapplicability of bulk data or the relatively low solid solubility of N in Ta (1.8 at% at 500°C)[24] compared to N in Mo (up to 28 at%)[25]. For high implanted dose ($2\times10^{16}/cm^2$), the peak concentration of N exceeds 2 at%. In case of Ta films, tantalum nitride phases may have already started to

form, thus immobilizing the implanted N. Whereas, N implanted into Mo at the same dose may still be in the form of a solid solution with a high diffusivity.

Since refractory metals are often contaminated by oxygen during deposition, it is important to know how oxygen can affect our experimental results. Figure 5a) to c) shows the redistribution of ^{16}O after various sample treatments. Two samples were implanted with 2×10^{16} N/cm^2, one had no annealing, the other was annealed at 510°C for 120 min., but did not form a significant amount of silicide. The third sample was implanted with 0.5×10^{16} N/cm^2 and annealed at 510°C for 180 min., most of the Mo film has reacted into $MoSi_2$. Some important points about the behavior of O can be picked out. (1) The total quantity of ^{16}O is conserved in the these samples, which had three different thermal treatments. This conservation indicates:that the Si cap prevents any O diffusion across it during annealing. (2) In the unannealed sample, O builds up towards the sample surface, reaching a peak concentration of 25 at%. It is believed that this build up is due to heating up of the vacuum chamber during evaporation, leading to faster outgassing from the chamber wall, towards the end of the film deposition. (3) In the high ^{15}N dose sample, a large portion of the O congregates near the surface during annealing, while the rest of the O spreads out uniformily in the Mo layer. (4) In the low ^{15}N dose sample, O is uniformily incorporated into the growing silicide layer. From these observations, we know that any effect that O may have on the growth kinetics of $MoSi_2$ is not intensified by prolonged annealing, because no O diffuses into the sample. Since a large amount of the O tends to accumulate near the surface, away from the Mo/$MoSi_2$ interface, O effects on the silicide reaction is automatically reduced. However, the small amount of oxygen which still remains near the Mo/Si interface may explain the incubation time for the sample with no ^{15}N implantation. This O accumulation can also explain the

residual Mo bump which persists after long annealing. It is possible that the combined effect of O and N accumulation may suppress silicide formation more effectively than either type of impurities alone.

IV CONCLUSIONS

A fast diffusion of N implanted into a Mo film is observed at an annealing temperature of 510°C. An interfacial N layer is trapped between Mo and the top Si encapsulation. The concentration of this layer is porportional to the implantation dose and does not change during subsequent silicide formation. The remaining N spreads uniformly in Mo and can have either no effect ($0.5\times10^{16}/cm^2$) or can significantly slow down ($1\times10^{16}/cm^2$) the $MoSi_2$ growth rate, or can inhibit $MoSi_2$ growth ($2\times10^{16}/cm^2$) for up to 90 min. annealing time, depending on the implanted dose. For the high dose ($2\times10^{16}/cm^2$) implanted sample, silicide reaction can be forced to completion by using a higher annealing temperature of 550°C. Nitrogen is incorporated into the silicide in the way that preserves the concentration ratio of N to Mo atoms before and after silicide formation.

ACKNOWLEDGEMENTS

The authors would like to acknowledge Ali Ghaffari for technical assistances. Discussions with M.Bartur, C.D.Lien and F.C.T.So have been very interesting and helpful.

REFERENCES

1 A.K.Sinha, *J.Vac.Sci.Technol.*, 19(1981)778.

2 S.P.Muraka, *J.Vac.Sci.Technol.*, 17(1980)775.

3 M.Bartur and M-A.Nicolet, *J.Electroch.Soc.*, 131(1984)371.

4 T.P.Chow, *IEEE Trans.Electr.Dev.*, ED-30(1983)598.

5 M.J.Kim and D.Brown, *IEEE Trans.Electr.Dev.*, ED-30(1983)398.

6 W.W.Fuller,S.A.Wolf,D.V.Gubser,E.F.Skelton and T.L.Francavilla, *J.Vac.Sci.Technol.*, A1(1983)517.

7 W.E.Pickett,B.M.Klein and D.A.Papaconstantopoulos, *Physica*, 107B(1981)667.

8 M-A.Nicolet and M.Bartur, *J.Vac.Sci.Technol.*, 19(1981)786.

9 R.S.Nowicki and I.Wang, *J.Vac.Sci.Technol.*, 15(1978)235.

10 M.F.Zhu,F.C.T.So and M-A.Nicolet, *Thin Solid Films*, (to be published)

11 L.T.Lamout,Jr., *J.Vac.Sci.Technol.*, 10(1973)251.

12 N.W.Cheung,M-A.Nicolet,M.Wittmer,C.A.Evans,Jr. and T.T.Sheng, *Thin Solid Films*, 79(1981)51.

13 J.L.Vossen, *J.Vac.Sci.Technol.*, 19(1981)761.

14 S.Nagata and F.Shoji, *Jap.J.Appl.Phys.*, 10(1971)11.

15 R.S.Nowicki,W.D.Buckley,W.D.Mackintosh,I.V.Mitchell, *J.Vac.Sci.Technol.*, 11(1974)675.

16 F.Neppel,G.Menzel and U.Schwabe, *J.Electroch.Soc.*, 130(1983)1174.

17 S.T.Picraux, *Nucl.Instr.Meth.* ,149(1978)289.

18 J.Baglin,F.d'Heurle,S.Petersson and C.Serrano, *Appl.Phys.Lett.*, 33(1978)289.

19 G.Bomchil,D.Bensahel,A.Golanski,F.Ferriell,G.Auvert,A.Perio and J.C.Pfister, *Appl.Phys.Lett.* ,41(1982)46.

20 K.T.Ho,C.D.Lien,M-A.Nicolet and D.M.Scott, MRS Proceedings Volume *Thin Films and Interfaces*, edited by J.E.E.Baglin,D.R.Campbell and W.K.Chu, (North-Holland,New York,in press).

21 K.T.Ho and M-A.Nicolet, (to be published)

22 E.Fromm and E.Gebhart, *Gase und Kohlenstuff in Metallen*, (Springer,Berlin,1976).

23 K.T.Ho,C.D.Lien,M-A.Nicolet and D.M.Scott, MRS Proceedings Volume *Thin Films and Interfaces*, edited by J.E.E.Baglin,D.R.Campbell and W.K.Chu, (North-Holland,New York,in press).

24 R.P.Elliott, *Constitution of Binary Alloys, First Supplement*, McGraw-Hill,New York,1965.

25 M.Hansen and K.Anderko, *Constitution of Binary Alloys*, McGraw-Hill,New york,1958.

FIGURE CAPTIONS

figure 1 Growth kinetics of $MoSi_2$. Implanted N can either have no effect on or slow down the silicide growth rate, or inhibits silicide formation, depending on the implanted dose. An incubation time is observed for all samples.

figure 2 Low dose (0.5×10^{16} N/cm^2) implanted sample before and after 510°C annealing for 180 min. Annealed sample has a sharp N peak at the silicide/Si cap interface. The rest of the N content is uniformily incorporated into $MoSi_2$.

figure 3 (a) RBS spectra for the high dose (2×10^{16} n/cm^2) sample: as implanted, after 120 min. annealing at 510°C, and after an additional 30 min. annealing at 550°C. b) Nitrogen profile for the as implanted sample. c) After 510°C annealing for 120 min., very little reaction has occurred. nitrogen redistributes uniformily in the Mo film, at a concentration of 1.5 at%. In addition, a large peak formed near the surface. d) By raising the annealing temperature to 550°C, silicide reaction proceeds to completion in 30 min. Nitrogen is uniformily incorporated into $MoSi_2$, keeping the concentration ratio of N to Mo constant.

figure 4 Schematic description of the N redistribution process. The Model is based on the results shown in figure 3.

figure 5 Redistribution of the incorporated ^{16}O. Oxygen uniformily redistributes during 510°C annealing in unreacted Mo, and is uniformily incorporated into the silicide when reaction occurs at 550°C. The total quantity of O is conserved in the three samples shown.

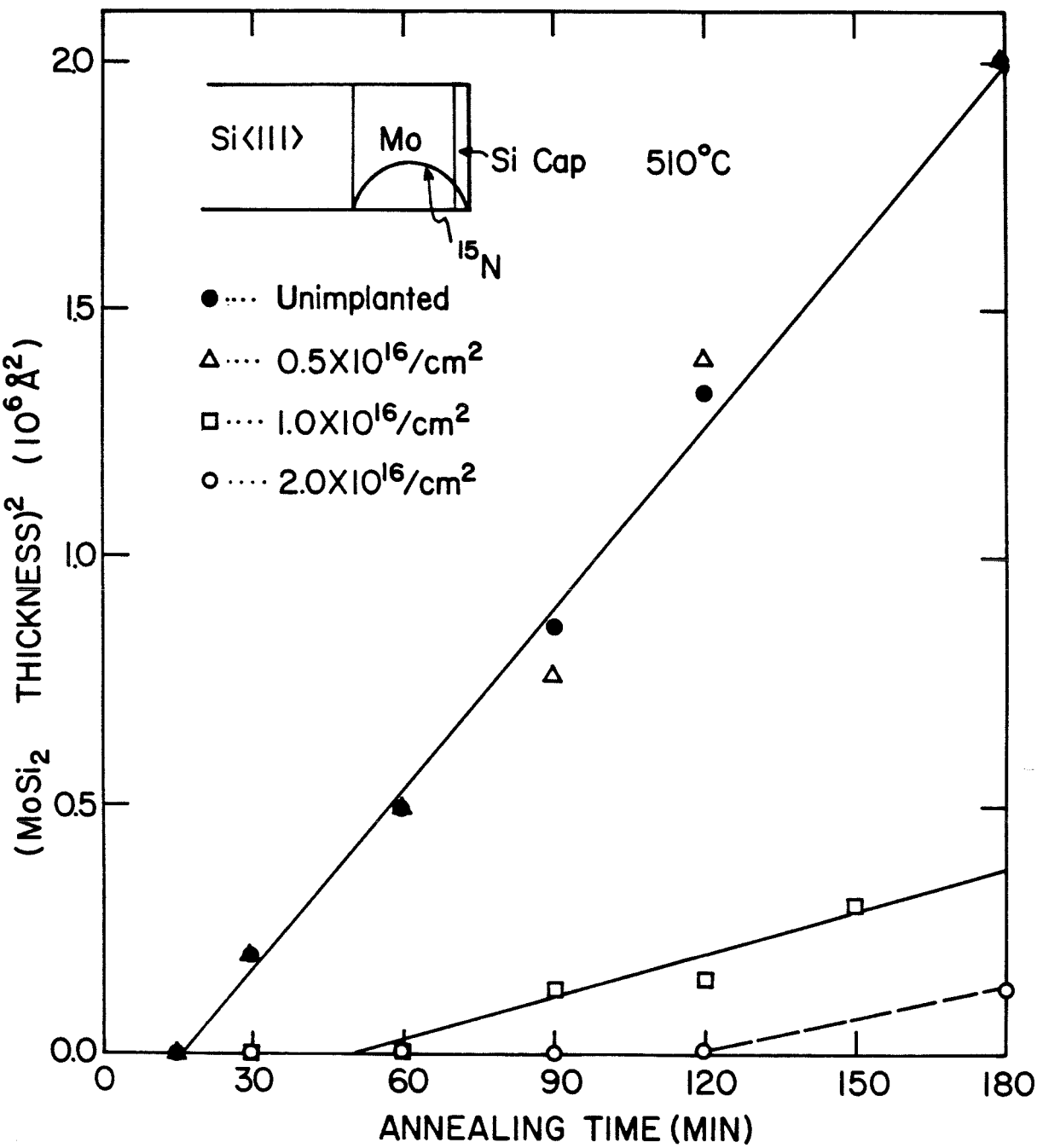
Si<111>
Mo
Si Cap
510°C
^{15}N
Unimplanted
0.5X10^{16}/cm^2
1.0X10^{16}/cm^2
2.0X10^{16}/cm^2
(MoSi$_2$ THICKNESS)^2 (10^{6}Å^2)
2.0
1.5
1.0
0.5
0.0
0
30
60
90
120
150
180
ANNEALING TIME (MIN)

fig.1

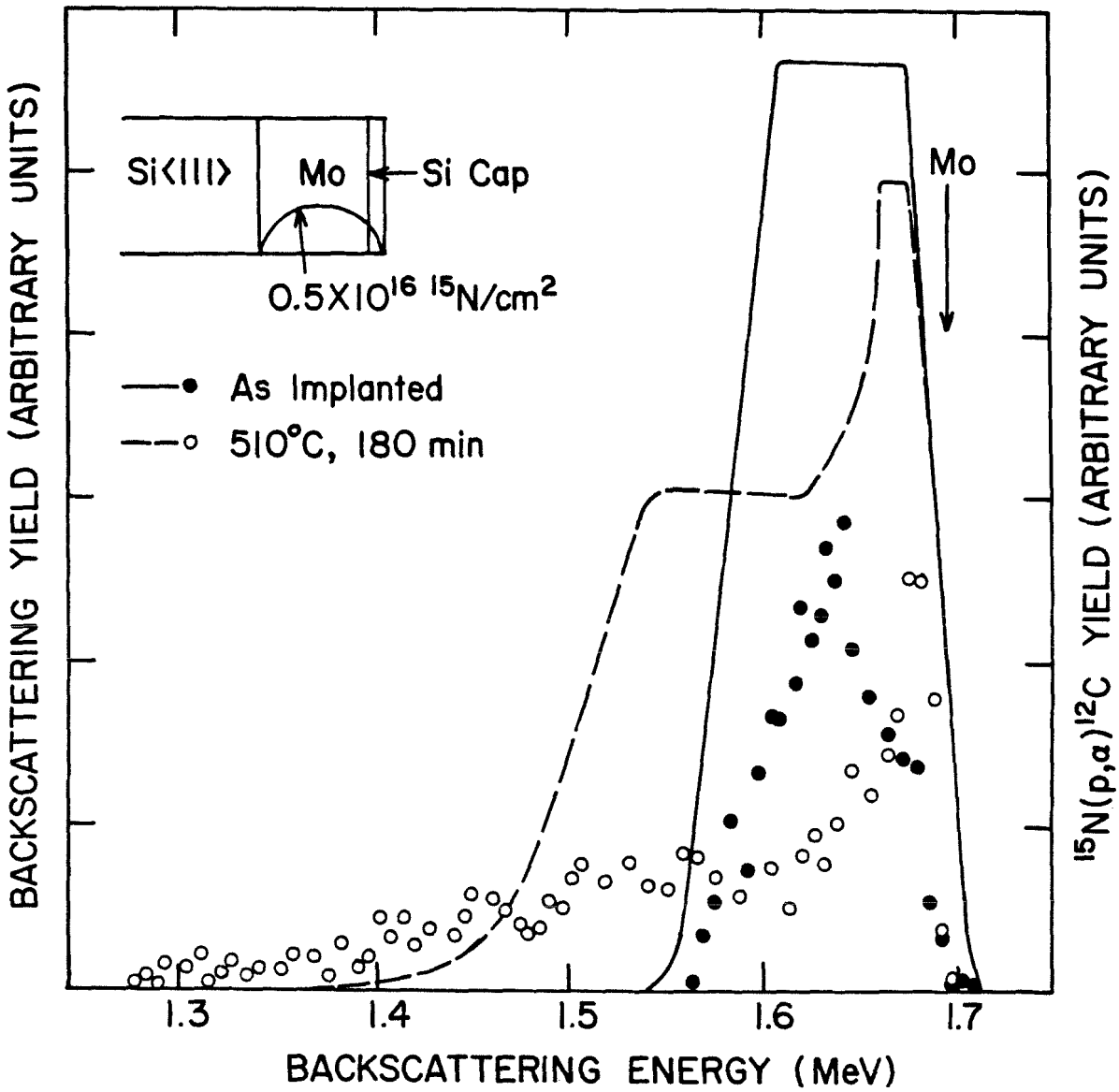
Si<111>
Mo
Si Cap
0.5X10^16 15N/cm2
As Implanted
510°C, 180 min
Mo
BACKSCATTERING YIELD (ARBITRARY UNITS)
15N(p,α)12C YIELD (ARBITRARY UNITS)
1.3
1.4
1.5
1.6
1.7
BACKSCATTERING ENERGY (MeV)

fig.2

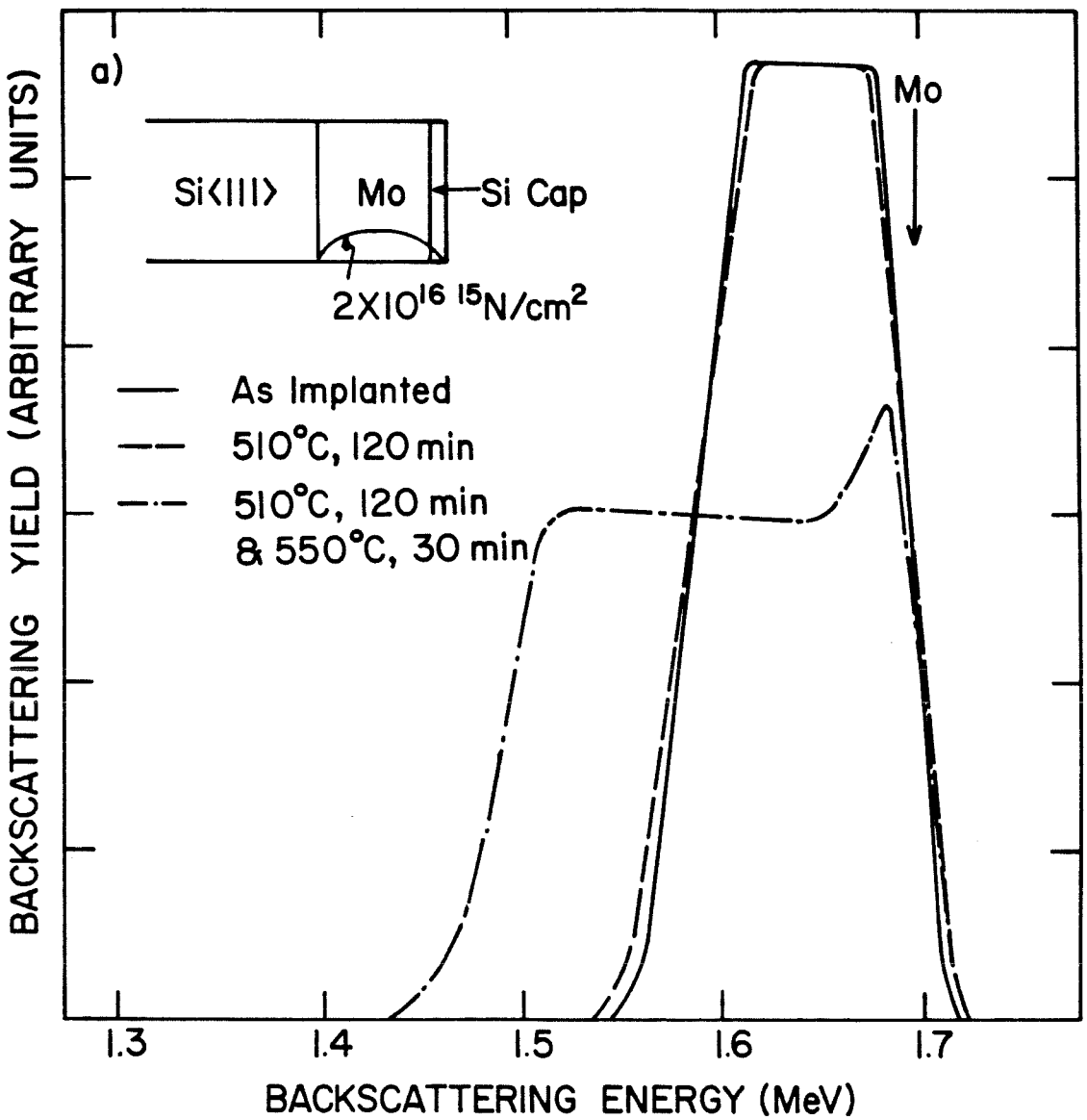
a)
Si<111>
Mo
Si Cap
2X10^16 15N/cm2
As Implanted
510°C, 120 min
510°C, 120 min
& 550°C, 30 min
Mo
BACKSCATTERING YIELD (ARBITRARY UNITS)
1.3
1.4
1.5
1.6
1.7
BACKSCATTERING ENERGY (MeV)

fig.3a

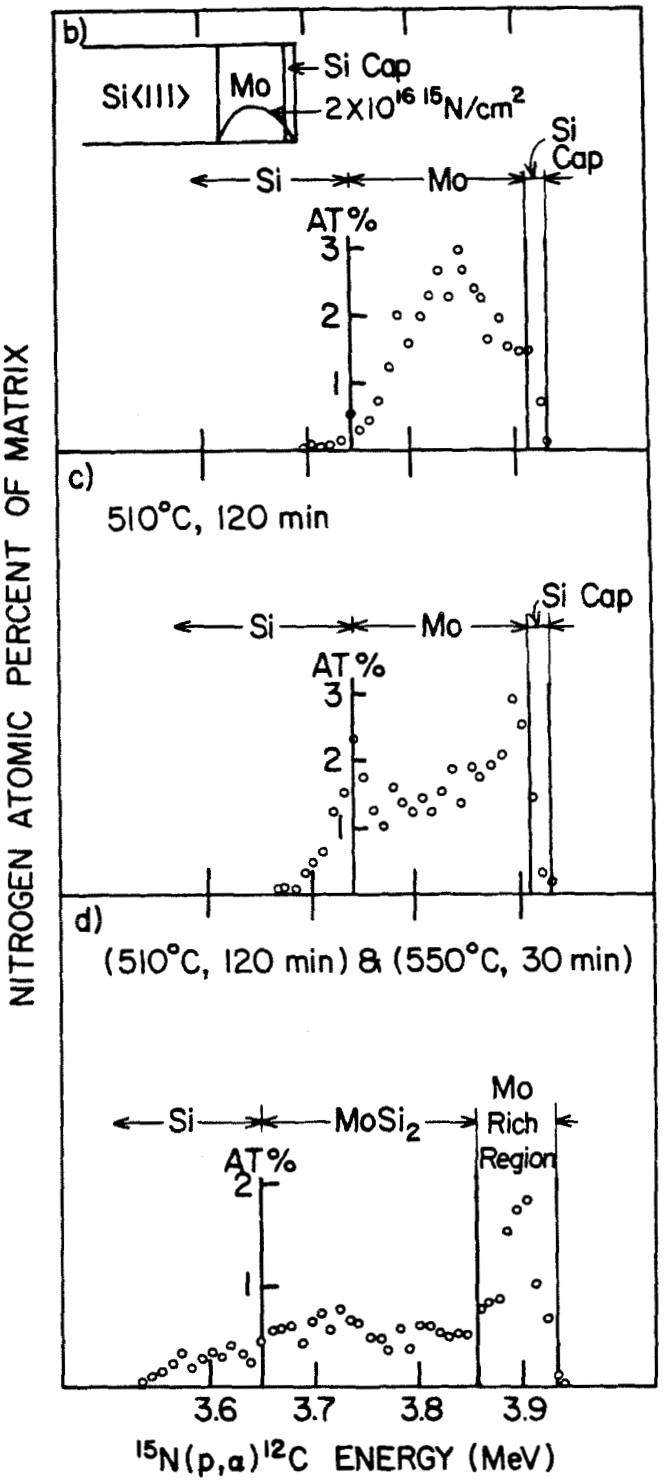
b)
Si<111>
Mo
Si Cap
2X10^16 15N/cm^2
Si
Cap
Si
Mo
AT%
3
2
1
c)
510°C, 120 min
Si Cap
Si
Mo
AT%
3
2
1
d)
(510°C, 120 min) & (550°C, 30 min)
Si
MoSi2
Mo
Rich
Region
AT%
2
1
3.6
3.7
3.8
3.9
15N(p,α)12C ENERGY (MeV)
NITROGEN ATOMIC PERCENT OF MATRIX

fig.3b,c,d

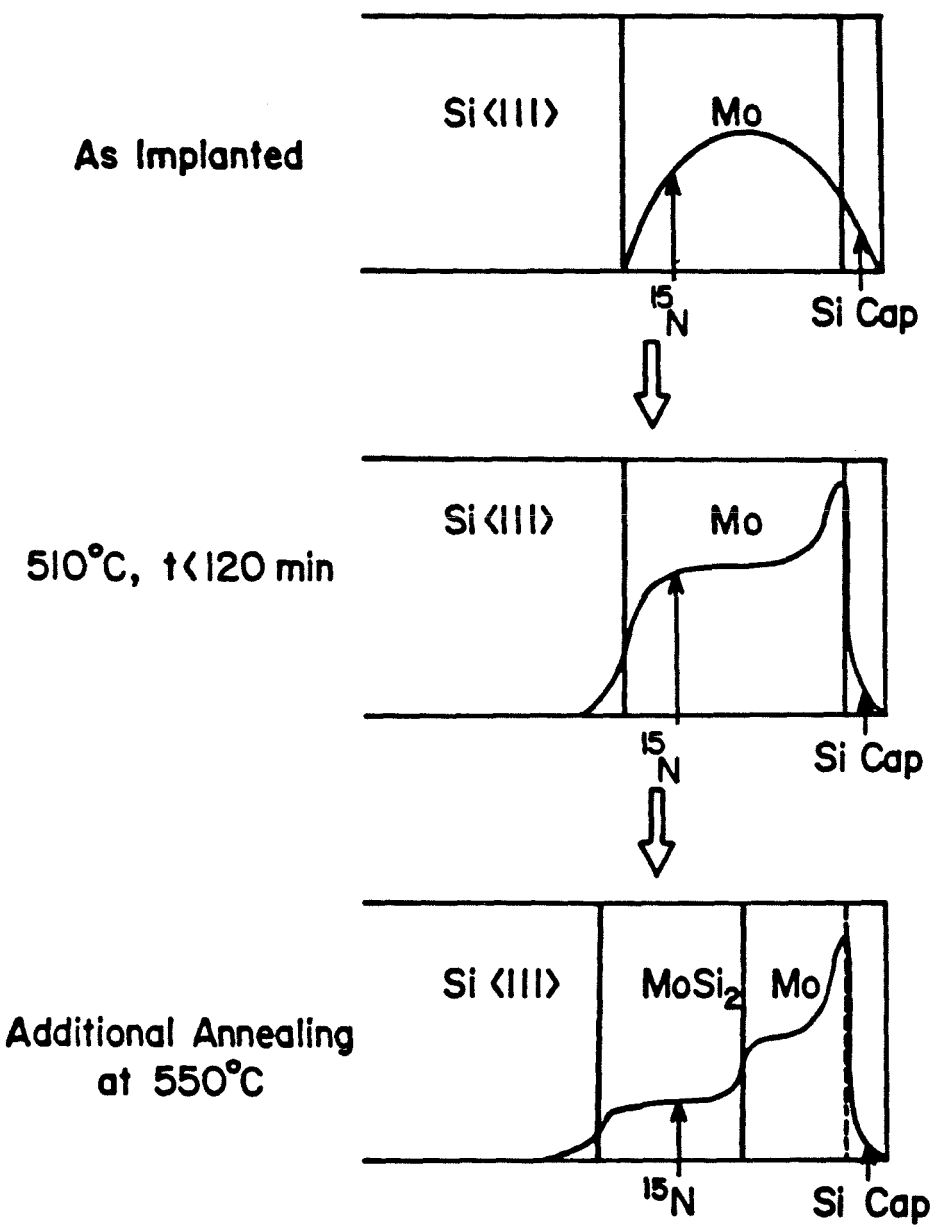
As Implanted
Si⟨111⟩
Mo
15N
Si Cap
510°C, t<120 min
Si⟨111⟩
Mo
15N
Si Cap
Additional Annealing
at 550°C
Si ⟨111⟩
MoSi2
Mo
15N
Si Cap

fig.4

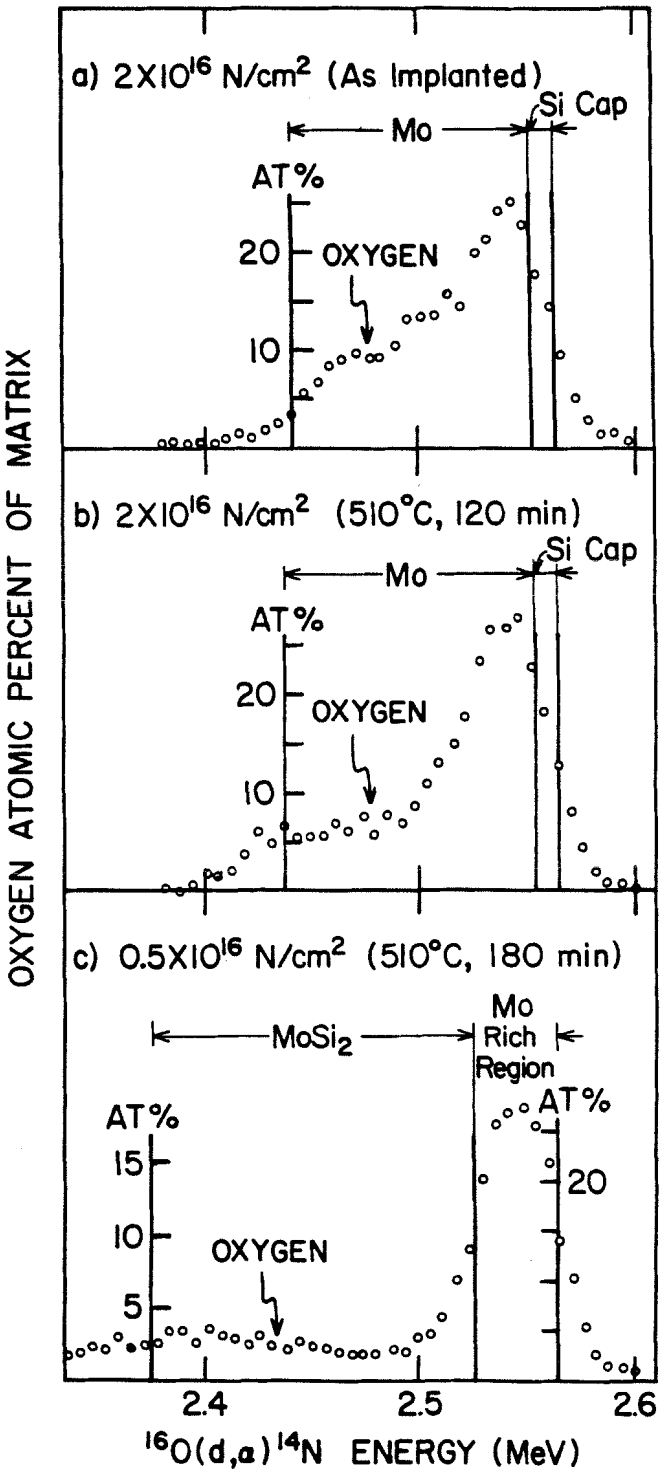
a) 2X10^16 N/cm^2 (As Implanted)
Si Cap
Mo
AT%
20
OXYGEN
10
b) 2X10^16 N/cm^2 (510°C, 120 min)
Si Cap
Mo
AT%
20
OXYGEN
10
c) 0.5X10^16 N/cm^2 (510°C, 180 min)
MoSi2
Mo Rich Region
AT%
15
10
OXYGEN
5
AT%
20
2.4
2.5
2.6
16O(d,α)14N ENERGY (MeV)
OXYGEN ATOMIC PERCENT OF MATRIX

fig.5

APPENDIX D

AN INERT MARKER STUDY FOR PALLADIUM SILICIDE FORMATION: Si MOVES IN POLYCRYSTALLINE Pd_2Si

K.T.Ho,C.D.Lien,U.Shreter, and M-A. Nicolet

California Institute of Technology,

Pasadena,California,91125

ABSTRACT

A novel use of Ti marker is introduced to investigate the moving species during Pd_2Si formation on <111> and <100> Si substrates. Silicide formed from amorphous Si is also studied using a W marker. Although these markers are observed to alter the silicide formation in the initial stage, the moving species can be identified once a normal growth rate is resumed. It is found that Si is the only moving species for all three types of Si crystallinity. However, Pd will participate in mass transport when Si motion becomes obstructed.

I INTRODUCTION

Pd_2Si is one of the most extensively studied metal silicides, both because of its viability as an integrated circuit contact material, due to palladium's dissolving power for surface oxides[1], and its various unique characteristics. Pd_2Si has a low formation temperature, but is stable up to ~750°C[2]. Of the many metal silicides which grow epitaxially on crystalline Si substrates, only Pd_2Si occurs as the first phase[3,4,5]. Reports on properties of Pd_2Si such as the epitaxial quality[6], electrical properties[7], formation kinetics and mechanism[2,6], and impurity effects[8] are abundant in literature.

One uncertainty about Pd_2Si which still remains is the identity of the moving species responsible for the growth. The identity of the dominant moving

species is relevant for processing considerations such as lateral silicide growth from contact windows[9,10],smoothness of silicide silicon interface and generic trends in silicide oxidation rates that are associated with the moving species[11]. Two earlier works by Chu et al.[12] and Pretorius et al.[13] reported that both Pd and Si move during Pd_2Si formation from a Pd film on single crystalline Si. However, it was recently pointed out by Scott and Nicolet that a reinterpretation of the experimental data from the above two references is possible and that an agreement can be reached with their new result that Si is actually the dominant moving species[8]. Other works have contained information on the moving species. Föll and Ho[14] concluded that both elements move based on the incorporation of interfacial oxides within the final silicide layer. However, Scott et al.[1] proposed that Pd motion is involved only during the initial oxide reducing process. The dissolved oxide layer is then incorporated in the silicide during the subsequent Si motion, which gives a final appearance of two species moving simultaniously. Cheung et al.[6] suggested that the interfacial voids observed at the Pd/silicide interface may be due to a predominant motion of Pd. They further suggested that moving species may differ for silicides formed from <111>,<100> Si substrates, and amorphous Si. More recently, Lien and Nicolet[15] using an epitaxial structure concludes that Pd is the moving species. The same authors, in another study[16], repeated the interfacial oxide marker experiment, and find that both species move in the unirradiated sample, but only Si moves after breaking up the interfacial oxide by Xe irradiation. These previous results along with the results from this study to be explained in the following text are summarized in table I. The structure of the Pd_2Si layer grown on <111> Si is reported to be polycrystalline or poorly epitaxial in every case except Lien and Nicolet's[15] work, as labelled in the footnotes. This fact will be important for the discussions at the end of the paper. The variation in opinions from previous studies is evident and motivated the present marker investigation

using substrates of different orientations and amorphous Si.

TABLE I

Results of previous studies.

AUTHORS	REF.	MARKER	INITIAL LOCATION OF MARKER	YEAR	Si TYPE	IDENTI-FICATION
W.K.Chu et al.	12	Argon	in Si	1975		Both
R.Pretorius et al.	13	^{31}Si	Top layer of Si	1978	<100>	Both
N.Cheung et al.	6	Kirkendall voids	at Pd/Pd_2Si & Pd_2Si/Si interfaces	1979	<111> <100> a. Si	Both Pd Pd
H.Föll et al.	14	Interfacial oxide	at Pd/Si interface	1981	<111>	Both
D.M.Scott et al.	8	oxygen	in Pd	1983	<100>	Si
C.D.Lien et al.	15	Epitaxial structure	Pd_2Si	1984	<111>	Pd[a]
C.D.Lien et al.	16	Interfacial oxide	at Pd_2Si interface	1984	<111>	no i.i.[b]: Both w. i.i.[c]: Si
K.T.Ho et al.	This work	W,Ti	in Pd_2Si	1984	<111> <100> a.Si	Si(Pd)

a) in epitaxial Pd_2Si
b) no i.i. = No ion irradiation
c) w. i.i. = with ion irradiation

The concept of an inert marker has been demonstrated by Chu et al.[12] using the implanted noble gases Xe and Ar. Van Gurp et al.[17] introduced an evaporated discontinuous W film as a marker which eliminates implantation damage to the sample lattice. We studied silicide formation from amorphous Si with the latter marker type. The sample configuration consists of a W marker placed between the Pd film, which is evaporated on an oxidized Si substrate, and the top amorphous Si layer. This configuration is advantageous for analysis by backscattering spectrometry, because backscattering signal of the heavier W will not interfere with the signal of the lighter Pd. However, to form silicide from single crystalline Si, Pd must be evaporated on top of the Si substrate and the marker, which produces an interference between the signals of the Pd film and

the W marker. A lighter element Ti is therefore used in place of the W. Since Ti has a smaller backscattering cross section, a thicker layer is desirable, which however goes against the criterion that a marker should not interfere with the silicide formation.

II EXPERIMENTAL PROCEDURES

Samples were e-gun evaporated in an oil-free high vacuum system pumped to $3x10^{-6}$ torr pressure. For silicide formation on <111> and <100> Si substrates, Pd films were deposited simultaneously by loading half wafers of each orientation side by side. The cleaning procedures for oxidized Si substrates consisted of ultrasonic cleaning in trichloroethylene, acetone, and methanol. The <111> and <100> Si wafers had, in addition to the above, an etch in 20% HF, followed by an RCA solution etch (H_2O_2 :NH_4OH:H_2O in the ratio 1:1:5), and finally another etch in 6% HF. A sequence of evaporations in the order :~20 Å Pd, ~10ÅTi, ~20 Å Si and finally 1550 Å Pd was then carried out with $4x10^{-7}$ background pressure during evaporation. The Pd evaporation rate was ~20Å/s. The purpose of the sandwich layers next to the marker is to cause it to be incorporated into the silicide layer during the initial stage of annealing and thereby minimize the possibility of interfacial dragging. The sample with amorphous Si was evaporated in the reverse order on an oxidized Si wafer. Amorphous Si of 970Å thickness was evaporated on top of sandwich layers containing ~20Å Pd,~6Å W and ~20Å Si ,which were evaporated on 1900 Å Pd. Annealing was carried out in $5x10^{-7}$ vacuum. The annealing temperatures used were 250, 300 and 350°C for samples with a W, a thin Ti and a thick Ti marker, respectively. Silicide thicknesses were measured by 2 Mev $^4He^+$ backscattering spectrometry, with the detector set at an angle of 170° against the incident beam. No x-ray diffraction was performed to verify the silicide phase formed, since the formation of Pd_2Si has been extensively reported in the literature.[2,3,6]

The ratio of the Pd and Si backscattering peak heights does confirm a stoichiometry consistent with that of Pd_2Si.

Silicide growth requires the mass flow of one or both elements across the marker, leaving a different amount of material in front of it. This is equivalent to having a cover layer of changing energy loss, and therefore produces a shift in the position of the marker signal in the backscattering spectrum.

III RESULTS AND DISCUSSION

The spectra for the Pd/< 111> Si sample before and after annealing at 300 °C for 7 min. are shown in figure 1a. Some spreading of the marker signal occurred during the silicide growth. The spreading is not strictly consistent with the notion of an inert marker. However, if the spread is symmetrical and small, the peak of the distribution still fulfills the function of an inert marker. The marker shift, ΔE, is taken to be the amount by which the center of the marker peak has moved. Since two sample configurations are studied, we must adopt a sign convention for ΔE that is consistently used, irrespective of the sample configuration being referred to. In the following discussion, a ΔE which designates dominant Si motion will be taken as positive. By this convention, the Pd/< 111> Si sample shows a marker shift of +9.4 keV after forming 1580 Å of Pd_2Si. The Pd/< 100> Si sample, whose spectra are not shown, has a Pd_2Si layer of 1440 Å thickness and a marker shift of +11.3 keV after the same heat treatment. Figure 1b shows the spectra for the Pd/amorphous Si sample, which has a W marker, before and after annealing at 250°C for 25 min. A ΔE value of +22.5 keV is measured for a silicide thickness of 1830 Å.

In figure 2a, marker shifts for the three sample configurations are plotted as a function of the corresponding silicide thicknesses. The top and bottom

solid lines are the calculated values for the two extreme cases of Si or Pd moving only, respectively. It is found that the data points can be fitted very well to lines which have the same slopes as the calculated solid line that assumes that only Si moves. However, these three lines do not have zero intercepts as observed in previous marker experiments.[12,16] For the Pd/<111> sample, up to 1060 Å of silicide forms without producing a marker shift. To investigate this anomalous initial behavior, we plotted the growth kinetics of these samples and compared them to a reference sample which had no marker(see figure 2b). In all cases the growth rates are the same, however an incubation time is seen for samples with a marker layer, as has been reported by van Gurp et al.[17] This delayed reaction of Pd with Si was also reported by Bower and Mayer for Si with a thin surface oxide layer[18]. These facts suggest that a different growth mechanism prevails during the initial annealing period when a barrier action, apparently associated with the marker, must first be overcome. From a similiar experiment involving a thin interfacial oxide, Scott et al.[1] proposed that Pd acts as the moving species during the penetration of the oxide barrier; Si assumes its natural role as the dominant moving species only after a uniform dissolution of the obstructive oxide by the growing silicide layer has occurred. Alternatively, when the oxide layer is first broken up by Xe irradiation, as was carried out by Lien and Nicolet[16], Si is identified as the moving species. We propose that, in our case, the presence of the marker layer only partially obstructs Si flow, such that both Pd and Si contribute to the mass transport, giving a negligible marker shift in the initial stage of silicide formation. Once a smooth transport of Si becomes possible, as indicated by the unhindered silicide growth rate, Si then becomes the dominant moving species.

To check this assumption, a second set of samples was prepared using a thicker marker of ~20 Å Ti. The annealing temperature was raised to 350°C to

facilitate breaking down of this thicker barrier. The marker shifts as a function of silicide thickness and the growth kinetics of the silicide for this set of samples are plotted in figure 3a and 3b. An apparent dominance of Pd motion is indeed observed at the start of annealing; the corresponding growth kinetics is irregular and slow. With increasing silicide thickness, the growth rates accelerate towards that of the reference sample. Simultaneously, the marker shifts indicate a rising contribution of Si to the total mass transport. These results strongly support a dual moving species model for Pd_2Si growth. Silicon serves as the dominant moving species whenever its diffusion in the silicide layer is free of obstructing barriers (eg. impurities, epitaxial structure). When a free Si diffusion becomes hindered, Pd participation in the mass transport will be activated. This dual moving species process can be recognized by an accompanying reduction in the silicide growth rate as compared to a sample in which Si diffusion is unobstructed. Qualitatively, the greater the participation of Pd motion, the greater will be the reduction in the silicide growth rate.

The capricious nature of Pd to participate in diffusion when Si traffic is impeded may explain much of the confusion which has clouded the past studies. In particular, a comparison should be made to the structural marker study of Lien and Nicolet[15], in which it is found that Pd diffuses through an epitaxial Pd_2Si layer and supports the epitaxial growth of Pd_2Si on an <111> Si substrate. The dominance of Pd motion in that case can be justified by assuming that lattice diffusivity of Si in good quality epitaxial Pd_2Si is low and therefore Pd diffusion dominates. A good epitaxial quality of the Pd_2Si layer is verified by channeling. The silicide formed on our <111> substrates is expected to have poorer epitaxial quality than that formed (at 400)deC) by Lien and Nicolet, because of the incorporation of impurities (Ti) and our lower annealing temperature (300°C). Indeed, TEM studies have shown that our silicide

film on the <111> substrate is composed of preferentially oriented polycrystallites with grain sizes ranging from 300 to 900 Å. The grain boundaries should serve very well as open channels for Si diffusion. Further verification of a poor epitaxial quality comes from channeling measurements. The channeled RBS signal of Pd in Pd_2Si showed no more than 2% decrease in yield, compared to the more than 15% decrease in the channeling yield of Lien and Nicolet[15]. Therefore, for our <111> samples, Si diffusion is not impeded and Si is the dominant moving species.

It is instructive to review the results listed in Table I in the light of the dual-moving-species model proposed here. Chu et al.[12] implanted $1 \times 10^{16}/cm^2$ into Si as a marker. Although Ar surely behaves differently than N in bulk Si, it is possible, but not certain, that Ar can form a barrier to Si diffusion the way N does. The result of the experiment then will indicate that both species move, as was in fact reported. The actual initial position of the Ar marker, however, seems to be in doubt in that experiment[8]. Pretorius et al.[13] also concluded that Pd and Si both move, based on experiments with radioactive ^{31}Si tracer and arguments that were later refined by invoking physically realistic models, but without changing the conclusion[19]. The annealings in their experiment were carried out at 400°C, which is substantially higher than most other experiments and may not be a negligible factor. The substrate cleaning procedure is not reported in that paper and it is possible that an initial Pd motion was activated by impurities. Föll and Ho's interfacial oxide does not qualify as an inert marker according to the present view, and as was already pointed out by Scott et al[1]. The invalidity of the interfacial oxide as a marker is further confirmed by the results of Lien and Nicolet[16], who finds that the outcome differs before and after ion irradiation. The oxygen marker studies of Scott and Nicolet[8], as well as the structure marker study of Lien and Nicolet[15] support the dual-moving-species

model explicitly. All these experimental studies are thus compatible with the notion of dual moving species. Only Cheung et al.'s result are difficult to reconcile with the present model. Their conclusion is based on the observation of interfacial voids in cross-sectional TEM micrographs that are interpreted as Kirkendall voids[6]. It would be very desirable to repeat some of these experiments with special attention given to the details of sample preparation, the Si configuration, and the annealing temperature that the dual-moving-species model dictates. In particular, that model predicts that the growth rate of epitaxial Pd_2Si on <111> Si should be significantly less than that of polycrystalline Pd_2Si on Si of a different structure. The results of Cheung et al. are in qualitative agreement with that prediction. The present investigation should also be repeated with other marker species, since the inert nature of any particular marker can never be firmly established.

When the dual moving species model is applied to a study of Pd_2Si formation in the presence of nitrogen implanted into Si, further confirmations are found. The N profiles before and after silicide formation are shown in figure 4. The horizontal axes are labeled in energy to aid the visualization of the relocation of the energy stopping medium. The signal heights are the normalized nuclear reaction yields; however, the vertical axes are also labeled in atomic per cent of nitrogen in its respective matrices. Nitrogen becomes completely incorporated into Pd_2Si after a thermal treatment of 580 min. at 230°C and 10 hr. at 350°C. The peak concentration increases over the original value and the profile width becomes correspondingly narrower. Another significant feature is the shift of the entire peak towards lower energy (deeper into the sample). The alteration of the profile shape can only come about by a greater loss of Si than the gain of Pd in the nitrogen-concentrated region (comparison is made with the quantity of each element weighted by its stopping

cross section factor). The peaking of the N profile suppresses the diffusion of Si and initiates that of Pd, leading to a medium of greater stopping power in front of the N peak and thus the observed shift along the energy axis.

IV CONCLUSION

We have shown that Si is the dominant moving species during the formation of Pd_2Si under a normal condition. The criterion for a normal condition is that the silicide layer is polycrystalline and the growth rate is the same as that of a reference sample without a marker. Pd diffusion participates in the mass transport when Si motion becomes obstructed(i.e. by an oxide or impurity layer, or an epitaxial silicide structure).

ACKNOWLEDGEMENTS

The authors would like to acknowledge Ali Ghaffari for technical assistance. The implanter part of this study was financially supported by the U.S.Department of Energy through an agreement with the National Aeronautics and Space Administration and monitored by the Jet Propulsion Laboratory, California Institute of Technology (D. Burger).

REFERENCES

1 D.M.Scott, S.S.Lau, R.L.Pfeffer, R.A.Lux, J.Mikkelson, L.Wielunski and M-A. Nicolet, *Thin Solid Film*, 104(1983)227.

2 K.N.Tu and J.W.Mayer in J.M.Poate, K.N.Tu and J.W.Mayer(eds.), *Thin Films-Interdiffusion and Reactions*, Wiley, New York, 1978, p359.

3 M-A.Nicolet and S.S.Lau, in N.G.Einspruch and G.B.Larrabee(eds.), *VLSI Electronics*, *Vol.6*, Academic Press, New York, 1983.

4 R.T.Tung, J.M.Poate, J.C.Bean, J.M.Gibson and D.C.Jacobson in P.S.Ho and K.N.Tu (eds.), *Proc. Symp. on Thin Films and Interfaces*, North-Holland, New York, 1982, p79.

5 H.Ishiwara in J.E.E.Baglin and J.M.Poate(eds.), *Proc. Symp. on Thin Film Interfaces and Interactions* Electrochem.Soc., Princeton, New Jersey, 1980,V80-2, p159.

6 N.Cheung, S.S.Lau, M-A.Nicolet and J.W.Mayer, reference 5, p494.

7 M.Wittmer, P.L.Smith, P.W.Lew and M-A.Nicolet, *Solid St.Elect.*, 21(1978)573.

8 D.M.Scott and M-A.Nicolet, *Nucl.Instr.Meth.* 209/210(1983)297.

9 S.P.Murarka, *J.Vac.Sc.Technol.*, 17(1980)775.

10 L.R.Zheng, L.S.Hung,J.W.Mayer, G.Majni and G.Ottaviani, *Appl.Phys.Lett*, 41(1982)646.

11 M.Bartur, *Thin Solid Films*, 107(1983)55.

12 W.K.Chu, S.S.Lau, J.W.Mayer, H.Müller and K.N.Tu, *Thin Solid Films*, 25,(1975)393.

13 R.Pretorius, C.L.Ramiller, M-A.Nicolet, *Nucl.Instr.Meth.*, 149(1978)629.

14 H.Föll and P.S.Ho, *J.Appl.Lett.*, 52(1981)5510.

15 C.D.Lien and M-A.Nicolet, to be published.

16 C.D.Lien and M-A.Nicolet, to be published.

17 V.J.Van Gurp, D.Sigurd and W.F.Van der Weg, *Appl.Phys.Lett.*, 29(1976)159.

18 R.W.Bower and J.W.Mayer, *Appl.Phys.Lett.*, 20(1972)359.

19 C.D.Lien and M-A.Nicolet, to be published.

FIGURE CAPTIONS

figure 1 (a) Pd_2Si formation from a <111> Si substrate, with ~10 Å Ti marker embedded in sandwiched layers of ~20 Å Pd and ~20 Å Si. A marker shift can be measured from the relocation of the Ti peak before and after annealing at 300°C for 7 min. (b) Pd_2Si formation from amorphous Si is studied with a ~6 Å W marker. RBS spectra show a broadening of the W signal as well as a shift in its peak position, after annealing at 250°C for 25 min.

figure 2 (a) Energy shift of Ti and W markers plotted as a function of the silicide thicknesses in the respective samples. The top and bottom solid lines are determined from energy stopping calculations for the two extreme cases of only one species moving. By allowing for initial stages of zero marker motion, lines that correspond to the case where only Si moves can be fitted to the data points for all three types of Si crystal- linity. The <111> and <100> samples have a Ti marker ~10 Å thick. The sample with amorphous Si has a W marker ~6 Å thick. (b) A comparison of Pd_2Si growth kinetics of samples with(open symbols) and without markers(full dots) shows that the growth rates are the same, but after an incubation period for samples with a marker. The initial suppression of interdiffusion and reaction is due to a barrier action associated with the marker.

figure 3 (a) With a Ti marker ~20 Å thick,a complex diffusion behavior is observed. The initial silicide grows by an apparent dominance of Pd motion, which subsequently subsides in favor of a predominant Si motion, after a substantial Pd_2Si thickness is attained. (b) The time dependence of the Pd_2Si growth of samples with thick Ti

markers demonstrate varying degree of retardation. The growth rates slowly approach that of the reference sample without a marker as the silicide layers thicken.

figure 4 The narrowing and shifting of the N peak implanted in Si can only be explained by a two-mode diffusion process. First, a predominant Si motion leads to narrowing of the N profile while maintaining its closeness to the sample surface. As the N concentration increases, the Si diffusion is inhibited. A second mode involving Pd diffusion is then activated which shifts the entire N profile deeper into the sample bulk.

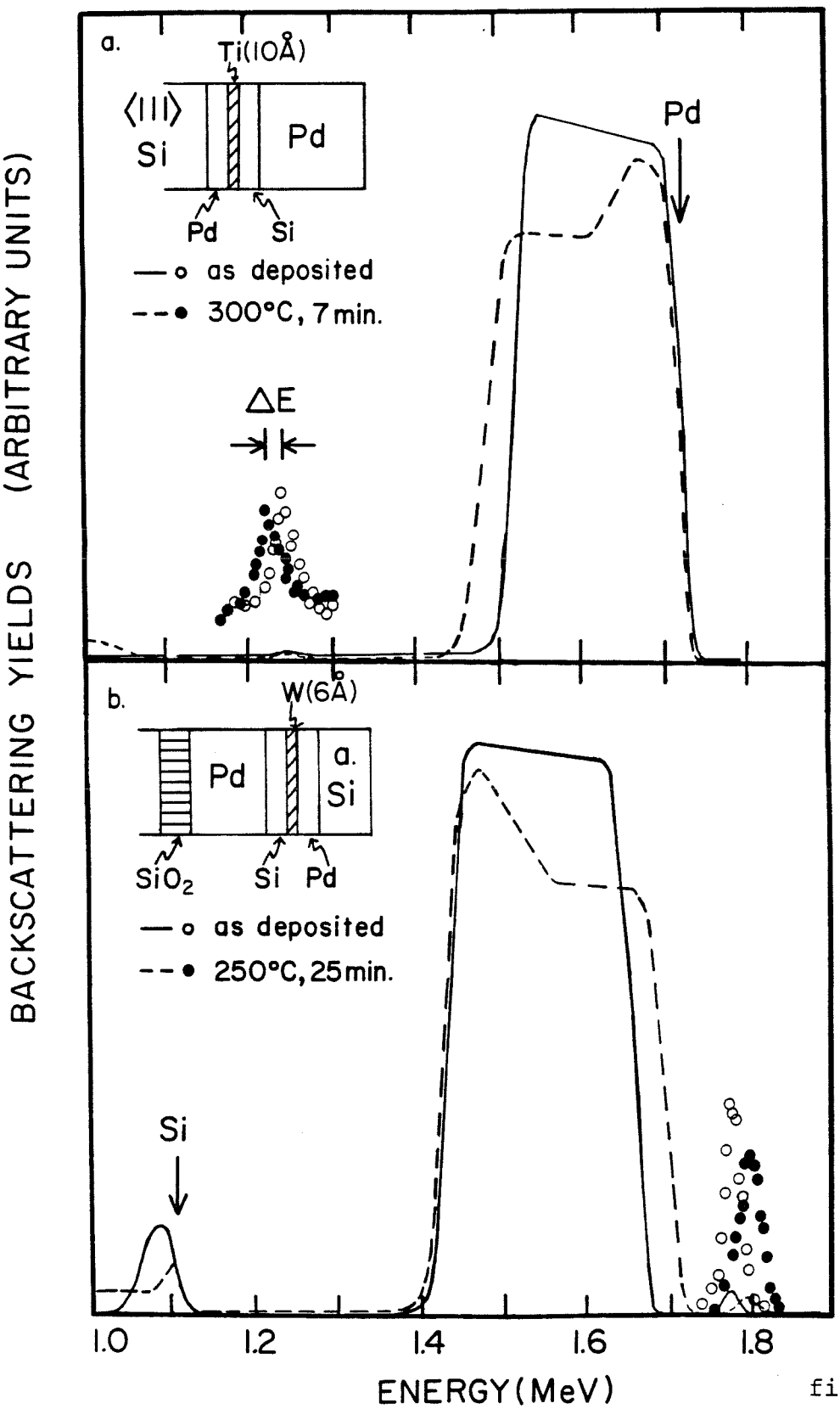
a.
Ti(10Å)
⟨111⟩
Si
Pd
Pd
Si
Pd
— o as deposited
- - - • 300°C, 7 min.
ΔE
b.
W(6Å)
Pd
a.
Si
SiO2
Si
Pd
— o as deposited
- - - • 250°C, 25 min.
Si
BACKSCATTERING YIELDS (ARBITRARY UNITS)
1.0
1.2
1.4
1.6
1.8
ENERGY (MeV)

fig.1

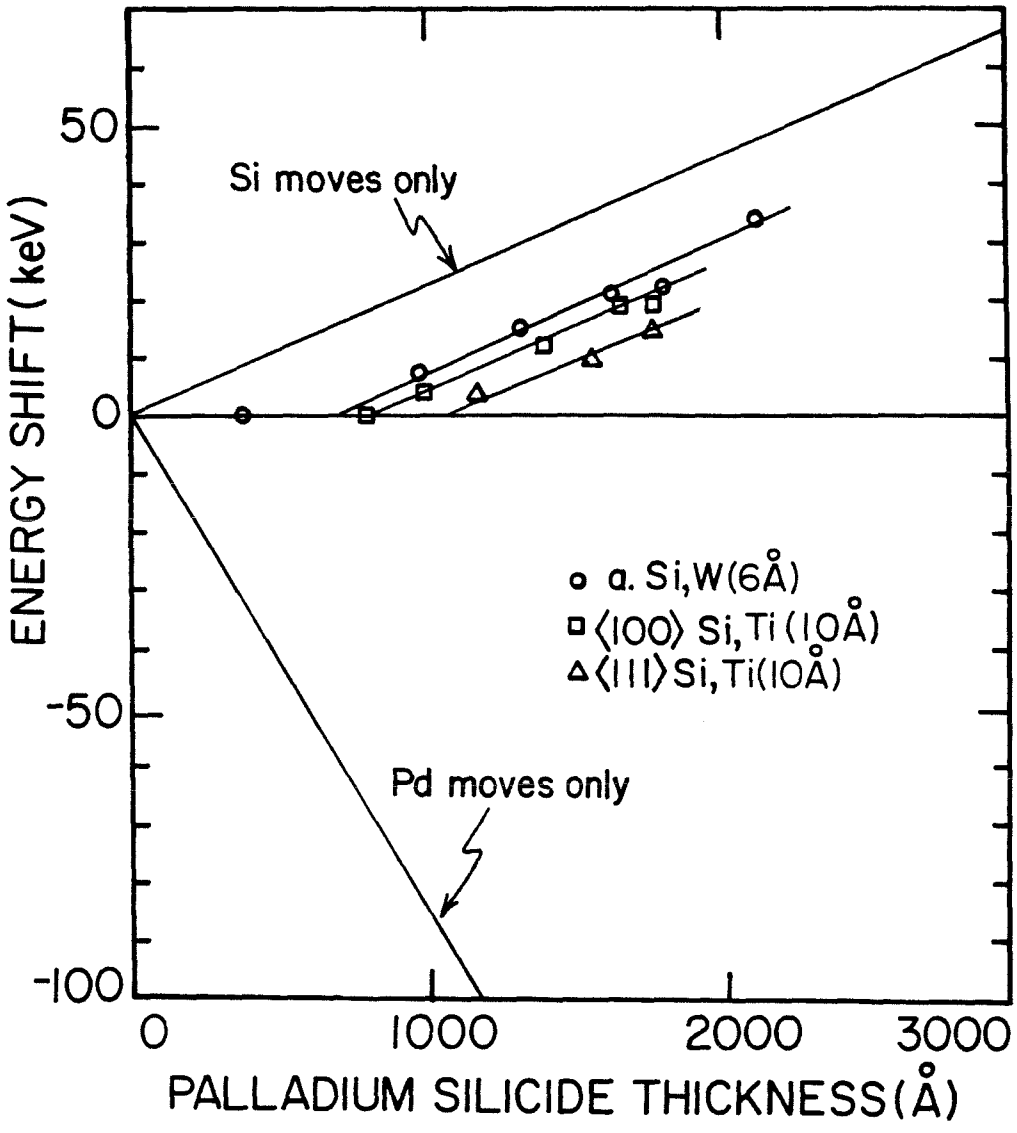
50
0
-50
-100
ENERGY SHIFT (keV)
Si moves only
Pd moves only
o a. Si,W(6Å)
□ ⟨100⟩ Si,Ti (10Å)
△ ⟨111⟩Si,Ti(10Å)
0
1000
2000
3000
PALLADIUM SILICIDE THICKNESS(Å)

fig.2a

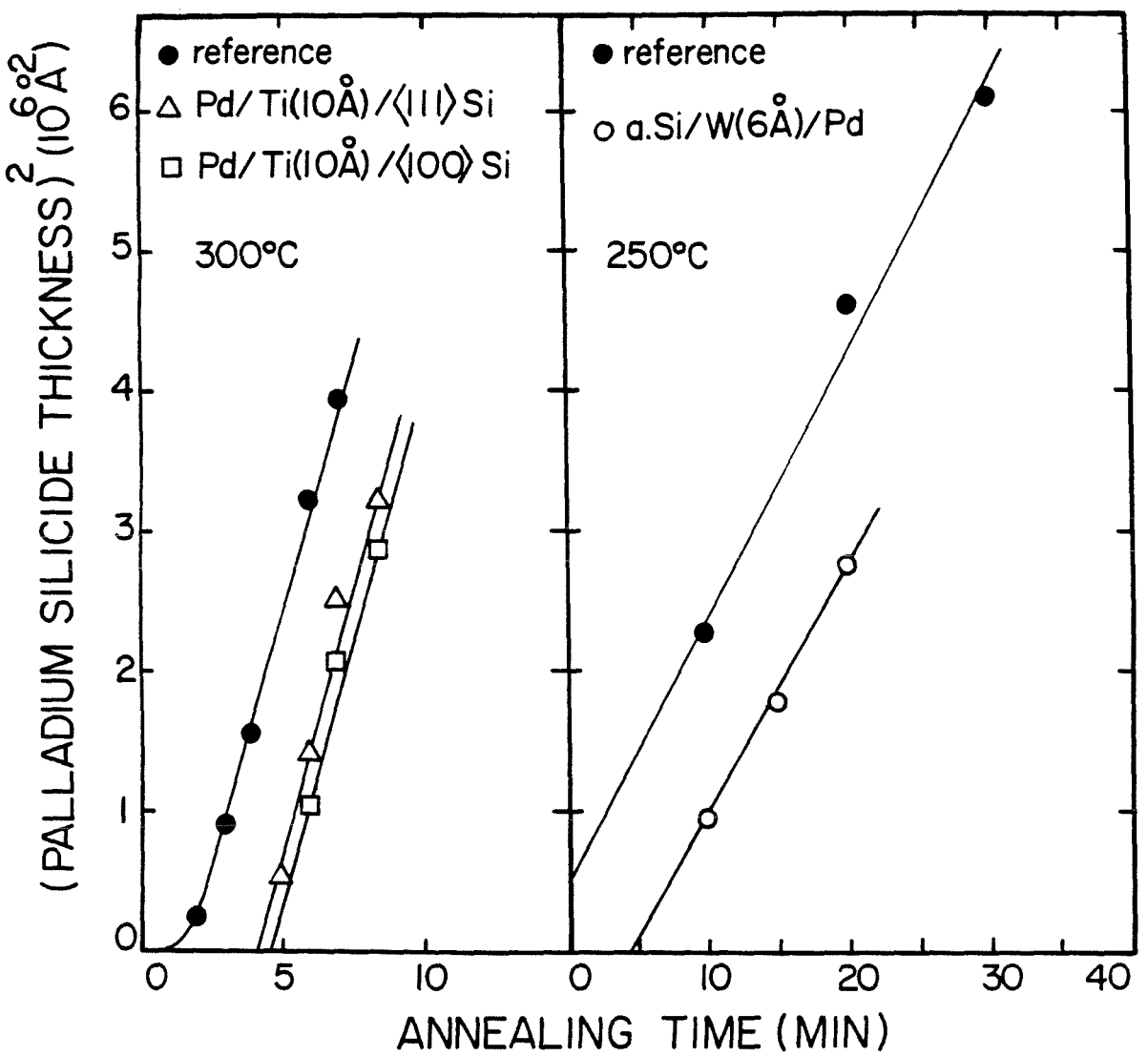
● reference
△ Pd/Ti(10Å)/⟨111⟩Si
□ Pd/Ti(10Å)/⟨100⟩Si
300°C
● reference
○ a.Si/W(6Å)/Pd
250°C
(PALLADIUM SILICIDE THICKNESS)² (10⁶Å²)
ANNEALING TIME (MIN)
0
1
2
3
4
5
6
0
5
10
0
10
20
30
40

fig.2b

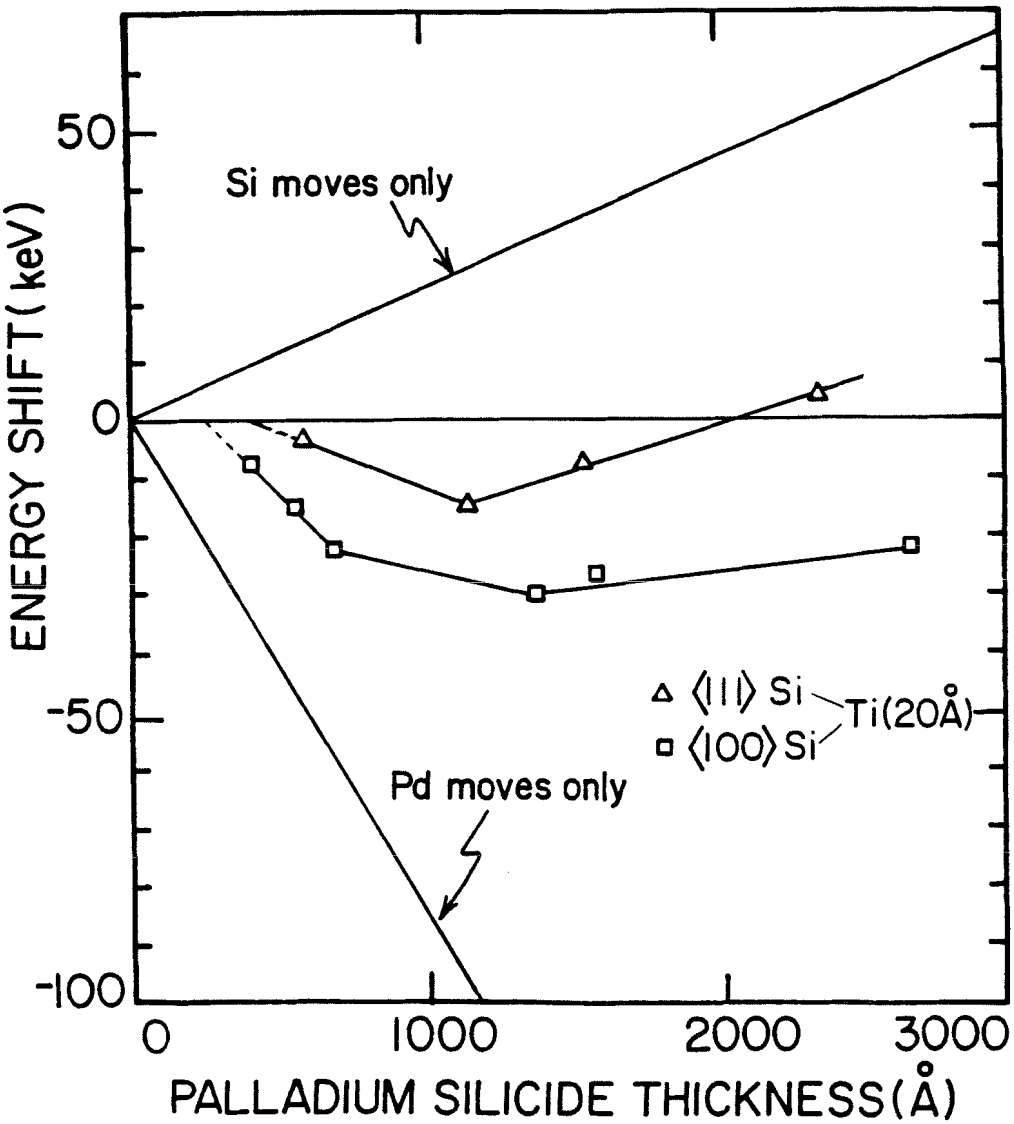
50
0
-50
-100
ENERGY SHIFT(keV)
Si moves only
Pd moves only
△ ⟨111⟩ Si
□ ⟨100⟩ Si
Ti(20Å)
0
1000
2000
3000
PALLADIUM SILICIDE THICKNESS(Å)

fig.3a

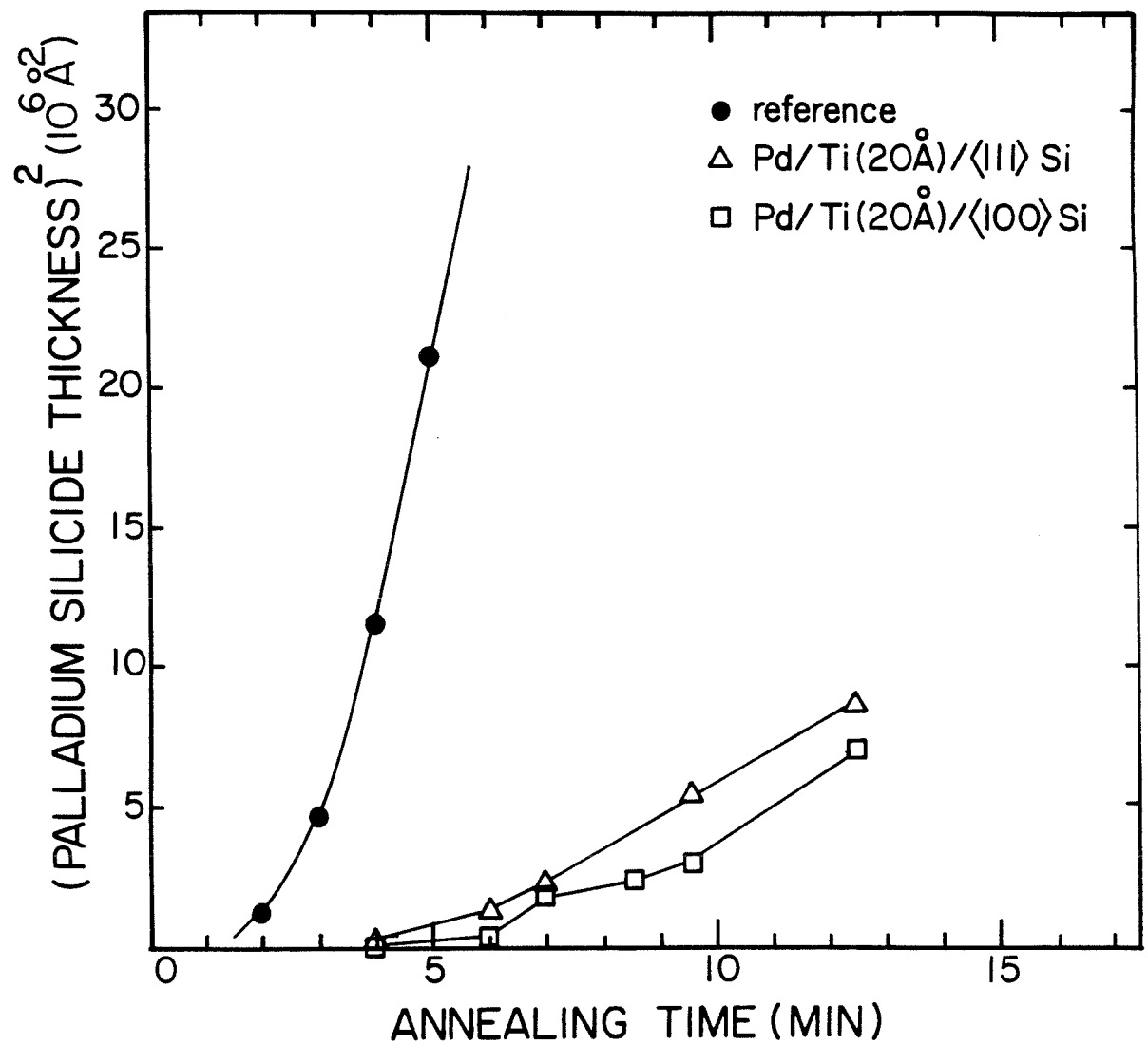
(PALLADIUM SILICIDE THICKNESS)² (10⁶ Å²)
30
25
20
15
10
5
0
5
10
15
ANNEALING TIME (MIN)
reference
Pd/Ti(20Å)/⟨111⟩Si
Pd/Ti(20Å)/⟨100⟩Si

fig.3b

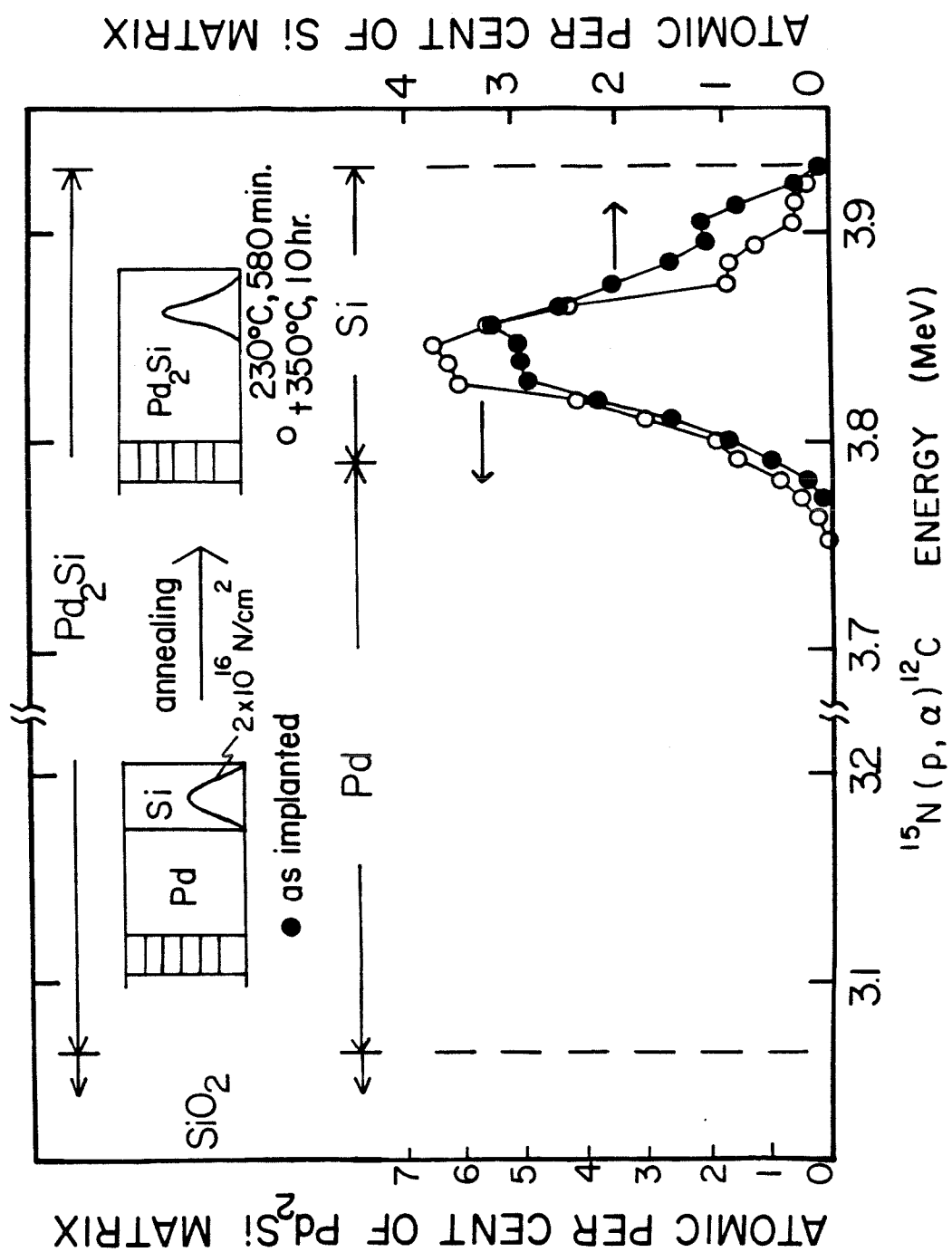
ATOMIC PER CENT OF Si MATRIX
ATOMIC PER CENT OF Pd2Si MATRIX
SiO2
Pd2Si
Si
Pd
Pd2Si
Si
Pd
annealing
2x10^16 N/cm^2
as implanted
230°C, 580 min.
+350°C, 10 hr.
15N (p, α) 12C ENERGY (MeV)
3.1
3.2
3.7
3.8
3.9

fig.4

APPENDIX E

PALLADIUM SICILIDE FORMATION UNDER THE INFLUENCE OF NITROGEN AND OXYGEN IMPURITIES

K.T.Ho, C.D.Lien and M-A.Nicolet

California Institute of Technology,

Pasadena, California, 91125

ABSTRACT

The effects of impurities on the growth of the Pd_2Si layer upon thermal annealing of an Pd film on < 100> and amorphous Si substrates is investigated. Nitrogen and oxygen impurities are introduced into either Pd or Si which are subsequently annealed to form Pd_2Si. The complementary techniques of Rutherford backscattering spectrometry ,and $^{15}N(p,\alpha)^{12}C$ or $^{18}O(p,\alpha)^{15}N$ nuclear reaction, are used to investigate the behavior of nitrogen or oxygen and the alterations each creates during silicide formation. Both nitrogen and oxygen retard the silicide growth rate if initially present in Si. When they are initially in Pd, there is no significant retardation; instead, an interesting "snow ploughing" effect of N or O by the reaction interface of Pd_2Si is observed. By using N implanted into Si as a marker, Pd and Si appear to trade roles as the moving species, when the silicide front reaches the nitrogen rich region.

I INTRODUCTION

The technological trend of scaling down the device size has made the manufacturing of small area contacts a challenging field of research. Metal silicides have been proposed as the contact material due to their chemical and thermal stability, and the selectibility and reproducibility of their Schottky barrier height when making contact to silicon[1,2]. Lateral confinement of contact

area exacerbates problems of high contact resistance and nonuniform reaction caused by interfacial contaminants or native oxides[3]. One possible solution may be offered by materials such as Pd and Ti which are known to dissolve the native oxide layer to produce an intimate contact to silicon[4,5,6]. Interfacial contaminants remain as a major cause of high contact resistance in various shallow contact schemes where only ~100Å of substrate Si is consumed[7]. Interfacial contaminants stay close to the active area even after silicide formation. The understanding of the effects of such contaminants is thus important for device quality considerations.

Recently various studies approached this problem by introducing specific types of impurity elements such as oxygen and nitrogen into silicide forming systems[8-11]. Various aspects such as the subsequent motion of the impurities during silicide formation, their effects on silicide growth kinetics and phases formed, compound formation involving the impurity element, and electrical properties of the resultant material have been modeled and analyzed in detail. Due to the wide range of diffusivity, solubility, heats of formation of competing compounds for different impurity-host combinations, a large variety of reaction modifications and final sample configurations can be observed. Some results have led to suggestive possibilities of making shallow contacts[12] and diffusion barriers[13] using impurity controlled behaviors of metal-silicon couples.

Previous work has shown that Pd is very permeable to ambient oxygen[14]. However, O incorporated in Pd does not alter the Pd_2Si growth kinetics. The present work addresses the effect of another common impurity, nitrogen, on Pd silicide formation, and reports additional results obtained for oxygen impurities. To model the behavior of nitrogen and oxygen in silicide forming systems, it is necessary to identify the moving species during the reaction. For Pd_2Si, the moving species has been a perplexing issue[14]. For this work, the

authors shall refer to the W marker results of Ho et al.[15], which identify Si as the dominant moving species for Pd silicide formed from amorphous Si.

II EXPERIMENTAL PROCEDURES

For experiments in which nitrogen was implanted into Pd, Pd films were evaporated either on an <100> Si wafer or on amorphous Si evaporated on an oxidized Si wafer. The <100> Si substrate was a commercially polished, n-type wafer, with a resistivity of .005-.02 Ω cm. The Pd film thicknesses were 4030Å and 1830Å, respectively, on the above two types of Si. The evaporated Si film was 2600Å thick. The rare nitrogen isotope ^{15}N was implanted into the Pd film at energies of 300 keV and 200 keV/N_2^+, with calculated ranges of R_p = 1325Å and 866Å, respectively. The R_p values were verified by experimental measurements. Implantation doses were 0.5, 1 and 2 × 10^{16}N/cm^2 for Pd on <100> Si and a single dose of 2 × 10^{16}N/cm^2 for Pd on amorphous Si. Silicide formation was thermally induced at annealing temperatures of 250°C and 200°C for these two sets of samples.

To study the effects of O in Pd, we evaporated 1700 Å of Pd on an <100> Si substrate of the type described in the last paragraph. Implantation of the rare isotope ^{18}O was performed at an energy of 260 Kev/O_2^+ to obtain a calculated projected range of 1010 Å. A single dose of 2 × 10^{16}/cm^2 was used, and samples were annealed at 250°C.

To study the effects of nitrogen and oxygen implanted into Si, 1860Å of amorphous Si was evaporated on 2900Å of Pd, which was itself evaporated first on an oxidized Si wafer. Nitrogen and oxygen in doses of 0.5, 1 and 2 × 10^{16}/cm^2 were implanted at an energy of 80 keV/N_2^+ or O_2^+, with an expected projected range of 1040Å and 890 Å, respectively. The annealing temperature used was 230°C for N-implanted samples and 225°C for O-implanted samples.

Both the oxidized and bare wafers were ultrasonically cleaned before loading into the evaporation system in trichloroethylene, acetone and methanol sequentially for 5 min. each. The bare Si substrate was, in addition, etched in 20% dilute HF solution, then immersed in an RCA solution (H_2O_2:NH_4OH:H_2O in the ratio of 1:1:5), and finally another etch in 6%HF.

Annealing was done in a vacuum furnace pumped to 5×10^{-7} Torr pressure. Evaporations were performed in an oil-free e-gun system at a pressure of 4×10^{-7} Torr. The deposition rate for both Pd and Si was 20Å/s. The silicide thicknesses were monitored by 2 MeV $^4He^+$ backscattering spectrometry at an detector angle of 170°. Nitrogen and oxygen impurities were profiled using the $^{15}N(p,\alpha)^{12}C$ and $^{18}O(p,\alpha)^{15}N$ nuclear reaction techniques. Samples were tilted at 60° against normal incidence to enhance the depth resolution to ~300Å. The proton incident energy was set at 1 MeV for ^{15}N activation and .75 MeV for ^{18}O activation. The detector was mounted in the plane defined by the sample normal and the proton beam, at an angle of 164° with respect to the incident beam, opposite to the direction of the sample tilt. Since Pd_2Si formation is already a well understood process, phase indentification by x-ray diffraction was not performed in this study.

III RESULTS AND DISCUSSION

A. Nitrogen in Pd

Growth curves of Pd_2Si for <100> crystalline Si and amorphous Si at temperatures of 250°C and 200°C, respectively, are shown in figure 1. Both unimplanted samples show initial $\sqrt{t}$ growth rates with nonzero intercepts when the straight lines are extrapolated to t=0. The slope of the line for 250°C agrees well with that of Scott and Nicolet[14]. When the silicide thickness exceeds ~3500Å, a slowing of the reaction rate is observed. This may be caused by either a large stress or the huge concentration of oxygen which permeates throughout the top

region of the Pd film.[14] The N implanted samples systematically show slightly slower growth rates compared to the reference sample. However, the thickness difference between implanted and unimplanted samples does not exceed experimental uncertainty until Pd_2Si thickness is above 2500 Å. Any dose dependence is too slight to be resolved from the uncertainty level of the experimental data.

In figure 2, the N profiles in the Pd/amorphous Si sample at various stages of thermal treatment is given by superimposing the Pd peak of backscattering spectra with the nuclear reaction spectra for nitrogen. The horizontal axis is labeled in energy of the backscattered α particle from the Pd in the sample. The energy axis of the nuclear reaction spectra is adjusted accordingly to align the N signals to the backscattering peaks of the host(Pd or Pd_2Si) lattices.

When the Pd film is partially reacted into Pd_2Si, some N is rejected from the silicide into the Pd side of the Pd/silicide interface. The rejection occurs for as long as pure Pd is being consumed by the reaction, until finally nitrogen is pushed to the Pd surface and exits from the film, resulting in 36 % loss in total quantity. The residual N content in the silicide amounts to 0.7 at%(0.7 N per lattice atom in Pd_2Si) and is uniform throughout the layer. The completely reacted sample was annealed at 225°C instead of the previous temperature of 200°C to shorten the annealing time.

For comparison, we note that when N is implanted into Pt rather than Pd, the subsequently formed Pt_2Si is totally free of N,[16]. This result is consistent with the fact that Pt is the moving species[17] and does not carry N with it during its diffusion across the silicide layer. This comparison strongly suggests that Pd is not the dominant moving species in the Pd_2Si formed in our experiment. The preceding paper[15] demonstrates that Si is the moving species in Pd_2Si formation except when the diffusion of Si is impeded. In our case, we can conclude that any

possible hindrance of Si diffusion is very slight in view of the unchanged silicide growth rate. We therefore approach the following analysis with the well supported premise that Si is the moving species.

If implanted nitrogen is strongly bonded to the Pd lattice, the moving Si should diffuse around nitrogen and cause it to be incorporated into the growing silicide layer. However, figure 2 clearly shows that N is partially "snow plowed" rather than completely incorporated. This is consistent with that fact that Pd does not have nitride phases[18], since nitrides are less likely to be mobile than nitrogen atoms in the Pd lattice. This "snow plow" effect may indicate that the solubility limit of N in Pd is much larger than that in Pd_2Si. Interfacial drag may be another mechanism which can explain the segregation effect. However, it is not clear whether an interfacial drag can have the same effect on bulk impurities as on interfacial impurities. These results are closely analogous to N behaviors in the Ta/Si system, where it is suspected that the metal forms a nitride only at large N concentrations.[8] As a last comment, we can suppose the Pd motion does contribute a minor fraction of the mass transport. Some N will be left behind by Pd and will accumulate at the Pd/Pd_2Si interface. This N will then be incorporated or segregated by the dominant flux of Si, leading to the same end picture. Therefore, the possibility of a minor Pd diffusion can not be excluded.

B. Oxygen in Palladium

A Pd_2Si growth curve at 250°C for a sample with O implanted into Pd is shown in figure 3, along with that of the correponding unimplanted reference sample. It is apparent that implanted O has no effect on Pd_2Si growth rate. This is to be expected in view of the large amount of ^{16}O that penetrates into Pd during annealing anyway. Both reference and implanted samples reproduced the growth rate reported by Scott and Nicolet[14]. The slight difference between the

growth rate of the reference sample in this set and that in the N-implanted set may be due to the factor of 2.4 in thicknesss ratio combined with the huge surface O content.

The evolution of the O profile indicates a strong segregation effect very similiar to that of implanted N. However, after the silicide formation reaches completion, oxygen distinguishes itself from nitrogen in that a major portion of the residual amount of oxygen resides in a large surface peak with only 15% loss in total quantity; as compared to the N case, where all residual amount in excess of the 0.7 at% that is uniformly incorporated in the silicide diffuses out of the sample. It can be conjectured that the thin O-rich layer, reported by Scott and Nicolet[14], at the sample surface may be capturing oxygen while allowing free passage of N. The amount of O incorporated in the silicide, neglecting the surface peak, has an average concentration of 0.9 at%. Finally, it should be mentioned that a different pattern of O redistribution was reported by Scott and Nicolet[14] The causes for the discrepancies still remain to be resolved.

C. Nitrogen in Silicon

Figure 5 shows Pd_2Si growth curves for implanted and as- deposited reference samples which have evaporated Si on top. The reference sample has a $\sqrt{t}$ growth rate. Whether a deviation from this growth pattern occurs for this reference sample at larger silicide thickness was not tested. It is expected that the Pd film is relatively free of oxygen contamination due to the top layer of Si acting as a cap. The silicide growth rate is clearly reduced by the implanted N. At the high dose of $2\times10^{16}N/cm^2$, the sample does not react beyond 2430Å of silicide after a 580 min. anneal at 230°C. If the silicide reaction is unhindered, a 3910 Å thick Pd_2Si layer can be formed from the evaporated Si. The N profile after this annealing step is shown in figure 6 as open circles. It can be seen that even though the Si/silicide interface has advanced a little beyond the peak of

the nitrogen profile, there is no detectable change in the shape of the N profile. This is consistent with the notion that a partial participation of Pd in the mass transport has begun, since, if only Si moves, nitrogen that is left behind is expected to pile up at the Si/silicide interface. The role conversion of Pd from a stationary species to a moving species has been observed in the preceding paper where the normal flow of Si is obstructed.[15]

Further reaction of the sample can be forced by raising the annealing temperature to 350°C and annealing for 10 hrs longer. The silicide reaction is completed after this thermal treatment as shown in figures 6 and 7. In figure 6, there is a bump on the backscattering signal of Si in Pd_2Si indicating a slight excess of Si in the near surface region. At the corresponding position in figure 7, the signal of Pd in Pd_2Si shows a significant dip. The superpositioned nitrogen signals in this spectrum shows that it is this excess nitrogen (and Si) in this region that is responsible for the drop in Pd signal. The N peak concentration after the complete reaction is ~6.3 at%. By assuming the stoichiometric ratio of N:Si = 4:3(for Si_3N_4) and Pd:Si = 2:1(for Pd_2Si), the lowering of the Pd concentration because of Si_3N_4 competing for Si is calculated to be 9.5 at%. This is close to the value of 8.7 at% measured for the dip in the Pd peak. Thermodynamics favors the formation of Si_3N_4(ΔH_f=-25.6 Kcal/gatom or -59.7 Kcal/Si atom)[19] over that of Pd_2Si(ΔH_f=-19.1 Kcal/gatom or -28.6 Kcal/Si atom)[20], in support of the above assumptions.

The complete reaction at 350°C causes an interesting alteration of the nitrogen profile, shown in figure 6. The profile narrows and the peak value rises. This change is consistent with a predominant initial Si motion. The entire profile is translated towards lower energy direction, which agrees with a predominant Pd mass transport during the end stage of the silicide reaction. The ability for Pd to convert into the moving species and consume the Si buried behind an

inert barrier is unique, and has been observed in other studies where a diffusion barrier exists and a high annealing temperature ($\geq$ 350°C) is used[4,15]. The tendency for the nitride barrier to yield at a higher temperature contrasts with what was observed for $TaSi_2$ formation[8], where Si is also the moving species during silicide formation. When an equivalent N dose is introduced into Si, $TaSi_2$ reaction does not proceed even though the annealing temperature (675°C) used was much higher than in the current study.

D. Oxygen in Silicon

Pd_2Si growth kinetics is also severely impeded when O is implanted into Si, as illustrated by figure 8. For an implanted dose of 2×10^{16} O/cm^2, Pd_2Si thickness saturates at 1340 Å after 150 min. annealing at 225 °C. The total thickness of Pd_2Si that can be formed from the evoporated Si is 3910 Å. The oxygen profile is unaltered after this thermal treatment. A high temperature annealing was not pursued in this case.

IV CONCLUSIONS

Nitrogen impurities in Pd or in Si have a minor retarding effect on Pd_2Si growth rate, which becomes more apparent at silicide thicknesses above 2500 Å. Only thin Pd_2Si thickness was used for studying O effects, and no alteration of silicide growth rate was observed. Although Si is the moving species, N and O are partially "snow ploughed" by the Pd/silicide interface. A uniform concentration of 0.7 at% of N or 0.9 at% of O is incorporated into the Pd_2Si lattice in each case. All excess nitrogen is finally ejected out of the Pd film, resulting a 36% loss in total quantity. Most of the excess oxygen accumulates in a large surface peak, resulting in only 15% loss in total quantity. When included in Si, both N and O will severely retard the silicide growth. The reaction continues at an elevated temperature with Pd as the diffusing species.

ACKNOWLEDGEMENTS

The authors would like to acknowledge Ali Ghaffari for technical assistance. The implanter part of this study was financially supported by the US Department of Energy through an agreement with the National Aeronautics and Space Administration and monitored by the Jet Propulsion Laboratory, California Institution of Technology (D. Burger).

REFERENCES

1 K.N.Tu and J.W.Mayer, in *Thin Films-Interdiffusion and Reactions* ,edited by J.M.Poate,K.N.Tu and J.W.Mayer (Wiley-Interscience,New York,1978), chap.10.

2 M-A Nicolet and S.S.Lau, in *VLSI Electronics* vol.6,edited by N.G.Einspruch and G.B.Larrabee, (Academic Press,New York,1983),chap.6.

3 J.L.Vossen, *J.Vac.Sci.Technol.*, 19,761(1981).

4 D.M.Scott,S.S.Lau,R.L.Pfeffer,R.A.Lux,J.Mikkelson,L.Wielunski and M-A.Nicolet, *Thin Solid Films*, 104,227(1983).

5 H.Föll and P.S.Ho, *J.Appl.Phys.*, 52(1981)5510.

6 K.N.Tu, *J.Vac.Sci.Technol.*, 19,760(1981).

7 S.Kritzinger and K.N.Tu, *J.Appl.Phys.*, 52,305(1981).

8 K.T.Ho,C.D.Lien,M-A.Nicolet and D.M.Scott, MRS Proceedings Volume *Thin Films and Interfaces*, edited by J.E.E.Baglin,D.R.Campbell and W.K.Chu, (North-Holland,New York,in press).

9 K.T.Ho,M-A.Nicolet and L.Wielunski, *Thin Solid Films*, 104,243(1983).

10 C.D.Lien.L.Wielunski,M-A.Nicolet and J.Stika, *Thin Solid Films*, 104,235(1983).

11 D.M.Scott Ph.D.Thesis,California Institute of Technology,1980.

12 T.Banwell,M-A.Nicolet and D.M.Scott, *Thin Solid Film*, 107,67(1983).

13 M-A.Nicolet and M.Bartur, *J.Vac.Sci.Technol.*, 19,786(1981).

14 D.M.Scott and M-A.Nicolet, *Nucl.Instr.Meth.*, 209/210,297(1983).

15 K.T.Ho,C.D.Lien,U.Shreter and M-A.Nicolet, preceding paper.

16 K.T.Ho and M-A.Nicolet, unpublished.

17 R.Pretorius, C.L.Ramiller, M-A.Nicolet, *Nucl.Instr.Meth.*, 149(1978)629.

18 M.Hansen and K.Anderko, *Constitution of Binary Alloys*, (McGraw-Hill,New York,1958),p.986.

19 R.C.Weast(ed.), *Handbook of Chemistry and Physics*, (CRC Press,Cleveland,1975).

20 S.P.Muraka, *Silicides for VLSI Applications*, (Academic Press,New York,1983),P.73.

FIGURE CAPTIONS

figure 1 Top set of curves: Thickness of Pd_2Si growth on <100> Si substrates, from Pd films annealed at temperature of 250°C. Samples implanted with N show a very similiar growth rate as the unimplanted reference. The curvature at large silicide thicknesses maybe due to heavy oxygen contamination near the Pd surface. Bottom set of curves: experiment repeated at 200°C with a single implantation dose of 2×10^{16} N/cm^2 and using amorphous Si. Implanted sample also shows a similiar growth rate as the reference.

figure 2 Nuclear reaction signals of nitrogen superimposed on Pd backscattering peak, Nitrogen piles up at the advancing Pd/silicide interface until it exits through the top surface at the completion of Pd consumption. There is no nitrogen loss at the intermediate stage of annealing.

figure 3 Oxygen implanted in Pd does not interfere with Pd_2Si growth rate. The growth rate found in this study coincides very closely with of Scott et al.

figure 4 A segregation effect of O in Pd is observed during Pd_2Si formation. The silicide lattice incorporates an average O concentration of 0.9 at%. Most of the remaining O accumulates in a large surface peak when silicide formation is completed. Samples are tilted 60° against normal during backscattering.

figure 5 Pd_2Si growth curves at 230°C with nitrogen implanted into the top Si layer.The growth rate is increasingly severely retarded

for increasing N dose. For the dose of $2\times10^{16}/cm^2$, silicide growth virtually comes to a halt after ~2000 Å.

figure 6 With N implanted into Si, silicide reaction stops at the N-rich region after 580 min. annealing at 230°C. Pd_2Si reaction can be forced to completion by raising annealing temperature to 350°C. There is a slight bump in the backscattering signal of Si at the near surface region. The relative movement of nitrogen signals indicate a complicated scheme of mass transport in which both Pd and Si diffusion contribute to the growth of the silicide. The backward shift of nitrogen signal in the fully reacted sample can be explained by a predominant Pd motion during the final stage of annealing.

figure 7 A dip in the Pd peak of the Pd_2Si layer coincides in position with the peak of the incorporated nitrogen. Calculation supports the assumption that the dip is caused by a depletion of Pd concentration in the region where Si is occupied by N due to the completing Si_3N_4 formation.

figure 8 Oxygen implanted in Si severely retards Pd_2Si growth rate. The effect of retardation is stronger with increasing O dose.

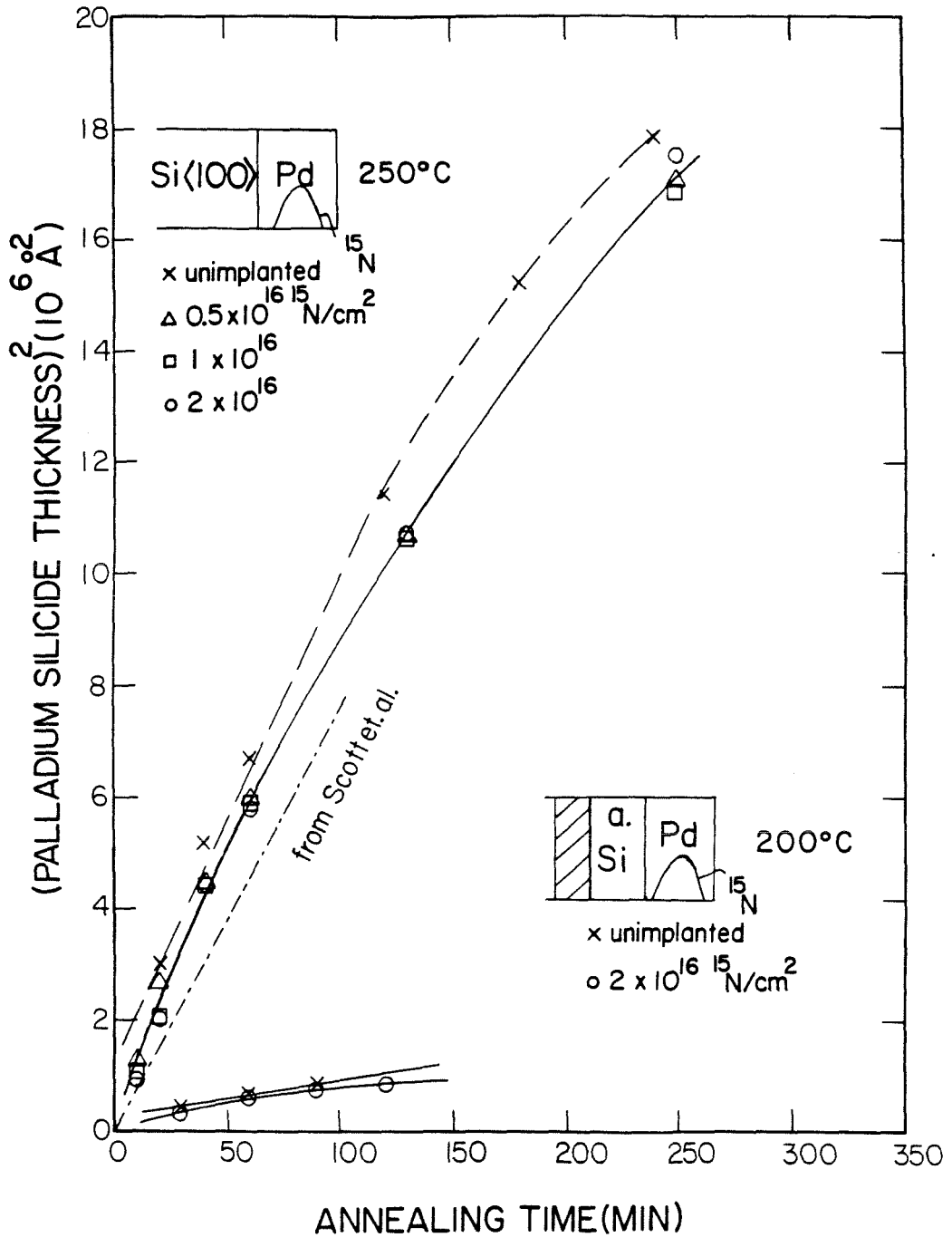
(PALLADIUM SILICIDE THICKNESS)^2 (10^6 Å^2)
ANNEALING TIME(MIN)
Si⟨100⟩ Pd
250°C
^{15}N
× unimplanted
△ 0.5×10^{16} ^{15}N/cm^2
□ 1×10^{16}
○ 2×10^{16}
from Scottet.al.
a. Si
Pd
200°C
^{15}N
× unimplanted
○ 2×10^{16} ^{15}N/cm^2

fig.1

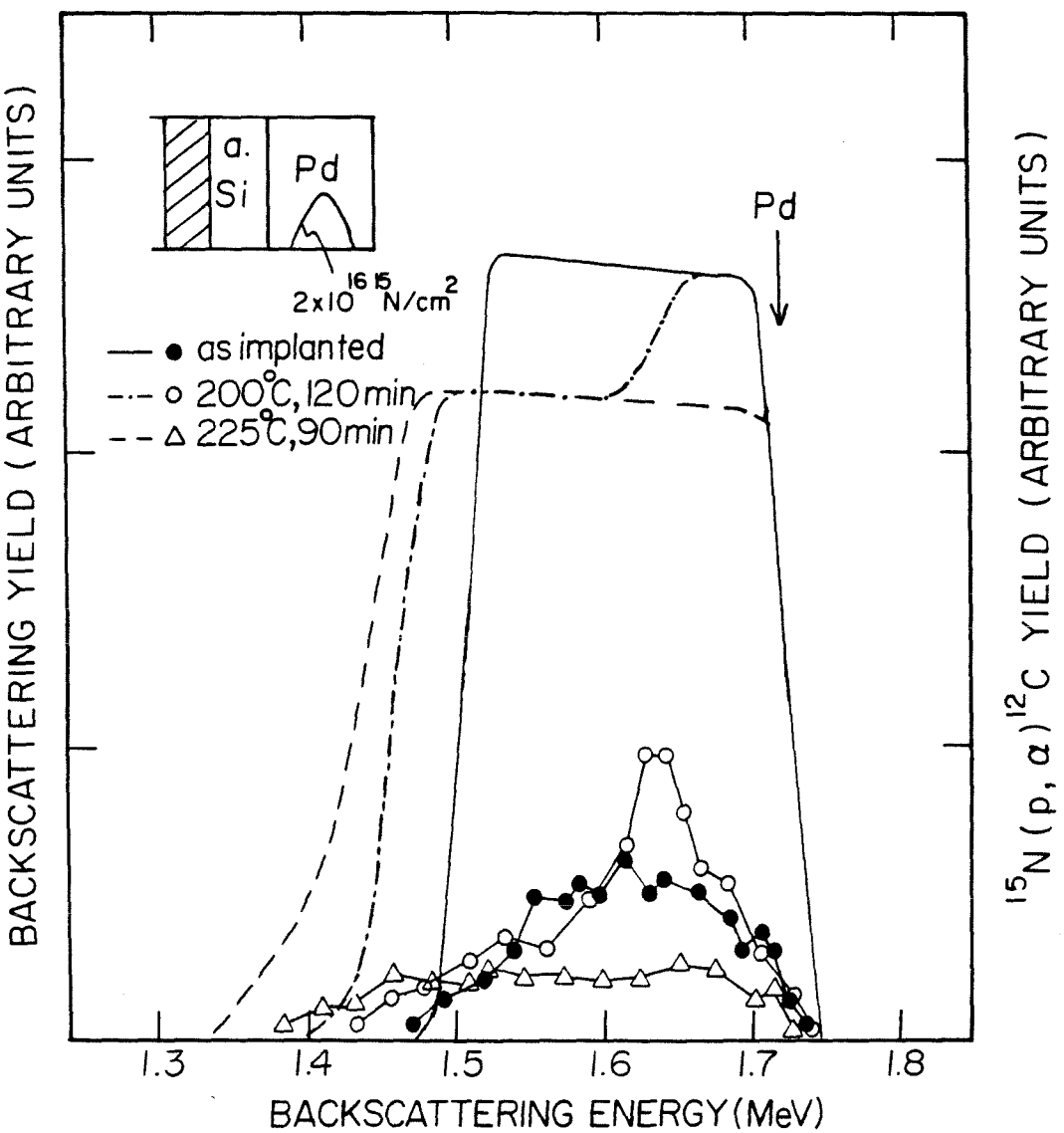
a.
Si
Pd
2x10^16 15 N/cm^2
Pd
as implanted
200°C, 120 min
225°C, 90 min
BACKSCATTERING YIELD (ARBITRARY UNITS)
15N (p, α) 12C YIELD (ARBITRARY UNITS)
1.3
1.4
1.5
1.6
1.7
1.8
BACKSCATTERING ENERGY (MeV)

fig.2

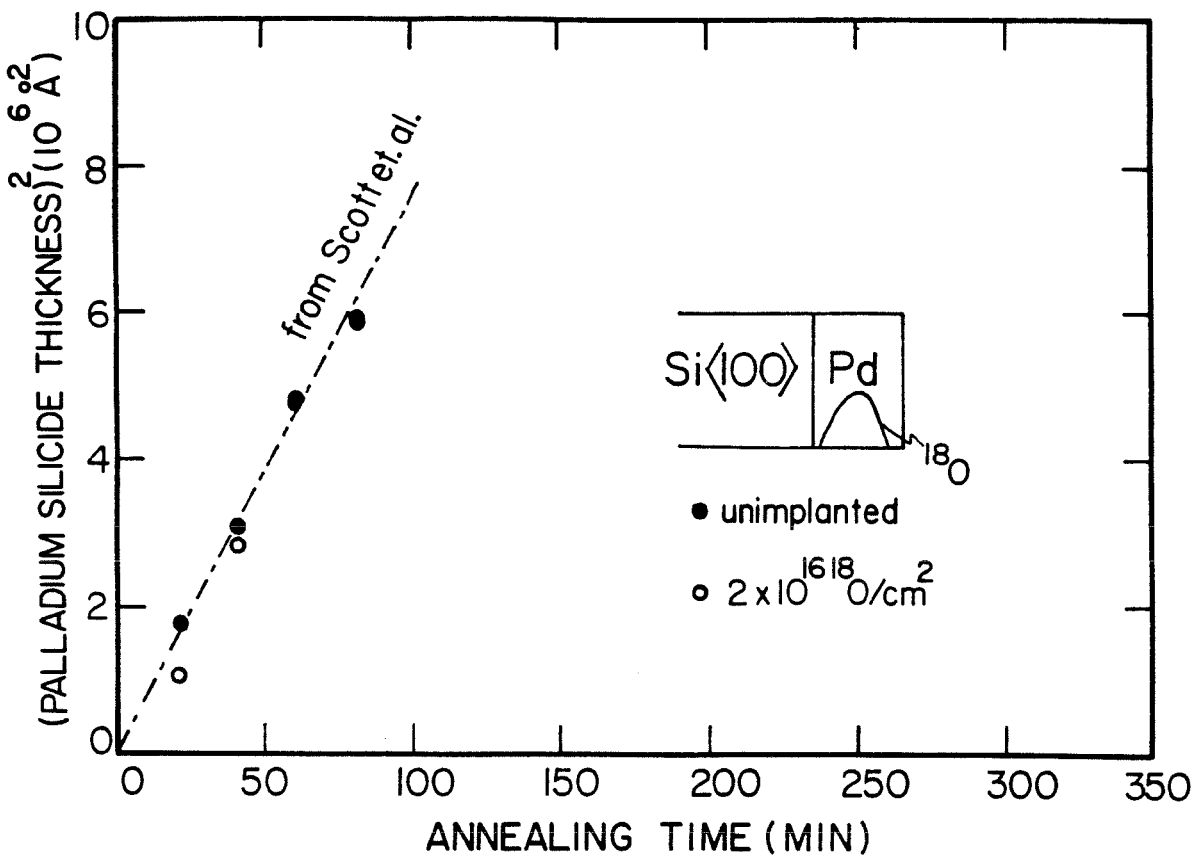
(PALLADIUM SILICIDE THICKNESS)^2 (10^6 Å^2)
ANNEALING TIME (MIN)
from Scott et. al.
Si⟨100⟩ Pd
^{18}O
● unimplanted
○ 2 x 10^{16} ^{18}O/cm^2
0
2
4
6
8
10
0
50
100
150
200
250
300
350

fig.3

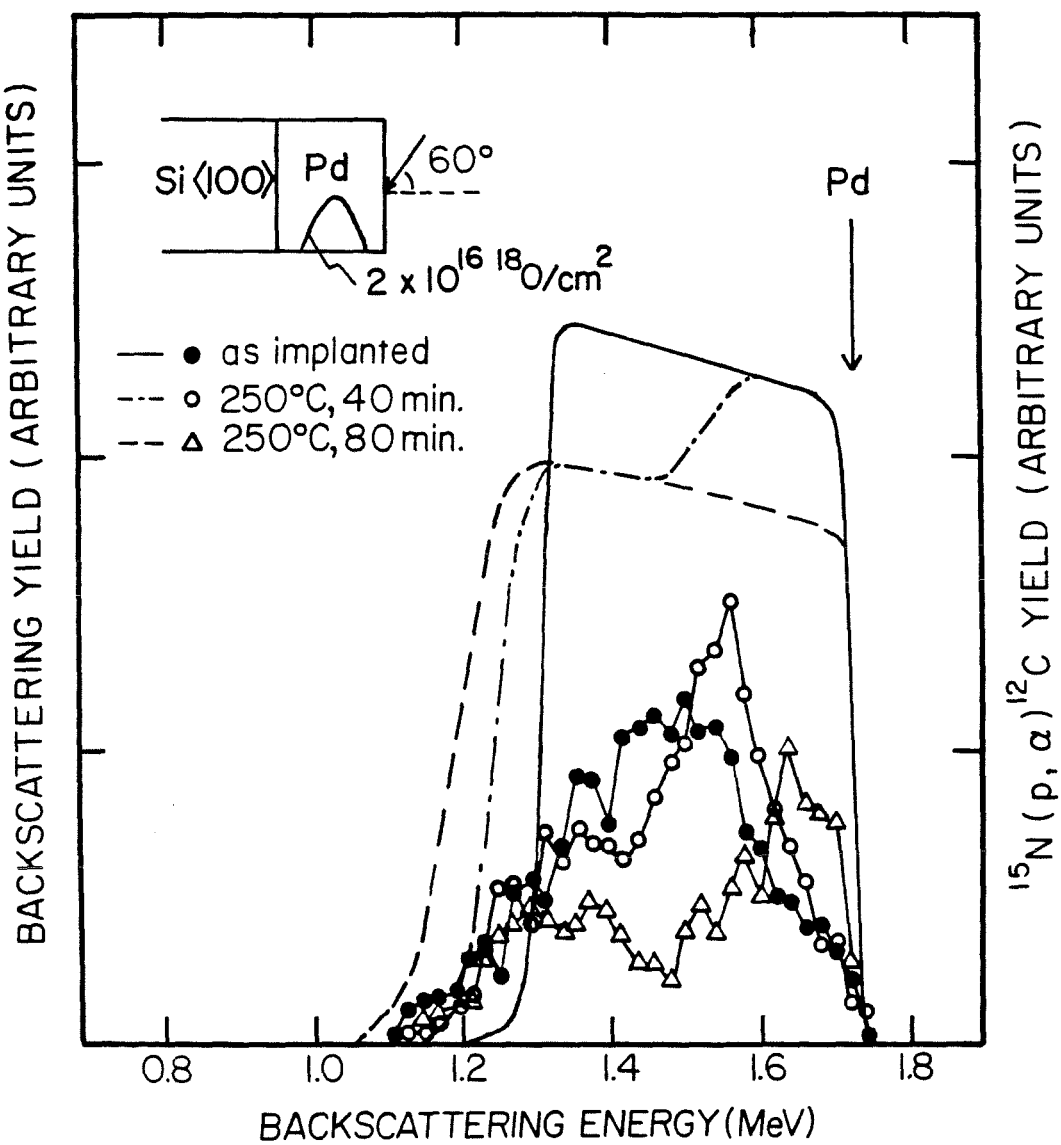
Si ⟨100⟩
Pd
60°
2 x 10^16 18O/cm^2
Pd
as implanted
250°C, 40 min.
250°C, 80 min.
BACKSCATTERING YIELD (ARBITRARY UNITS)
15N (p, α) 12C YIELD (ARBITRARY UNITS)
0.8
1.0
1.2
1.4
1.6
1.8
BACKSCATTERING ENERGY (MeV)

fig.4

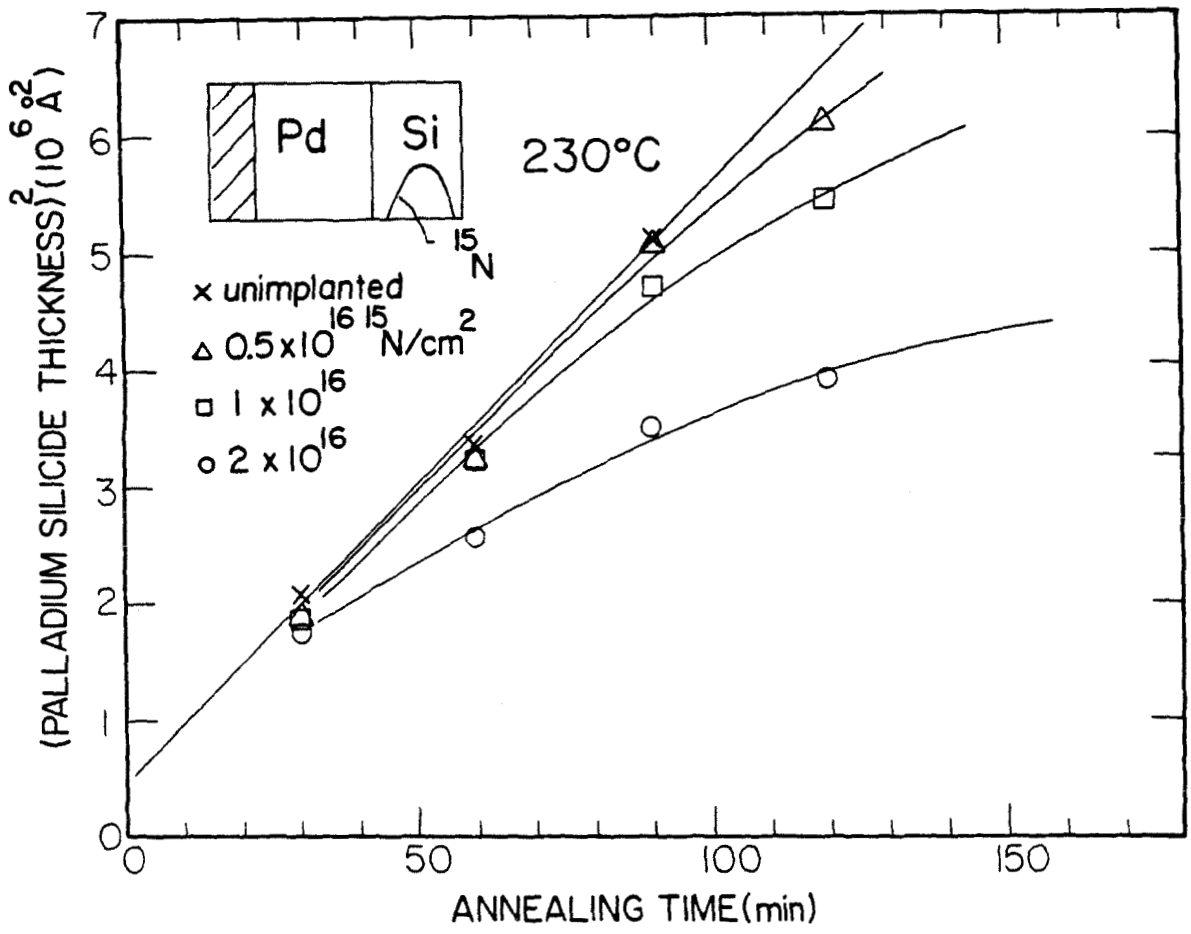
(PALLADIUM SILICIDE THICKNESS)^2(10^6 Å^2)
ANNEALING TIME(min)
Pd
Si
^{15}N
230°C
× unimplanted
△ 0.5×10^{16} ^{15}N/cm^2
□ 1×10^{16}
○ 2×10^{16}
0
1
2
3
4
5
6
7
0
50
100
150

fig.5

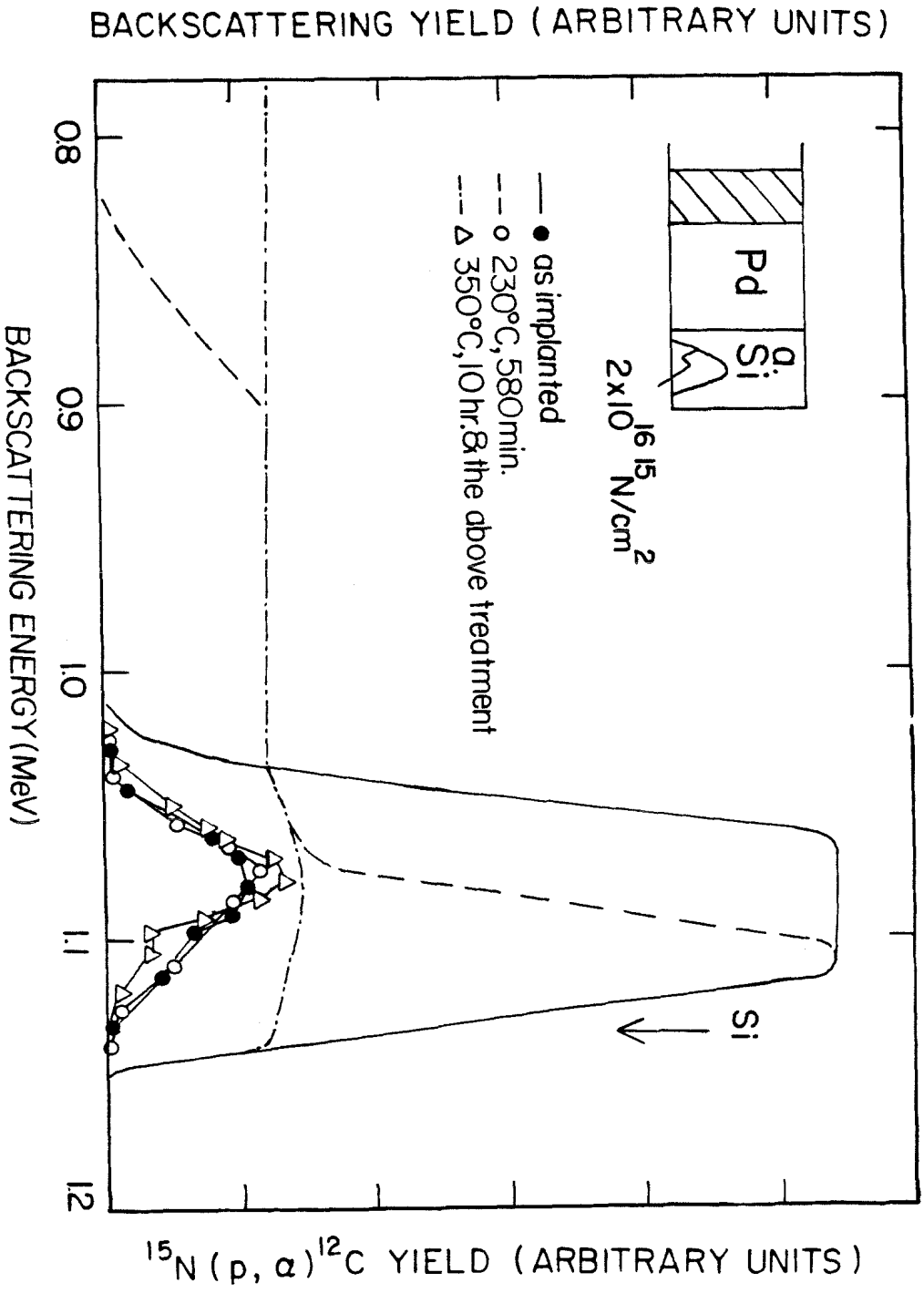
BACKSCATTERING YIELD (ARBITRARY UNITS)
Pd
a-Si
2x10^16 15N/cm^2
● as implanted
o 230°C, 580 min.
Δ 350°C, 10 hr. & the above treatment
Si
0.8
0.9
1.0
1.1
1.2
BACKSCATTERING ENERGY (MeV)
15N (p, α) 12C YIELD (ARBITRARY UNITS)

fig.6

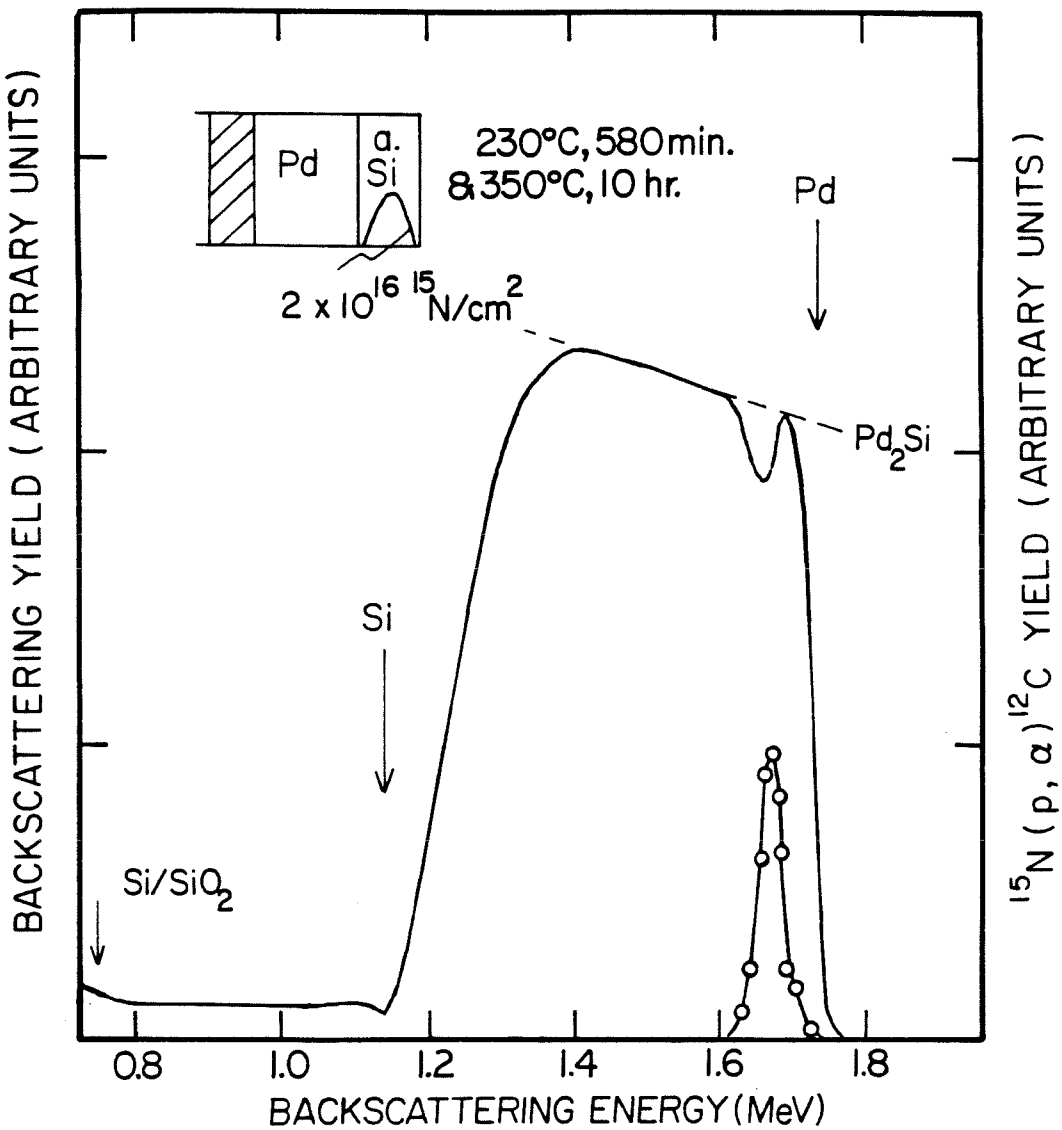
Pd
a. Si
230°C, 580 min.
& 350°C, 10 hr.
Pd
2 x 10^16 15N/cm^2
Pd2Si
Si
Si/SiO2
BACKSCATTERING YIELD (ARBITRARY UNITS)
15N (p, α) 12C YIELD (ARBITRARY UNITS)
0.8
1.0
1.2
1.4
1.6
1.8
BACKSCATTERING ENERGY (MeV)

fig.7

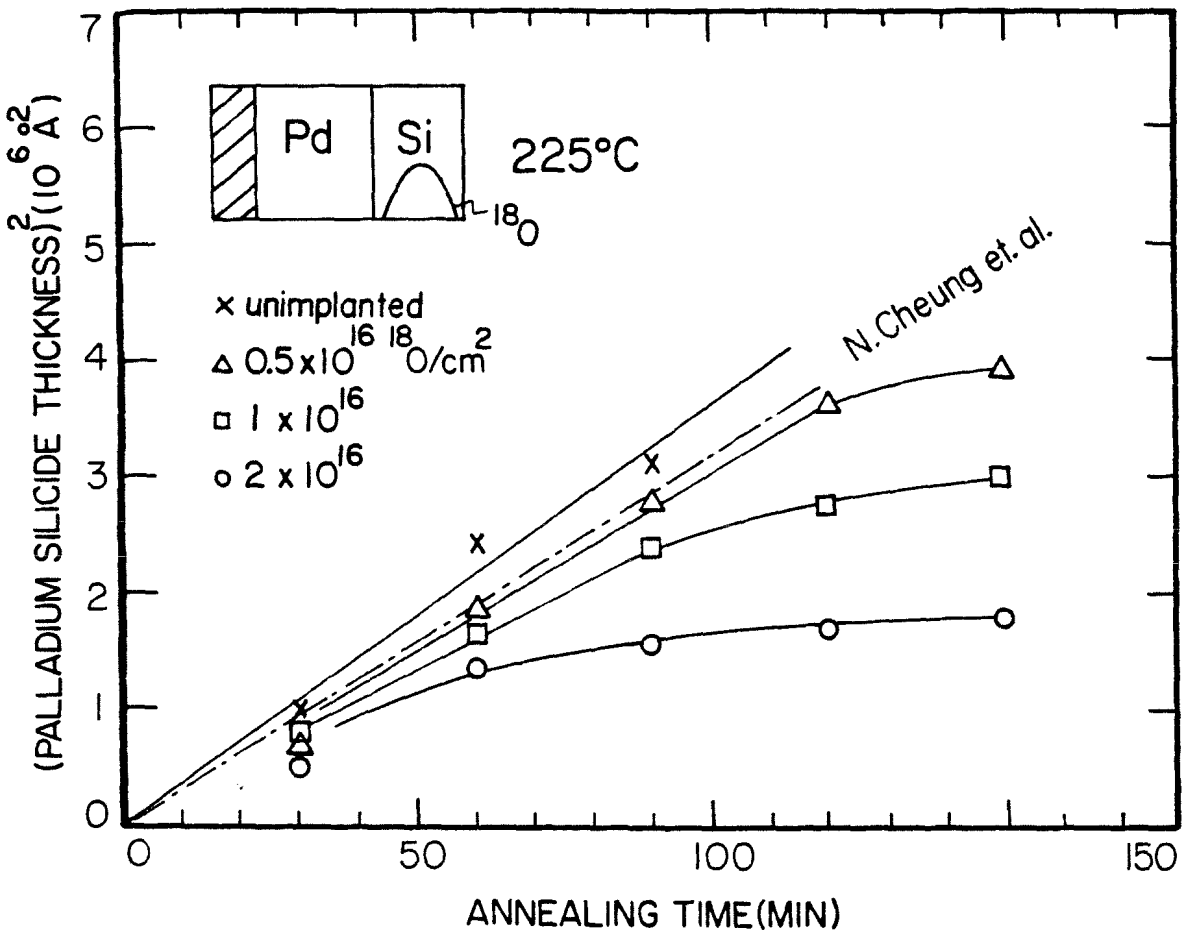
(PALLADIUM SILICIDE THICKNESS)^2(10^6 Å^2)
ANNEALING TIME(MIN)
0
50
100
150
1
2
3
4
5
6
7
Pd
Si
225°C
^{18}O
× unimplanted
△ 0.5×10^{16} ^{18}O/cm^2
□ 1×10^{16}
○ 2×10^{16}
N. Cheung et. al.

fig.8

APPENDIX F

SUBSTRATE ORIENTATION DEPENDENCE OF

ENHANCED EPITAXIAL REGROWTH OF SILICON

K.T.Ho,I.Suni[a)], and M-A. Nicolet

California Institute of Technology,

Pasadena, California, 91125

ABSTRACT

This work extends the study of dopant-enhanced epitaxial regrowth rate of amorphized Si from the <100> to the <110> and <111> orientations of Si. Boron and phosphorous dopants are considered. The annealing temperatures are 500 and 550°C. Phosphorous enhances the growth rates in all three orientations by a constant factor of 8.1± 0.9. Boron produces a higher enhancement factor of 12.2± 1.2, except in the case of <100>. Implications of the results on various growth models are considered. The crystalline quality of regrown <111> layers is improved in the doped samples.

I INTRODUCTION

Regrowth of Si by solid phase epitaxial(SPE) is a part of most device fabrication processes that use high dose implantation doping. Another recent example is the preamorphization of Si by self-implantation to control the projected range of boron implantation in a shallow junction[1]. Dopant enhanced SPE regrowth is thus gaining technological significance in addition to its scientific interest.

The original work on dopant-enhanced regrowth of Si was done by Csepregi et al.[2], who demonstrated that impurities such as B, P and As can

significantly accelerate the regrowth rates of amorphized Si on <100> substrates. Subsequently, Nishi et al.[3] looked at As doped amorphized layers on <100>,<110> and <111> substrates with detailed analysis of electrical activation during regrowth. It was shown that dopants become partially or totally activated as they get incorporated into the advancing recrystallized region. Recently, Suni et al.[4] and Lietoila et al.[5] demonstrated that the enhancement is an electrically activated effect by showing that p-type and n-type dopants together mutually compensate and do not produce an enhanced growth rate. Explanations of the enhancement in terms of electronic processes are given by Suni et al.[6] and Williams and Short[7]

These previous works have studied SPE regrowth principally on <100> Si substrates. The current work aims at a systematic survey of the enhanced regrowth on other substrate orientations, namely <111> and <110>, in addition to <100> which was also included for reference.

Substrate orientation dependence of SPE was first reported by Csepregi et al.[8] on undoped Si. The regrowth velocities of each orientation differ and decrease in the order $v_{100} > v_{110} > v_{111}$. A model based on geometrical arguments was used to explain this dependence. A recent atomistic model proposed by Narayan[9] correctly predicts the relative regrowth rates of the different orientations.

This work incorporates the above two subjects that have been separately studied before, namely, enhanced regrowth and substrate orientation dependence of Si SPE regrowth. Previous studies have shown that, for <100> Si, B doped samples grow faster than P doped ones. This work looks at such dopant dependences for B and P implantations.

II EXPERIMENTAL METHODS

The starting wafers were p type < 100> with resistivity of 1.5-2.5 Ω cm ($\sim 10^{16} B/cm^3$), p type < 110> with resistivity of .017 Ω cm ($\sim 5x\,10^{18} B/cm^3$), and n type < 111> with resistivity of .005-.020 Ω cm($\sim 1.5x\,10^{18}$to $1.5x10^{19} Sb/cm^3$). The principal axis of < 111> wafers was about 3° off the sample normal; while the < 110> and < 100> axes coincided with the respective sample normal. The wafers were cleaned and diced for one of three sequences of multiple implantations at liquid nitrogen temperature. The sequences were i)^{28}Si only (denoted as I), ii)^{28}Si, ^{11}B (denoted as B), iii)^{28}Si, ^{31}P (denoted as P). Si implantation preceded B and P implantations to ensure complete amorphization. Sample normals were tilted 8° from the incident ion beam to avoid channeling effects.

The dose and energy combination was selected such as to produce an extended region , approximately 6000 Å deep, of constant dopant concentration. Range tables by Smith[10] have been used to calculate the final dopant distributions, shown in figures 4 and 5. The implantation schedules are provided in table I.

The plateau of the B and P profiles corresponds to a concentration of about $2x10^{20}/cm^3$, well exceeding the degenerate doping level , but still below the solid solubility limit of B and P in Si in the temperature range used for regrowth[11]. Given the low diffusion coefficients of B and P in Si[11], no redistribution of the implanted dopants is expected during regrowth. Recent studies of Sadana et al.[12] also demonstrated the lack of redistribution of P in regrown amorphized Si. Annealing was done in a vacuum furnace at temperatures of 500°C or 550°C. Thicknesses of the amorphous layers are derived from channeling spectra obtained using 1.5

Mev $^4He^+$ ions.

III RESULTS

A. Dopant Dependence for Each Substrate Orientation

< 100> Si(fig.1):

Our regrowth rate for intrinsic Si is approximately 11.6 Å/min which is slightly higher than the value reported by Csepregi et al.[8] at 500°C. In the P implanted sample, the regrowth rate reaches a constant level of 92.4 Å/min in the uniformly doped region. The regrowth is even faster in the B implanted sample where the measured growth rate is approximately 241.0 Å/min. These rates are in fairly good agreement with previouly reported values.They are summarized in Table II.

There is an initial fast growth in the intrinsic sample which may be related to an incompletely amorphized region due to the trailing edge of the implanted Si profile. In the experiments of Csepregi et al., a low temperature (~450°C) preannealing was performed to eliminate the damaged region.[13] No initial fast growth is reported in those results.

< 110> Si(fig.2):

Regrowth enhancement by B and P doping is observed for the < 110> orientation as well, as shown in figure 2. Our intrinsic growth rate is 6.3 Å/min, faster than that of Csepregi et al.[8](shown in dashed line). The P implanted sample regrows at a constant rate of 45.1 Å/min in the uniformly doped region; while the B implanted sample regrows at a faster rate of 84 Å/min.

< 111> Si(fig.3):

Because the intrinsic regrowth rate of <111> Si at 500°C is impractically slow(~ 1.5 Å /min),this orientation was also studied at 550°C, so that an intrinsic growth curve can be obtained for comparison. The results for 500°C annealing are included in figures 4 and 5.

The intrinsic growth curve shows the same break as observed by Csepregi et al.[8], but at a larger regrown thickness. At 550°C,the slow growth progresses at a rate of 6.6 Å /min, and the fast growth, at a rate of 14.4 Å /min, both slightly higher that the corresponding rates reported by Csepregi et al. The P implanted sample reaches a constant growth rate of 129.0 Å /min, and the B implanted sample, a rate of 154.7 Å /min, in their respective uniformly doped regions.

B. Orientation Dependence with Fixed Dopant Type

Figures 4 and 5 show that the growth rates for different orientations are related in the same way in doped samples as they are in the intrinsic case, namely, $v_{100} > v_{110} > v_{111}$. At 500°C annealing temperature, the B<111> and P<111> samples appear to have two regrowth rates in the constant concentration region. Phosphorous doped samples become very nonuniform at the amorphous-crystalline interface after prolonged annealing. The end section of the P<111> growth curve therefore has an uncertain meaning and is left as a dash-dot line.

C. Additional Observations

In the six month period in which this experiment was carried out, scattering of data points did not exceed 17% in the worst case of B<110>. The growth curve for each doped sample (except the <111> samples at 500°C) was obtained from a number of specimens annealed only once. Each intrinsic growth curve (and the doped <111> samples at 500°C)

includes data points obtained by sequentially annealing of a few specimens. Reproducibility has been checked for some growth curves and good agreement was found.

The quality of SPE on <111> substrates is plagued by twin formations leading to bilinear growth and high channeling yields[14,15]. This is explained by Drosd and Washburn[18] and Narayan[9] to come from the requirement of 3 atoms to complete the first six-fold ring of a recrystallizing plane in <111> direction, as compared to 2 atoms required for <110> and 1 atom for <100> plane. The high chance of a twin formation is due to the high probability of the 3 atoms nucleating in the wrong configuration. We may assume that twin nucleations occur at a certain rate at the amorphous- crystalline interface, in competition with epitaxial regrowth. Since the growth front advances at a faster velocity in a doped sample, twin nucleation density per regrown thickness is expected to be correspondingly reduced. Faster regrowth therefore should improve the crystalline quality. This is verified by channeling spectra of the completely regrown samples shown in fig.6, in which B and P implanted samples demonstrate an overall reduction in yield. All regrown samples show a faster climb in yield, as compared to the virgin sample, from the surface to the original amorphous-crystalline interface, indicating dechanneling due to residual defects. This means that the crystalline quality is still severely degraded with respect to the virgin sample.

IV DISCUSSION

Various models have been proposed for the mechanism of SPE regrowth. Csepregi et al.[8] assume that an atom can be attached to the crystalline phase only at sites where at least two nearest neighboring atoms at the interface are already in crystalline positions. Geometrical

inspection then indicates that <111> plane is the slowest growing direction, giving rise to <111> facets.

In the model by Spaepen and Turnbull[16], attachment of each new atom to a crystalline site involves breaking one bond to rearrange the five- or seven-fold rings characteristic of the amorphous phase to a six-fold ring of the diamond crystalline phase.[17] This broken bond runs along a [110] ledge reconstructing crystalline sites in its path. Spaepen suggests that the bond breaking process is the controlling mechanism for SPE regrowth.

In the work by Drosd and Washburn[18] and that by Narayan[9], two similiar and congruent models of SPE regrowth are presented. Each involves nucleation of atomic steps on a flat crystalline plane at the amorphous-crystalline interface. The step then laterally spreads into a new crystalline layer. Drosd and Washburn attribute the SPE regrowth activation energy to the reorientation of a small group of atoms in the amorphous material at the interface. Narayan takes a very different view and proposes that the activation energy is that for the self diffusion in amorphous Si near the interface. Since Narayan argues that only migration energy is involved in this type of diffusion, this interpretation does not relate the activation energy to the formation of point defects.

It was pointed out by Csepregi et al.[19] that the activation energy of the SPE regrowth for both Si and Ge lies within the range quoted for the formation energy of vacancies in the respective materials. Based on this correlation, Suni et al.[6] suggested that vacancies at the amorphous-crystalline interface control and accelerate the bond breaking process which neccessarily precedes atomic rearrangement during recrystallization. The same authors estimated the reduction of regrowth activation energy by considering the energy levels of charged vacancies

and the shift of Fermi level induced by dopants. A qualitative agreement with experimental data was found.

Thus far, the controlling mechanism of SPE regrowth has been variously attributed to:

1)vacancy formation(Csepregi et al, Suni et al.)

2)bond breaking/propagation of loose bonds (Spaepen et al.)

3)self diffusion in amorphous Si (Narayan)

In order to shed light on this subject, a compilation of data by various authors is presented in table II to illuminate any consistency and patterns which may emerge from the many research efforts. Growth rates are seen to vary by up to 44% in the worst case. However, it should be noted that in the work done by Csepregi et al[2]. and Nishi et al.[3], the implantations did not produce a region of constant doping level. Although Csepregi et al. made the observation that the growth velocity becomes approximately constant for P concentration between 2 and 3 x $10^{20}/cm^3$, it is not clear how reliably growth rates can be measured in such situations. Other factors leading to discrepancies are offsets in temperature and impurities incorporated during implantation, such as nitrogen and carbon, which are known to slow down the growth velocities.[20] The < 100> orientation of each dopant type is studied most extensively, and may serve as the standard in making cross references.

The enhancement effect can be measured in terms of the enhancement factor defined as the ratio of the rates of the doped samples to the intrinsic sample of the same orientation. In < 100> Si the enhancement factor is 8.0 for P implanted samples, and 20.8 for B implanted samples. In < 110> Si, P produces an enhancement factor of 7.2, and B, a factor of 13.3.

The < 111> results are complicated by a bilinear growth characteristic of the intrinsic samples, with the final fast growth region dominated by formation of large twin planes inclined to the surface[8] This makes a quantitative comparison with doped samples difficult. However, the faster growth rate can be interpreted as the growth rate of < 111> oriented wafers averaged over the twined and perfectly epitaxial sections on the growth front. Since a predominant part of the amorphized region regrows at the fast rate, it is more practical to emphasize this rate. We therefore calculate the < 111> enhancement factor according to the faster intrinsic rate as is done by Csepregi et al.[2] At 550°C, the doped samples show only one growth rate in the constant concentration region, giving an enhancement factor of 9.0 for P implanted samples, and 11.0 for B implanted samples. At 500°C, both P and B implanted samples show two growth rates in the constant concentration region. Whether twin formations are responsible here for the different rates can not be determined without TEM studies. Both slow and faster growth rates of these samples are included in table III. Enhancement factors cannot be meaningfully defined in this case.

Table III provides an overview of the current experimental results. The enhancement factors due to P range from 7.2 to 9.0, which may be considered to be a constant value of 8.1 ± 0.9. The enhancement factor due to Boron is 12.2 ± 1.2. However, this value excludes the exceptionally high value of 20.8 for B< 100> .

Based on this interpretation of data, it can be stated that the primary mechanism responsible for regrowth enhancement is independent of the crystal orientation. The exceptionally high value for B< 100> then indicates that an addition mechanism for enhancement is taking effect in this sample configuration.

The model of Suni et al. which explains the enhancement by a reduction in activation energy due to dopant induced charged vacancies, would be in agreement with our findings. This is because in this model, all substrate related geometrical factors are included in the preexponential term, which is unaffected after doping. Narayan's model which described an enhanced self diffusion in amorphous Si is also consistent with the orientation independence. The model of Spaepen et al. looks at bond breaking and loose bond propagation. The interfacial conditions in which these processes occur differ for each orientation. Whether the enhancement according to this model should be constant is not clear. (It is also unclear that Spaepen et al. wanted to apply the model to other than the <111> orientation.)

Our <111> wafers have an original doping level within one order of magnitude of the implantated value. The question is whether this relatively high background enhances the regrowth. In the works of Csepregi et al.[2] and Suni et al.[6], various growth curves are superimposed on corresponding dopant profiles. We determine from their figures that any enhancement effect due to this background doping level is negligible.

V CONCLUSION

Dopant enhanced SPE regrowth has been demonstrated to take place for <111> and <110>, as well as <100> oriented Si, at both 500°C and 550°C. Samples implanted with P exhibit an enhancement factor of 8.1 ± 0.9; while B implanted samples have a factor of 12.2 ± 1.2, except in case of B<100>, which has a high value of 20.8. We find consistency with previously reported results that B is more effective than P in accelerating the SPE regrowth velocity. A constant enhancement factor for different orientations is, by itself, not sufficient to distinguish whether the primary

controlling mechanism of regrowth is due to vacancy formation, bond breaking and propagation, or self diffusion in amorphous Si, as proposed by various authors. The faster regrowth induced by B and P improves crystalline quality in the regrown layer by partially suppressing competing twin formations.

ACKNOWLEDGEMENT

The authors would like to thank Dr. S.S.Lau(University of California, San Diego) for valuable discussions. The implantation part of this study was financially supported by the U. S. Department of Energy through an agreement with the National Aeronautics and Space Administration and monitored by the Jet Propulsion Laboratory, California Institute of Technology(D. Burger).

REFERENCES

[a)]Permanent Address: Semiconductor Laboratory,Technical Research Centre of Finland, Otakaari 5A, SF 02150, Expo 15, Finland.

1 T.M.Liu and W.G.Oldham, ***extended abstract*** #406, ECS spring meeting(1983); to be published in *J.Electrochem.Soc.*

2 L.Csepregi,E.F.Kennedy,T.J.Gallagher and J.W.Mayer, *J.Appl.Phys. 48*, 4234(1977).

3 H. Nishi,T. Sakurai,and T. Furuya, *J.Electrochem.Soc. 125*, 461(1978).

4 I.Suni,G.Göltz,M.G.Grimaldi,and M-A.Nicolet, *Appl.Phys.Lett. 40*, 269(1982).

5 A.Lietoila,A.Wakita,T.W.Sigmon and J.F.Gibbons, *J.Appl.Phys. 53*, 4399(1982).

6 I.Suni,G.Göltz and M-A.Nicolet, *Thin Solid Film 93*, 171(1982).

7 J.S.Williams and K.T.Short, *Proceedings of the International Conference on Ion Beam Modification of Materials(IBMM-82),Grenoble, France, September, 10*, 123(1972).

8 L.Csepregi,E.F.Kennedy and J.W.Mayer, *J.Appl.Phys. 49*, 3906(1978).

9 J.Narayan, *J.Appl.Phys. 53*, 8607(1982).

10 B.Smith, *Ion Implantation Range Data for Silicon and Germanium Device Technologies (Research Studies Press, Forest Grove, Oregon, 1977).*

11 S.M.Sze, *Physics of Semiconductor Devices, 2nd Edition (Wiley-Interscience, New York, 1981).*

12 D.K.Sadana,J.Washburn and C.W.Magee, *J.Appl.Phys. 54*, 3479(1983).

13 S.S.Lau, private comm.

14 L.Csepregi,J.W.Mayer and T.W.Sigmon, *Appl.Phys.Lett. 29*, 92(1976).

15 G.Foti,L.Csepregi,E.Kennedy,P.Pronko and J.W.Mayer, *Physics Lett. 64A*, 265(1977).

16 F.Spaepen and D.Turnbull, in *Laser-Solid Interactions and Laser Procesing, edited by S.D.Ferris, H.J.Leamy, and J.M.Poate(American Institute of Physics, New York, 1979)*, p73.

17 F.Spaepen, *Acta Metall. 26* ,1167(1978).

18 R.Drosd and J.Washburn, *J.Appl.Phys. 53*, 397(1982).

19 L.Csepregi,R.Kullen,J.W.Mayer and T.W.Sigmon, *Solid State Comm. 21*, 1019(1977).

20 E.F.Kennedy,L.Csepregi,J.W.Mayer and T.W.Sigmon, *J.Appl.Phys. 48*, 4241(1977).

TABLE I

Implantation schedules for silicon, Boron, and Phosphorous. All implantaions were performed at LN_2 temperature, with the sample normal tilted by 8° from the beam to minimize channeling effects.

Dopant	Ion Species	Dose ($10^{15} atom/cm^2$)	Energy (Kev)
^{28}Si	Si^+	1	60
	Si^+	2	140
	Si^+	5	300
^{11}B	B^+	2.5	60
	B^+	3.4	115
	B^+	4.1	200
^{31}P	P_2^+	1.4	180
	P_2^+	2.5	320
	P^+	6.7	320

TABLE II

Regrowth Rates at 500°C

(Å/min)

	This Work	Csepregi et al.	Suni et al.	Nishi et al.	Lietoila[b] et al.
		(ref.2)	(ref.4)	(ref.3)	(ref.5)
Doping level ($10^{20}/cm^3$)	2	2-3	4	2 max	2
I<100>	11.6	10.0	7.0		6.93
<110>	6.3	3.5			
<111>		1.5[a]			
B<100>	241	200	177		
<110>	84				
<111>	18				
P<100>	92.4	61	88		52
<110>	45.1				
<111>					
As<100>		55	39.4	40	
<110>				11	
<111>				1.3	

[a] extrapolated from Arrhenius plot

[b] annealed at 503°C

TABLE III

Regrowth rates and enhancement factors.

I,P,and B doped <100>,<110>,and <111> Silicon.

		I	B	P
500°C	<100>	11.6	241 / 20.8	92.4 / 8.0
	<110>	6.3	84 / 13.3	45.1 / 7.2
	<111>	1.5[a] / 0.4	18 / 8.6	7.6 / 3.7
550°C	<111>	14.4	154.7 / 11.0	129 / 9.0

Growth rate / Enhancement Factor

a) Extrapolated from Arrhenius plot of Csepregi et al. (from Ref. 8).

Figure Captions

figure 1 Regrowth curves of doped and intrinsic < 100> Si, at an annealing temperature of 500°C. The dashed line is taken from Csepregi et al. Arrows next to the B and P growth curves indicate beginnings of constant concentration regions.

figure 2 Regrowth curves of < 110> Si at 500°C. The dashed line is taken from Csepregi et al.

figure 3 Regrowh curves of < 111> Si at an annealing temperature of 550°C. The slow and fast growth regions are similiar to the results of Csepregi et al.(dashed line)

figure 4 Substrate orientation dependence of regrowth rate for B implanted Si at 500°C annealing. Growth velocities decrease in the order $v_{100} > v_{110} > v_{111}$ similiar to intrinsic samples. The calculated concentration profile of the implanted Boron is also plotted. The area between dash lines is taken as the constant concentration region.

figure 5 Phosphorous implanted samples show the same substrate orientation dependence as the B implanted and intrinsic samples. The annealing temperature is 500°C. The calculated P concentration profile is also plotted. Due to the slow regrowth rate of the < 111> sample, the time scale is contracted by a factor of 3 to fit this growth curve into the figure. The P< 111> growth curve ends in a dash-dot line to indicate that the amorphous-crystalline interface has become very nonuniform.

figure 6 Channeling spectra of fully regrown Boron, Phosphorous, and Si

implanted < 111> samples, plotted against the channeled and random spectrum of an unimplanted sample. Implanted dopants reduce channeling yields as compared to the spectrum of the intrinsic sample, indicating an improvement of crystalline quality. The implanted samples were regrown at 550°C. The annealing times were 4hrs, 4hrs and 8hrs forB doped, P doped and intrinsic samples, respectively.

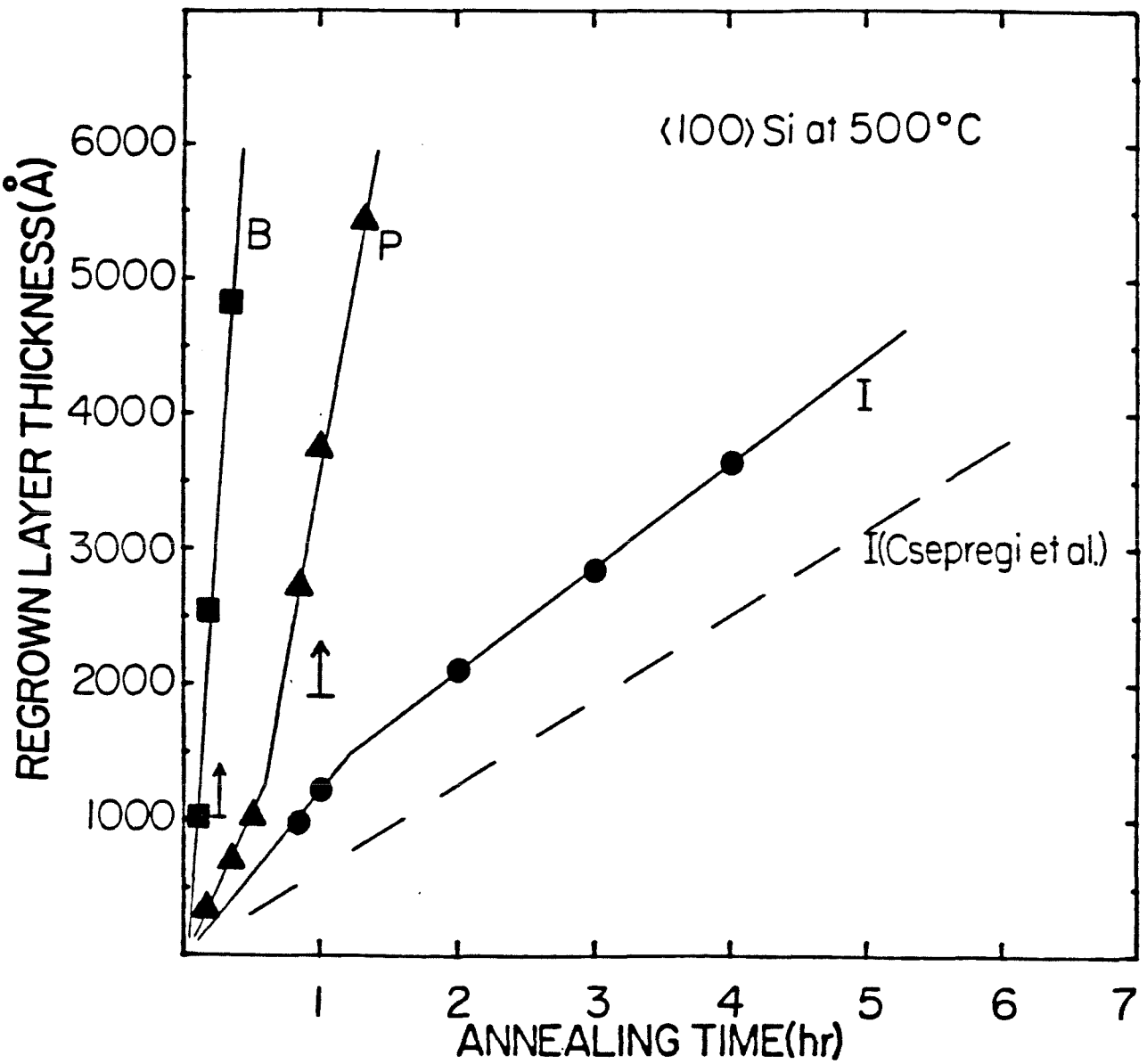
⟨100⟩ Si at 500°C
B
P
I
I(Csepregi et al.)
REGROWN LAYER THICKNESS(Å)
6000
5000
4000
3000
2000
1000
1
2
3
4
5
6
7
ANNEALING TIME(hr)

Fig. 1

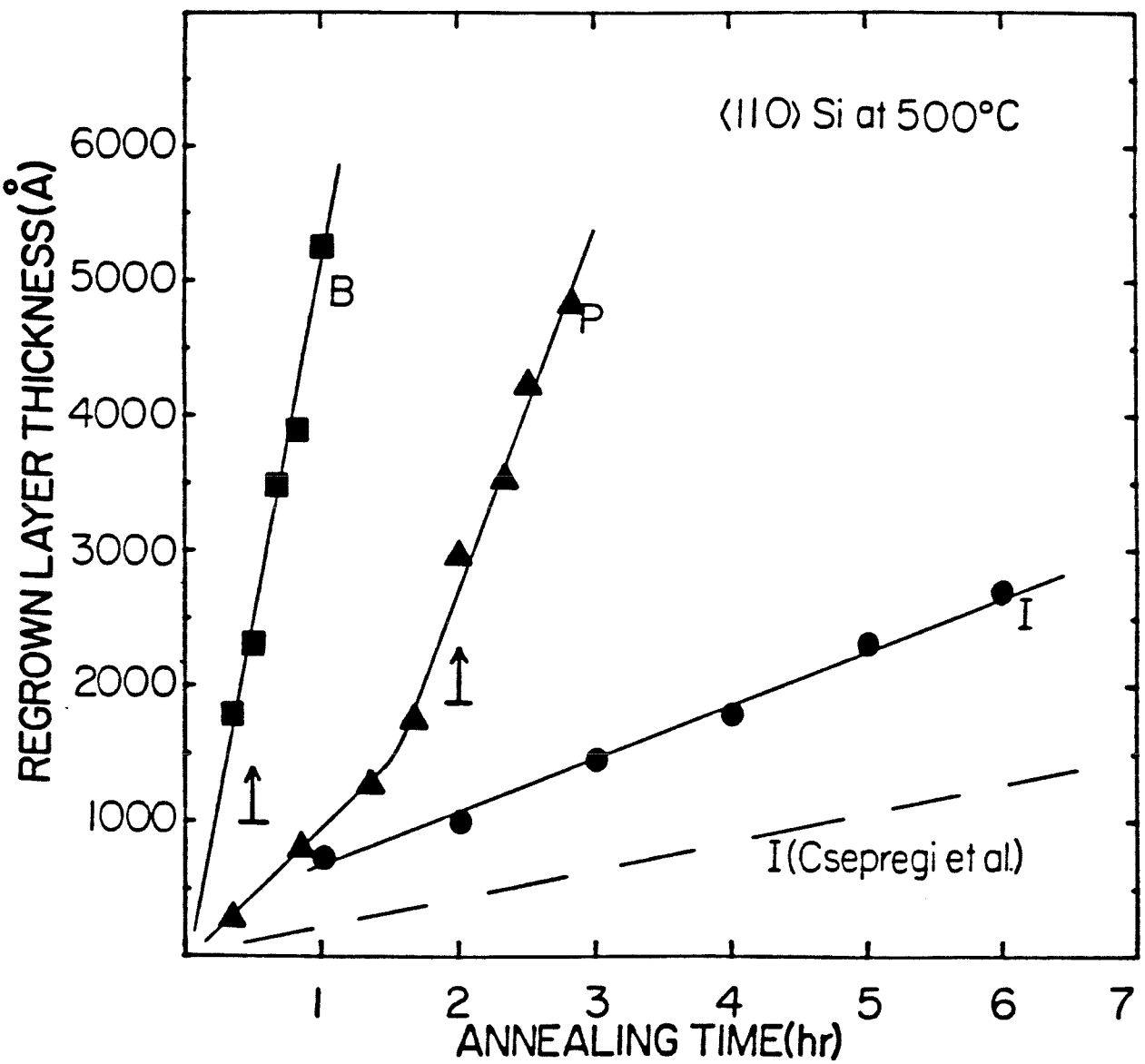
⟨110⟩ Si at 500°C
REGROWN LAYER THICKNESS(Å)
6000
5000
4000
3000
2000
1000
B
P
I
I(Csepregi et al.)
1
2
3
4
5
6
7
ANNEALING TIME(hr)

Fig. 2

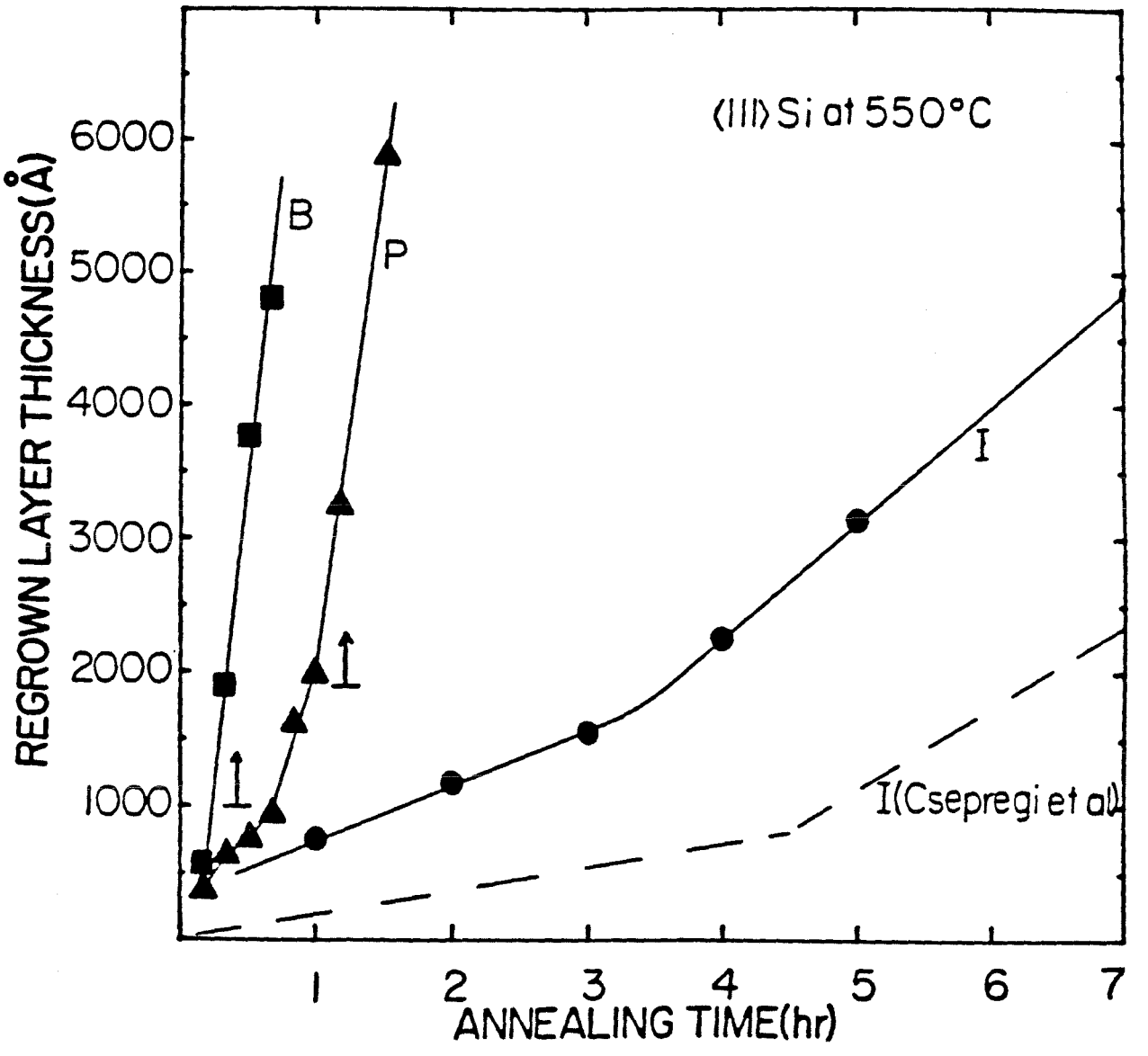
⟨111⟩Si at 550°C
B
P
I
I(Csepregi et al)
REGROWN LAYER THICKNESS(Å)
6000
5000
4000
3000
2000
1000
1
2
3
4
5
6
7
ANNEALING TIME(hr)

Fig. 3

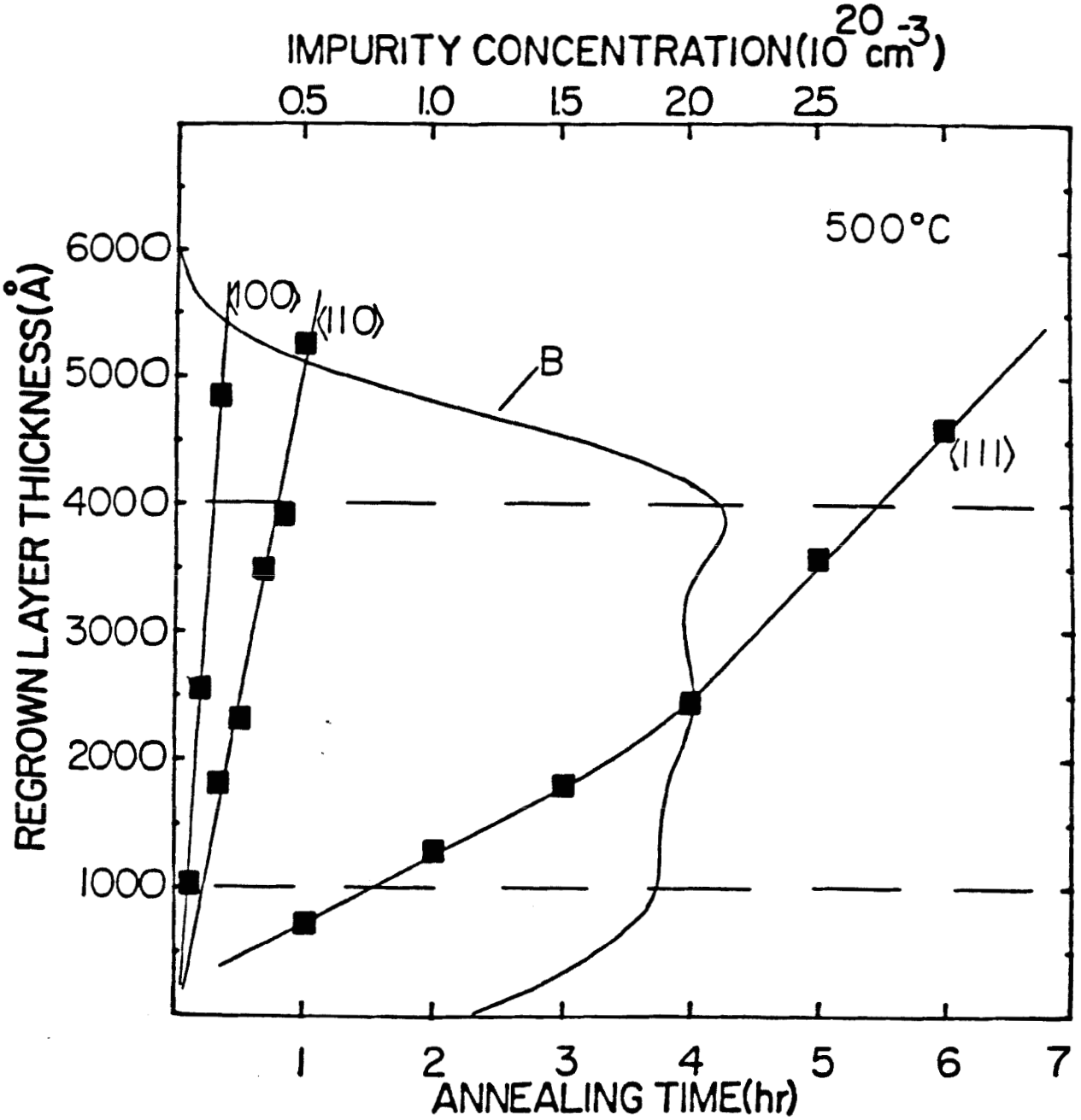
IMPURITY CONCENTRATION(10^{20} cm^{-3})
0.5
1.0
1.5
2.0
2.5
500°C
REGROWN LAYER THICKNESS(Å)
6000
5000
4000
3000
2000
1000
⟨100⟩
⟨110⟩
B
⟨111⟩
1
2
3
4
5
6
7
ANNEALING TIME(hr)

Fig. 4

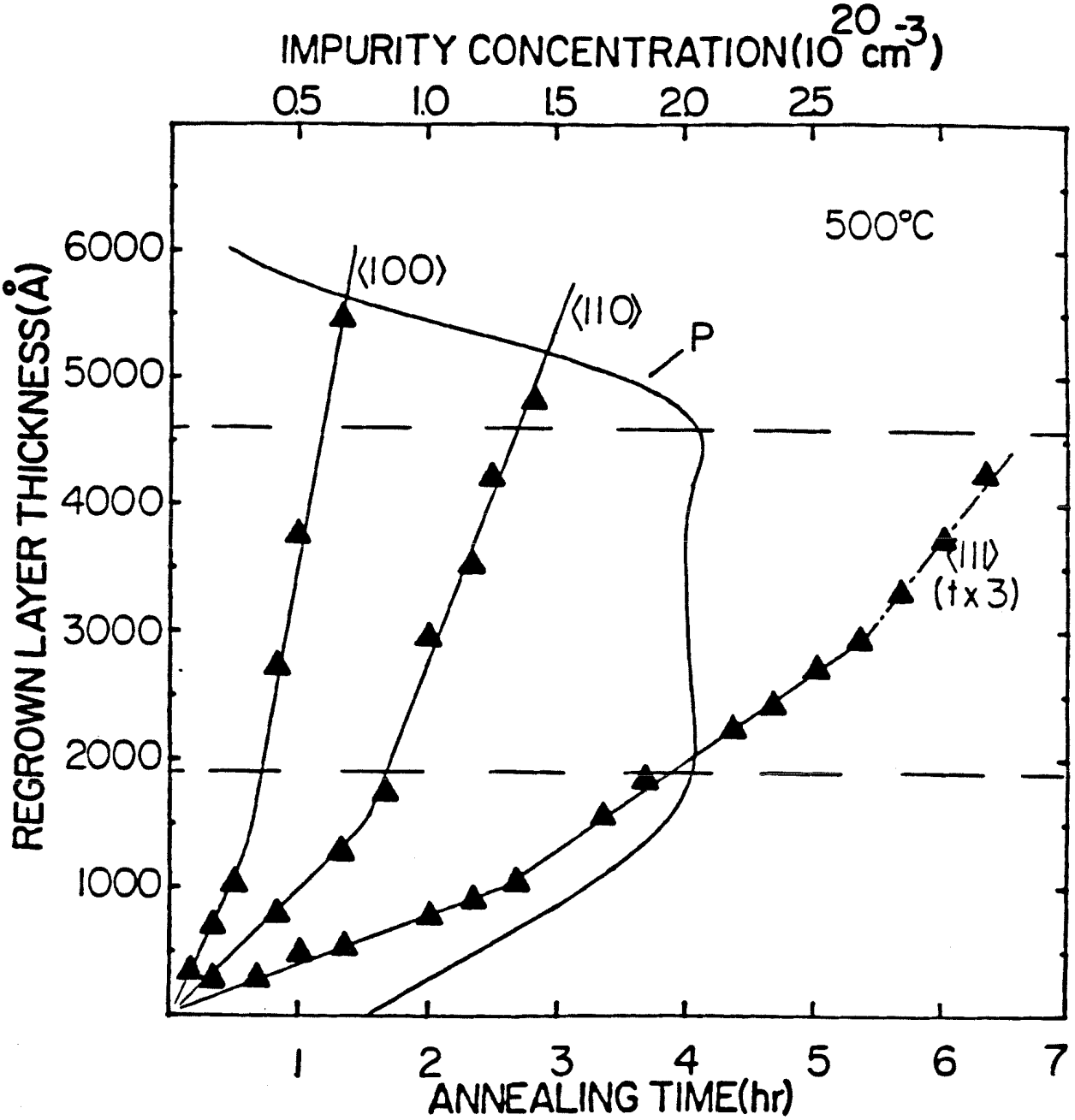
IMPURITY CONCENTRATION(10^{20} cm^{-3})
0.5
1.0
1.5
2.0
2.5
500°C
⟨100⟩
⟨110⟩
P
⟨111⟩
(t x 3)
REGROWN LAYER THICKNESS(Å)
6000
5000
4000
3000
2000
1000
1
2
3
4
5
6
7
ANNEALING TIME(hr)

Fig. 5

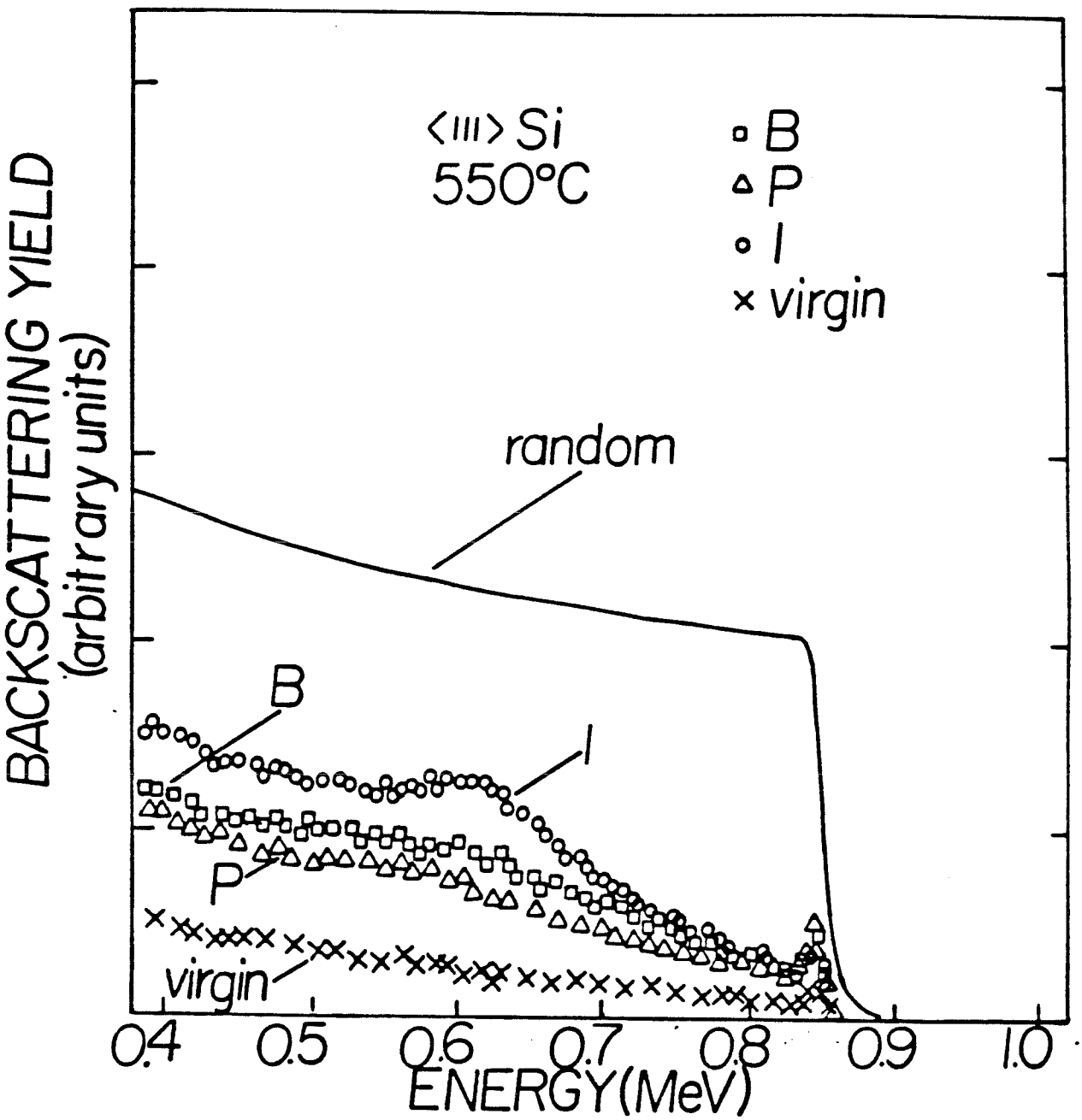
<111> Si
550°C
B
P
I
virgin
random
B
I
P
virgin
BACKSCATTERING YIELD
(arbitrary units)
0.4
0.5
0.6
0.7
0.8
0.9
1.0
ENERGY(MeV)

Fig. 6